DEPENDENCE OF THERMAL CONTROL COATING DEGRADATION UPON ELECTRON ENERGY

FINAL REPORT FOR THE PROGRAM:

STUDY OF SPACE ENVIRONMENT EFFECTS ON
THERMAL CONTROL COATINGS

MAY 1969

CONTRACT NO. NAS5-11164

PREPARED BY
THE BOEING COMPANY
AEROSPACE GROUP
SEATTLE, WASHINGTON

FOR

GODDARD SPACE FLIGHT CENTER
GREENBELT, MARYLAND

DEPENDENCE OF THERMAL CONTROL COATING DEGRADATION UPON ELECTRON ENERGY

FINAL REPORT FOR THE PROGRAM:

STUDY OF SPACE ENVIRONMENT EFFECTS ON
THERMAL CONTROL COATINGS

CONTRACT NO. NAS5-11164

GODDARD SPACE FLIGHT CENTER

CONTRACTING OFFICER: Charles L. Dunfee

TECHNICAL MONITOR: Charles H. Duncan

PREPARED BY: Lawrence B. Fogdall
TECHNICAL LEADER

Sheridan S. Cannaday
PRINCIPAL INVESTIGATOR

SUPERVISED BY: Richard F. Brown
PROGRAM MANAGER

THE BOEING COMPANY
AEROSPACE GROUP
SEATTLE, WASHINGTON

FOR

GODDARD SPACE FLIGHT CENTER
GREENBELT, MARYLAND

ABSTRACT

This document is the final report of work performed for NASA-Goddard Space Flight Center under Contract NAS5-11164. The effects of 20-keV, 50-keV, and 80-keV electrons on the reflectance of selected types of thermal control coatings and surfaces have been studied and compared. Both diffuse and specular materials of current interest for space application were exposed in the dark in a 10^{-8} torr vacuum to electron fluences as great as 10^{16} electrons/cm^2. The types of coatings and surfaces tested included diffuse white paints, a metallic gray paint, Kapton, metallized Teflon and lacquer, aluminum, and overcoated aluminum. The hemispherical spectral reflectance of each test specimen was measured in vacuum (in situ) before and after exposure, using an integrating sphere, a monochromator, and a continuous wavelength scan technique between 0.25 and 2.5 microns. Plots of reflectance or reflectance changes as a function of wavelength were obtained by computer-processing of test data, and are presented. It was concluded that reflectance degradation in most materials studied is strongly dependent upon electron energy. Relative effectiveness of 20-, 50-, and 80-keV electrons for causing spectral reflectance degradation was determined for those coatings showing sufficient damage. Quantitative fluence/energy equivalences are presented. In several types of coatings appreciable improvement in reflectance was observed with time after exposure, even though test specimens remained in the dark and in the 10^{-8} torr vacuum. Observance of this phenomenon — of importance for space vacuum environment applications — led to the performance of several additional tests and studies during the program period. Both the reflectance-degradation and the reflectance-recovery characteristics of the materials studied are reported.

SUMMARY OF CONCLUSIONS AND RECOMMENDATIONS

Exposures of coatings to 20-keV, 50-keV, and 80-keV energy electrons during Contract NAS5-11164 have resulted in significant findings and conclusions. The observance of in-vacuum reflectance changes has given the work increased significance for space applications. Accordingly, future work relating degradation and recovery phenomena and mechanisms is recommended herein.

From the 20-keV electron test, it is concluded that:

1. Degradation in white paints builds up more slowly than was found in earlier tests at 50 keV for Contract NAS5-9650. Absorptance bands in the infrared wavelength region are apparent in reflectance vs. wavelength curves, even after exposure to high electron fluences.

2. The most recent ZnO-methyl silicone coating, series 101-7 (type R), has successfully been made more resistant to low-energy electron damage. Nevertheless, substantial degradation occurs in Type R at 10^{15} and 10^{16} 20-keV electron fluences.

3. The visible-region "silicate-band" damage in types D_3, E_3, and F_3 occurs in substantial amounts, even for this low energy. Additional damage due to the presence of TiO_2 and ZnO occurs in the types possessing them as pigments. Thus type D_3, with Al_2O_3 pigment only, is the most stable of the three types under electron exposure.

4. Other coatings tested with 20-keV electrons (Kapton, Alzak, overcoated aluminum) sustain only limited amounts of reflectance degradation, if any.

From the 80-keV electron test, it is concluded that:

5. Degradation in white paints is more severe at each exposure fluence, compared to damage resulting from lower energy electrons. Absorptance structure in the infrared wavelength region is removed at lower fluences than happens with lower energy electrons. Damage is chiefly in the infrared except for the case of

aluminum oxide-potassium silicate (type D_3) in which degradation is confined to the "silicate band" in the visible and ultraviolet wavelength regions.

6. The visible-region silicate absorption band is induced to even greater amounts by 80-keV electrons. In addition, the presence of TiO_2 and ZnO pigments in coating types E_3 and F_3 causes them to incur "catastrophic" amounts of reflectance degradation at 10^{16} 80-keV electrons/cm^2.

7. Similar "catastrophic" reflectance damage is measured in the following coatings after exposure to 10^{16} 80-keV electrons/cm^2:

a. types M and R ZnO—methyl silicone
b. type O rutile TiO_2—methyl silicone
c. type N Kapton H film

8. Exposure to 10^{16} 80-keV electrons/cm^2 is sufficient to convert the specular appearance of each Teflon coating to a crazed, mottled gray appearance.

Upon comparison of test results at different energies, it is concluded that:

9. Degradation in white paints is substantial for each energy studied, and quite severe in some cases. In every case, exposure to 20-keV electrons causes less damage than exposure to electrons of higher energy. Degradation caused by 50-keV electrons (for those surfaces tested) is rather like degradation caused by 80-keV electrons. In a few cases, in fact, results at 50 keV are virtually indistinguishable from those at 80 keV. Degradation in the white paints from 20-keV electrons is less able to mask the existence of infrared absorption bands than is damage by 50-keV and 80-keV electrons.

10. Type O rutile TiO_2—methyl silicone offers the greatest stability of the white diffuse coatings tested in an electron environment, provided fluences above 10^{15} electrons/cm^2 are not expected to be encountered in the application or mission. Because of type O's poor performance above 10^{15}, however, type L with anatase TiO_2 is a better TiO_2—silicone selection for such an application.

11. The following coatings and surface are extremely resistant to reflectance change when exposed to electrons in the 20-keV to 80-keV range: leafing aluminum—silicone (type I), vapor-deposited aluminum over lacquer (type J), aluminum oxide over aluminum (type G), silicon dioxide over aluminum (type H), and buffed aluminum (type K). The main change in type H is improvement in reflectance in the ultraviolet wavelength region.

12. Alzak (types Z_3, Z_4, and Z_5) sustains more degradation from 20-keV electrons than from 80-keV electrons. Reflectance losses are mainly in the ultraviolet wavelength region.

13. The concept of potassium silicate (K_2SiO_3) actually being best represented by ($K_2O \cdot SiO_2$) fits well with results obtained in this program. Damage in coatings bearing potassium silicate (D_3, E_3, and F_3) correlates well (as to wavelength region in which it peaks—0.6 micron) with that historically observed and reported for optical materials, including silica, Corning 7940, and borosilicate glass.

14. The newly-obtained 50-keV test data fit well, though not perfectly, with earlier 50-keV data obtained under Contract NAS5-9650.

From the recovery tests, it is concluded that:

15. In-vacuum reflectance recovery or improvement with time after the end of an electron exposure is a real, validly observed phenomenon in some types of coatings. The amount or rate of recovery may be easily observed, or difficult to detect, depending upon the type of material or coating involved.

16. In-vacuum reflectance recovery proceeds more quickly to remove greater fractions of the original degradation caused by exposure to 20-keV electrons, compared to that removed with time after 50-keV or 80-keV electron exposure. Previous observations of reflectance improvement when exposure to ultraviolet radiation follows electron exposure (Contract NAS5-9650) may also be interpreted as in-vacuum reflectance recovery successfully competing with ultraviolet-induced degradation.

17. Let a "segmented exposure" be defined as one in which alternating periods of irradiation and measurement (with irradiation having been interrupted) occur. Similarly, let "unsegmented exposure" refer to continuous irradiation to a "final" radiation level without interruption at intermediate levels for measurement. Then, it is found that segmented and unsegmented electron exposures yield substantially the same results (reflectance changes) in the types of coatings tested, when compared at a "final" fluence of 3×10^{14} 20-keV electrons/cm^2.

18. Both the rate and the extent of in-vacuum reflectance recovery in the various coatings and surfaces studied are functions of electron energy, electron fluence, and time after end of exposure. There is some indication that rate and extent of recovery are dependent upon specimen temperature. Additional study would be needed to determine any dependence upon the type of radiation received before recovery is observed (e.g., protons, solar photons, etc.), and any dependence upon exposure flux or intensity.

It is recommended that this program be followed by:

1. Continuation of coating exposures to additional simulated space environmental conditions, and further test technique development to increase accuracy of simulation. Included would be separate and simultaneous exposures to solar electromagnetic energy and particles (both electrons and protons) in energy regions not already studied. This will allow better prediction of coating performance and survival.

2. Studies to determine damage mechanisms, in order to effect hardened coating development. A damage model would be developed from future experimental results and further analysis of available data. Emphasis should be placed on relating the absorption of solar energy as a function of distance into a coating, to radiation penetration depth, dose, and displacement density. An effort should also be made to determine the roles of residual gas species and charge migration on the damage and recovery of coatings.

ACKNOWLEDGMENTS

Those who prepared or supervised the preparation of this report acknowledge with thanks the assistance of several persons on the staff of the Boeing Radiation Effects Laboratory. Persons contributing to the program include:

Richard R. Brown	Program Leader
Lawrence B. Fogdall	Technical Leader
Sheridan S. Cannaday	Principal Investigator
Loren D. Milliman	Computer Software
Chalmers R. Brittain, Jr.	Data Reduction and Document Preparation
Edward D. Sullivan	Test Monitoring

KEY WORDS

Damage Mechanisms	Monochromator
Electron radiation	Radiation effects
Energy dependence	Space simulation
Hemispherical reflectance	Spectral reflectance
In situ (In vacuum)	Thermal control coatings
In situ reflectometer	Vacuum

LIST OF FIGURES

LIST OF FIGURES (continued)

LIST OF FIGURES (continued)

LIST OF FIGURES (continued)

LIST OF FIGURES (continued)

LIST OF TABLES

1.0 INTRODUCTION

This program, under NASA-Goddard Contract NAS5-11164, has been a follow-on effort to earlier electron, proton, and ultraviolet radiation studies conducted by Boeing for NASA-Goddard. The connection between the two efforts is described below.

1.1 PROGRAM DESCRIPTION

This program involved exposure of some 23 types of thermal control coatings and surfaces to 20-keV electrons and to 80-keV electrons, in two separate tests. The intent was to build upon 50-keV electron results obtained in an earlier program, Contract NAS5-9650, and to establish the electron energy dependence for degradation across the 20-keV to 80-keV electron energy range. The spectrum of trapped electron radiation includes this energy range.

Thirteen of the 23 coating types are common to the earlier 50-keV electron tests for Contract NAS5-9650 and the more recent tests for this program. Of the remaining ten types, four were available at the beginning of this program, and so were tested at both 20 keV and 80 keV. The other six types, all Teflon-based coatings, were received after the start of this program, and thus were exposed during the second test, at 80 keV.

Brief descriptions of each of the 23 tested types of coatings and surfaces are contained in Table 1, which is part of Section 2.1.

Both the 20-keV electron test and the 80-keV electron test provided the following exposure fluences or levels at which specimen hemispherical reflectance measurements were made: 1×10^{13}, 5×10^{13}, 1×10^{14}, 3×10^{14}, 1×10^{15}, and 1×10^{16} electrons/cm^2. More detailed information for each test, including the electron exposure rates used to reach each fluence, will be found in Tables 2 and 3, which are part of Sections 2.2 and 2.3, respectively.

Reflectance measurements made were continuous-scan charts over the 0.25- to 2.5-micron wavelength region. The measurement method involves an integrating sphere in vacuum (10^{-8} torr range) and a Beckman DK-2A Far UV spectrophotometer outside the test chamber (see also References 1 and 2). Besides allowing the making of charts with very high resolution of reflectance structure with wavelength, this system includes encoders inside the spectrophotometer so that data is simultaneously punched onto cards (via a Datex automatic data collection system) for subsequent computer processing.

As tests for this program proceeded, several unexpected phenomena were observed which led us to perform additional tests within the program period. The observance of measurable increases in sample reflectance with time, when compared with the degraded reflectance condition measured immediately following an electron exposure, prompted us to conduct several in-vacuum (in situ) reflectance recovery studies, each lasting several hours or even days. Depending on the coating type, and on the overall time involved, the amount of in-vacuum reflectance recovery was observed to be as much as 50 percent of the originally measured reflectance degradation. Several types of coatings exhibited no in-vacuum recovery. The largest amounts of in-vacuum recovery were observed during the 20-keV electron test. Lesser amounts were observed at 80 keV.

Both the 20-keV test and the 80-keV test consisted of exposing samples progressively to higher and higher electron fluences on a segmented basis with interruptions at each chosen fluence level for reflectance measurements to be made. Because of the significant amounts of reflectance recovery observed in several types of coatings, it was apparent that a continuous exposure of samples to a reasonably high fluence, conducted on an unsegmented basis, should be made to validate the data obtained on a segmented-exposure basis. Such a continuous, unsegmented exposure was made with 20-keV electrons, to a fluence of 3×10^{14} electrons/cm^2, and the data compared with measurements arising from the segmented exposures to 3×10^{14} electrons/cm^2.

Each test was conducted with the samples in good thermal contact with the

test chamber's temperature-controlled sample wheel. The temperature-controlling fluid used for the tests was externally-supplied, unrecycled water, whose temperature customarily varies throughout the year from about 20°C in the summer to about 5°C in the winter. The 20-keV electron test was performed at a time when the sample wheel was controlled to 10 ± 1°C, while the 80-keV electron test took place with the sample wheel at 6 ± 1°C. To see if any reflectance-changing effects could be observed from changes in temperature, the sample wheel was brought to room temperature (19-20°C) at the completion of the 80-keV electron test. No reflectance changes attributable to this 14C° change were observed.

This program involves a comparison of the earlier (50-keV) test data from Contract NAS5-9650 with 20-keV and 80-keV data from this program's tests. Continuous-scan reflectance data over the 0.25- to 2.5-micron wavelength region was obtained in both programs, but in the earlier program was analyzed only at selected wavelengths. The decision was made to expand the amount of 50-keV data readily available, by conducting a new 50-keV test to 1×10^{15} electrons/cm^2 on selected types of coatings. The result is punched-card, computer-ready test data of the same type which was generated in the 20-keV and 80-keV electron tests, allowing the energy dependences and degradation equivalences in Section 2.5 to be presented more accurately and with more detail.

More detailed discussion of these additional experiments is contained in Section 2.4.

1.2 SCOPE OF PROGRAM RESULTS

This report contains considerable new in situ data characterizing the effects of electron exposure upon the reflectance properties of 23 types of thermal control coatings. As opposed to being just "degradation" or "damage" data, the results instead constitute a more "fundamental" or "basic" energy study. The report includes descriptions of energy dependences observed and electron energy/fluence equivalences determined. It is tempting to try to relate the raw and/or computer-processed reflectance results to expressions of how energy is deposited in the test materials—what could be termed depth-dose profile (interaction with distance into

the material). One could begin with well-established range-energy relations for electrons; however, these are limited to a few familiar cases such as air, water, aluminum, and lead. Then, considering the test materials, any results obtained would be, strictly speaking, applicable only to buffed aluminum (sample type K). To be sure, one can easily determine that 20-keV electrons penetrate approximately 3 microns in aluminum, while 50-keV and 80-keV electrons have ranges of about 15 microns and 33 microns, respectively, in aluminum. The ranges of electrons in the other test materials can be estimated by using an approximation that such ranges are inversely proportional to the electron density of those materials (Reference 3). Upon recalling, however, the complexity of the materials under test—tetrafluoroethylene, polydimethylsiloxane, and other organics; potassium silicate, with one or two metal oxides bound in intimate mixture, multilayered specular surfaces and other inorganics—it becomes sheer guesswork to determine an effective Z (electron number per atom), much less an average electron density, without detailed information concerning the composition and preparation of each type of test specimen.

Qualitatively, one can say assuredly that the range of 80-keV electrons is greater than that of 50-keV electrons, which is greater than the range of 20-keV electrons in all the coating materials tested. One can observe that the order of magnitude of electron penetration range—several microns—is within the span of several physical specimen parameters which are pertinent:

(1) the thickness of the uppermost layer in certain coatings—the 1.1 microns of Al_2O_3 in type G, the 2.5 microns of SiO_x in type H;

(2) the unspecified microns-thick layer of opaque aluminum over coating type J;

(3) the 2- and 3-mil layers of Kapton H film and leafing aluminum (in types N and I, respectively); and

(4) the white paint coatings of up to 11 mils (280 microns) in thickness.

Thus, in some coating types the incident electrons are decelerated and captured within a "homogeneous" material, while in others they pass through a multilayer

structure, each layer with its own dE/dx (derivative of energy loss with distance). The result is nothing less than an exceedingly complex model of the way in which the energy of incident particles is absorbed in real test specimen materials, and of the relationship between this absorption and coating reflectance.

Compounding the importance of all this is the fact that different wavelengths of "light"—ultraviolet, visible, and infrared—which are incident on the coatings while in use, penetrate the various materials to varying depths while being fractionally reflected and absorbed. That is, due to dispersion and other phenomena, both pigments and the other materials have "skin depths" to which incoming light is fractionally transmitted. This depth profile must be folded into the profile which is purely the effect of electron radiation.

Finally, the data analysis which obviously is within the scope of this program is the one which has been performed, and which is evident in the remainder of this document. Conducting the more fundamental investigations just spoken of—which would constitute "damage mechanism" studies—is not to be dismissed, but rather is recommended for the future. Such studies would require samples whose preparation had been carefully controlled and documented, to enable more precise characterization.

2.0 DETAILED REPORT OF PROGRAM RESULTS

This section describes each electron test which was conducted for this program, and the results obtained on each type of coating or surface tested.

2.1 TEST SPECIMENS

The types of specimens tested are described in Table 1. Thirteen types of samples, B through O, had been exposed to 50-keV electrons in the earlier program, NAS5-9650, while the remaining ten types listed in Table 1, R through Z_5, were exposed to electron radiation for the first time in this program. All specimens were held in a clean environment prior to the beginning of tests, and were handled and mounted carefully (on edge) when being installed in sample holders for testing.

Table 1. Coating Types and Radiation Environments in Which Tested

Type Code	Description of Coating (Pigment--binder)	Exposed to		
		20-keV Electrons	80-keV Electrons	50-keV Electrons
B S-13	Zinc oxide—methyl silicone. Approx. 9 mils of S-13 on top of a thin coat of GE S54044 primer	x	x	x
D_3	Alpha-phase aluminum oxide—PS-7 potassium silicate. Approx. 11 mils of paint, applied directly to substrate.	x	x	
E_3	Rutile titanium dioxide/aluminum oxide—PS-7 potassium silicate. Approx. 4 mils of paint, applied as with type D_3.	x	x	x
F_3	Zinc oxide/aluminum oxide—PS-7 potassium silicate. Approx. 5 mils of paint, applied as with type D_3.	x	x	x
G	Vapor-deposited aluminum oxide (11,000 A) on top of 1000 A of aluminum evaporated onto a buffed, chemically cleaned, and glow discharge cleaned, substrate. (Prepared by Dr. Georg Hass of Fort Belvoir.)	x	x	

Table 1. Coating Types and Radiation Environments in Which Tested (Continued)

Type Code	Description of Coating (Pigment--binder)	Exposed to		
		20-keV Electrons	80-keV Electrons	50-keV Electrons
H	Silicon dioxide deposited in vacuum onto a buffed and degreased aluminum substrate.	×	×	
I	Leafing aluminum—mixed Dow Corning 805 and 806A phenylated silicones. Approx. 3 mils total in 3 coats.	×	×	
J	Vapor-deposited aluminum on a lacquered aluminum substrate.	×	×	
K	Buffed and vapor-degreased aluminum substrate.	×	×	
L_1	Anatase titanium dioxide---Dow Corning Q92-0090 methyl silicone, mixed 3 parts paint to 1 part catalyst. Like type A, but approx. 5 mils of paint on top of 2 mils of Cat-a-Lac white primer.	×	×	×
M S-13G	Treated zinc oxide—methyl silicone. Approx. 10 to 12 mils of an early formulation of S-13G, over S54044 primer.	×	×	×
N	2-mil Kapton H film over a thin aluminum coat on an aluminum substrate.	×	×	
O	Rutile titanium dioxide—GE RTV 602 methyl silicone, mixed 2 parts pigment to 1 part vehicle.	×	×	
R	Treated zinc oxide—methyl silicone. Goddard Series 101-7-1.	×	×	×
TA-2	2-mil Teflon aluminized to opacity		×	
TA-5	5-mil Teflon aluminized to opacity		×	
TA-10	10-mil Teflon aluminized to opacity		×	
TS-2	2-mil Teflon silvered to opacity		×	
TS-5	5-mil Teflon silvered to opacity		×	
TS-10	10-mil Teflon silvered to opacity		×	
Z_3	0.15-mil anodized aluminum (Alzak)	×	×	
Z_4	0.22-mil anodized aluminum (Alzak)	×	×	
Z_5	0.34-mil anodized aluminum (Alzak)	×	×	

2.2 20-KEV ELECTRON TEST

The exposure of 17 types of thermal control coatings and surfaces to 20-keV electrons (as listed in Table 1) was the first test to take place as part of this program. The electron fluences or exposure levels at which spectral reflectance measurements were made on each test specimen, and the electron flux or rate used to achieve each exposure level, are shown in Table 2. During each exposure segment the electron flux was controlled to within ±5 percent of the nominal value listed in Table 2. Each exposure time is known to within one percent.

Table 2. 20-keV Test Points and Exposure Rates

Electron Fluences for Measurements	Electron Flux
Pre-irradiation	----------
1.0×10^{13} e/cm^2	1.0×10^{10} e/cm^2-sec
5.0×10^{13}	1.0×10^{10}
1.0×10^{14}	1.0×10^{10}
3.0×10^{14}	1.0×10^{10}
1.0×10^{15}	1.0×10^{10}
1.0×10^{16}	1.4×10^{11}

Substantial reflectance degradation was measured in all diffuse white coatings (paints) tested. In several coating types heavy damage was observed even at the lower electron fluences. Other types resisted reflectance degradation until the highest electron fluences (10^{15} - 10^{16}) were reached, and then degraded severely.

The extent of damage induced by 20-keV electrons in three tested zinc oxide—methyl silicone coatings (types B, M, and R) is shown in Figures 1, 2, and 3. Type B (S-13), for which data is shown in Figure 1, has the largest reflectance drop of all the white paints tested, at the first electron fluence measurement point, 10^{13} electrons/cm^2. At each higher fluence test point, however, additional

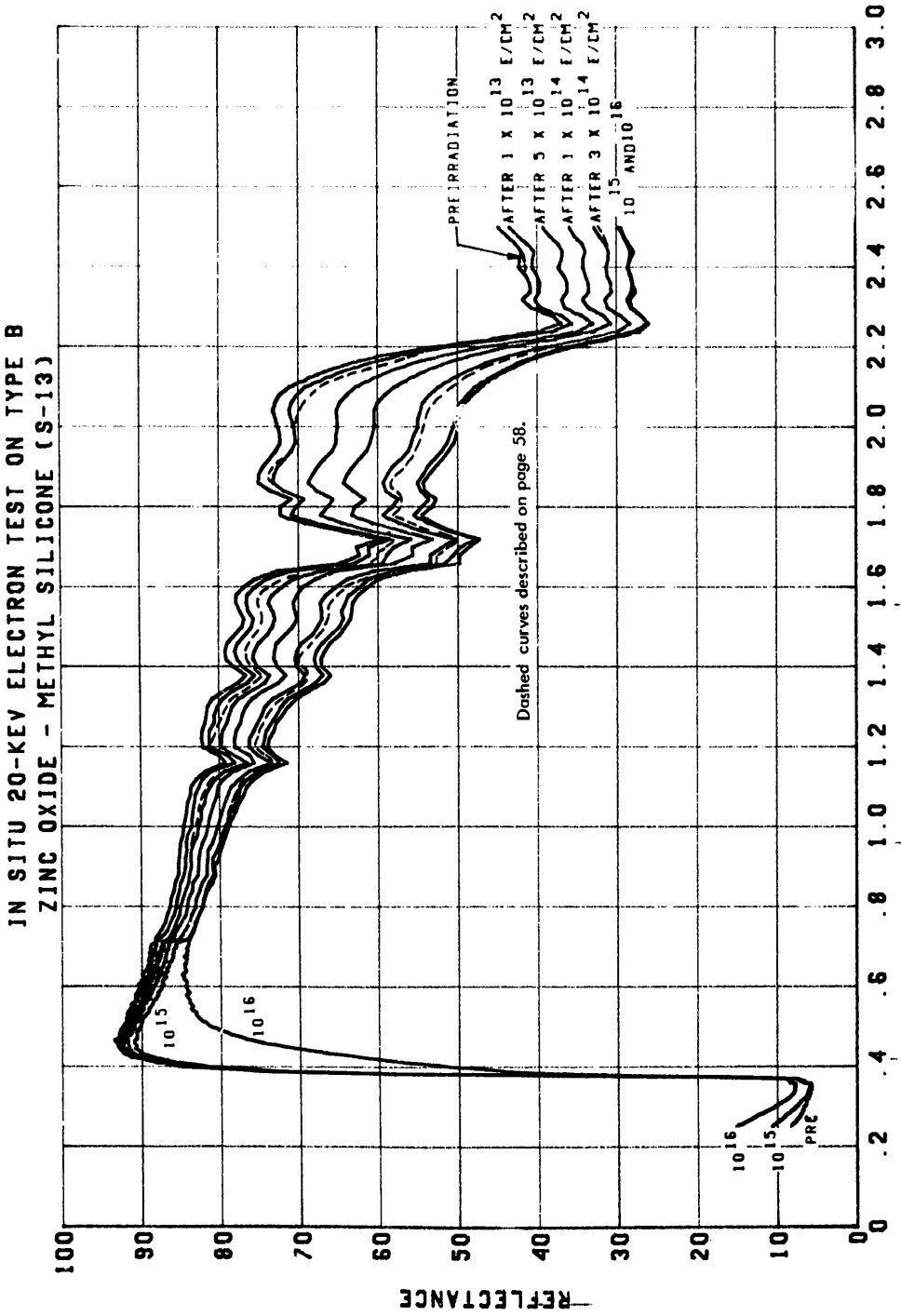

Figure 1. Effects of 20-KeV Electrons on S-13 (Type B)

degradation per "unit fluence" is observed to be less. In other words, by the time the 10^{14} fluence range is reached, there is already a tendency for damage to saturate. At 10^{15} 20-keV electrons/cm^2 nearly all infrared wavelength region damage has occurred in S-13, while in the visible wavelength region reflectance losses are beginning to build up. Figure 1 shows that visible-region damage becomes substantial only at 10^{16} 20-keV electrons/cm^2.

It is appropriate to point out here that the ultraviolet reflectance appearing in plots of several white paints tested may be augmented by the phenomenon of fluorescence. Ultraviolet-region reflectance traces which appear to be showing increases in reflectance after radiation exposure (Figure 1 being an example of this) may be influenced by visible-region fluorescence which the photomultiplier is detecting. References 1 and 2 discuss in detail the reflectance-measuring equipment, geometry and techniques being used in these tests. The principle involved is the same as that used in the majority of similar facilities, in that monochromatic energy illuminates the sample being measured, but the photomultiplier is able to detect from the sample all wavelengths to which it is sensitive. Thus, if incident ultraviolet energy causes the sample to fluoresce, the photomultiplier will see this as reflectance. If radiation exposure causes increased efficiency for fluorescence, the photomultiplier will see this as increased reflectance. Both phenomena—reflectance and fluorescence—represent non-absorbed energy, minimizing any effect on calculations of solar absorptance (α_s) values. Optical techniques exist for discriminating against fluorescence effects, but the negligible effects on α_s calculations does not justify modification considerations, except in the study of damage mechanisms or in non-thermal control applications requiring ultraviolet reflectance stability (Reference 4).

Figure 2 shows how type M (an early formulation of S-13G, silicate-treated zinc oxide—methyl silicone) responds to 20-keV electron exposure. There is little reflectance change at 10^{13} electrons/cm^2, but at higher fluences the amount of degradation picks up dramatically (compare Figure 1). Little tendency towards saturation of infrared damage is evident until a fluence of about 10^{15} 20-keV

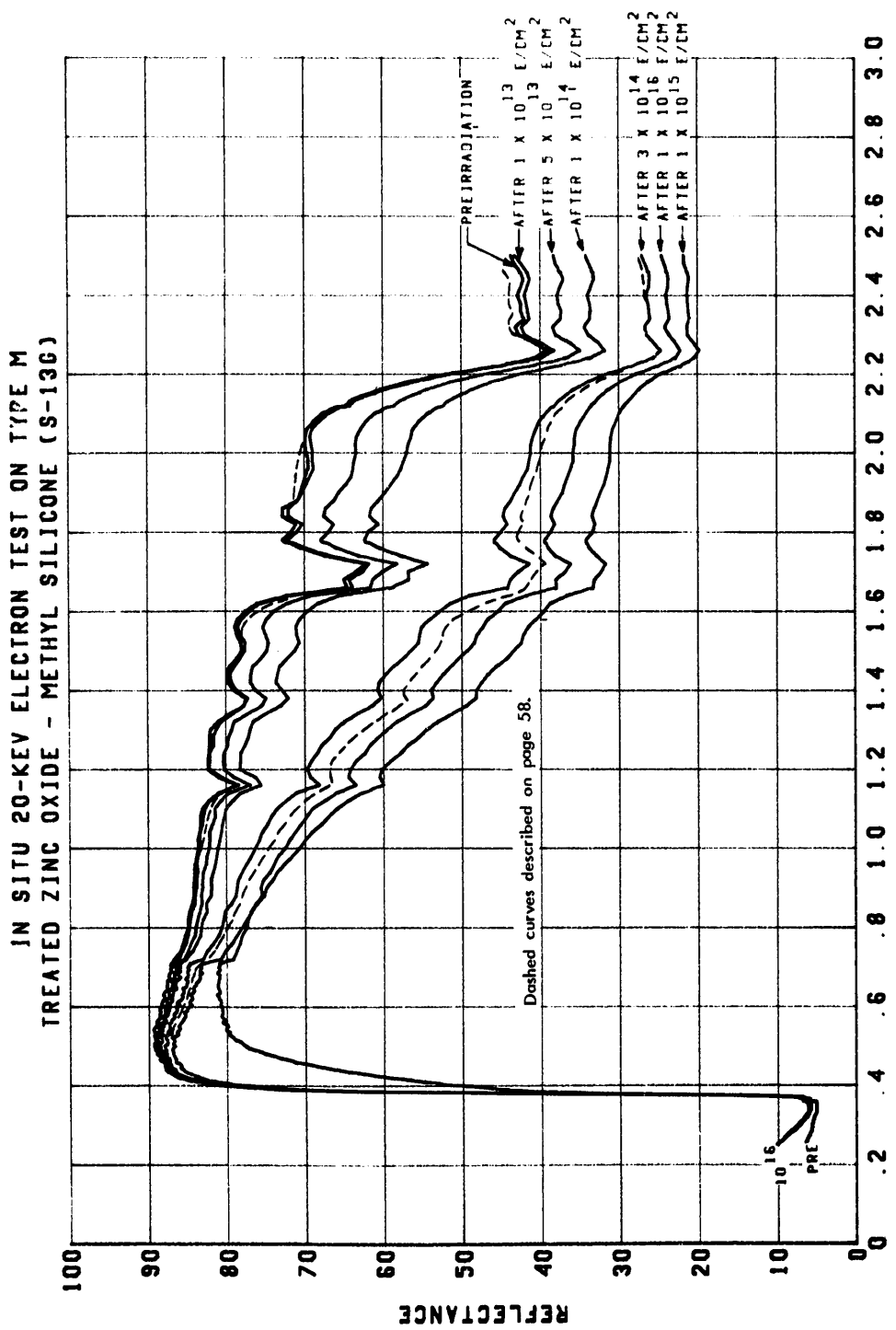

Figure 2. Effects of 20-keV Electrons on S-13G (Type M)

electrons/cm^2 is reached. Beyond this fluence level, degradation in the visible region increases substantially. Because of the in-vacuum reflectance recovery observed during this test (see Sections 1.1 and 2.4) there is a crossover of reflectance curves at about 0.8 micron, and infrared reflectance after 10^{16} electrons/cm^2 is measured to be a higher value than after 10^{15} 20-keV electrons/cm^2.

The latest NASA-Goddard treated zinc oxide—methyl silicone follow-on to S-13, Series 101-7-1 (type R), has successfully been made more resistant to low-energy electron damage, as Figure 3 shows. Infrared reflectance changes are largely confined to the 10^{14} fluence region. Visible-region reflectance degradation has been confined to values less than those incurred by types B and M. Extent of degradation is similar to that found in type B, and considerably less than that observed in type M.

Two types of titanium dioxide—methyl silicone coatings were exposed to 20-keV electrons. Type L_1, with anatase TiO_2 pigment, shows measurable degradation at 10^{13} electrons/cm^2, but even as higher electron fluences are reached degradation is confined to relatively small values. On the other hand, type O, with rutile TiO_2, greatly resists reflectance change, even in the 10^{14} fluence range. However, damage becomes significant at 10^{15} 20-keV electrons/cm^2, and quite heavy at 10^{16}. The contrasting behavior of these two coatings may be observed from Figures 4 and 5.

Two type O specimens were exposed in this 20-keV electron test. It was noticed that one of these specimens acquired a speckled or spotted appearance after a fluence of 10^{15} electrons/cm^2 was reached. The other sample did not acquire such an appearance even after 10^{16} electrons/cm^2. The total number of speckles over the whole sample area was about 25 (an actual count was not made). Each speckle comprised an extremely small area, being perhaps the size of a small pinhole. Each speckle appeared a rather dark gray, suggesting reduction of titanium dioxide to metallic titanium. The speckles all but disappeared when the chamber was backfilled with dry air after the test was completed.

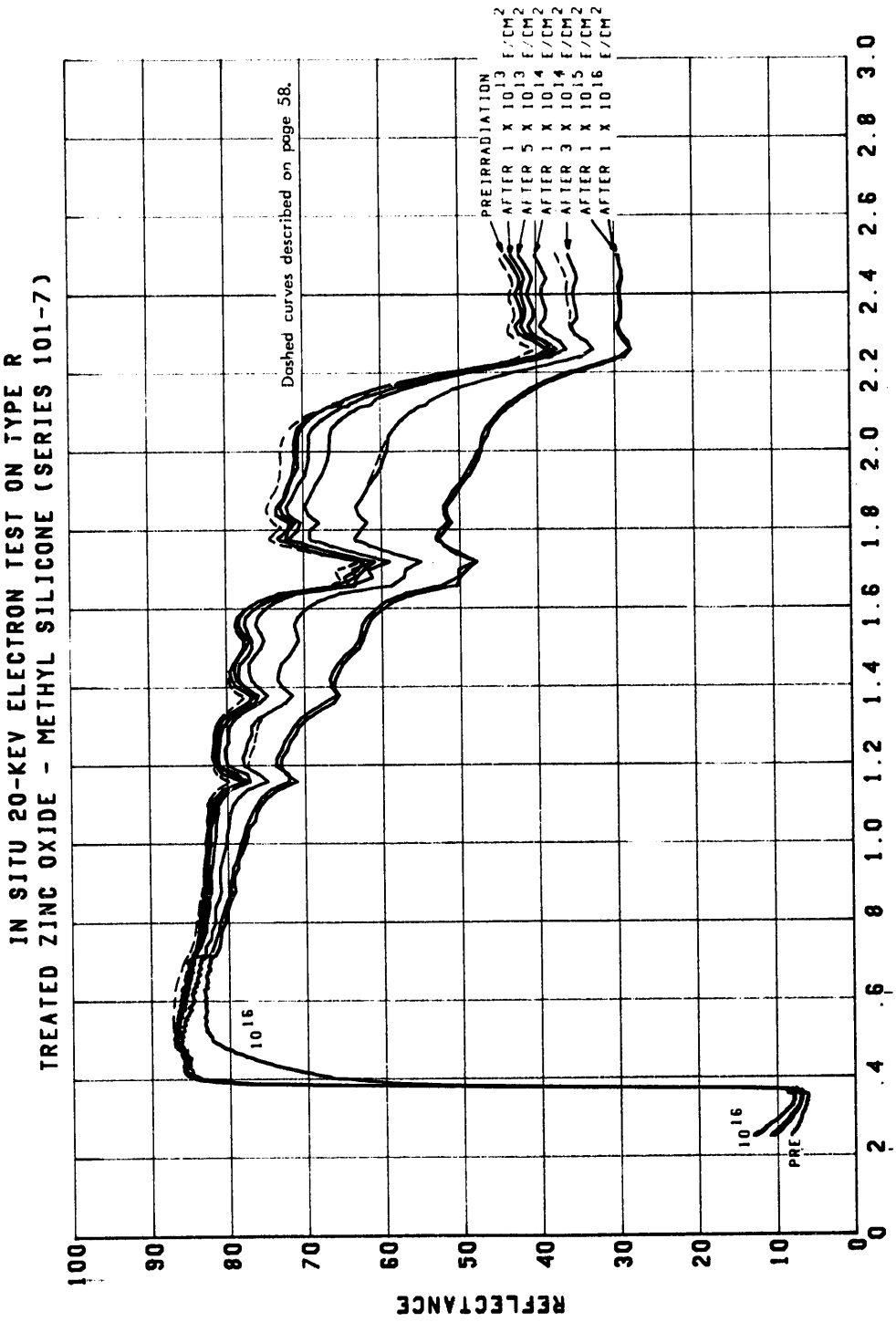

Figure 3. Effects of 20-keV Electrons on Series 101 (Type R)

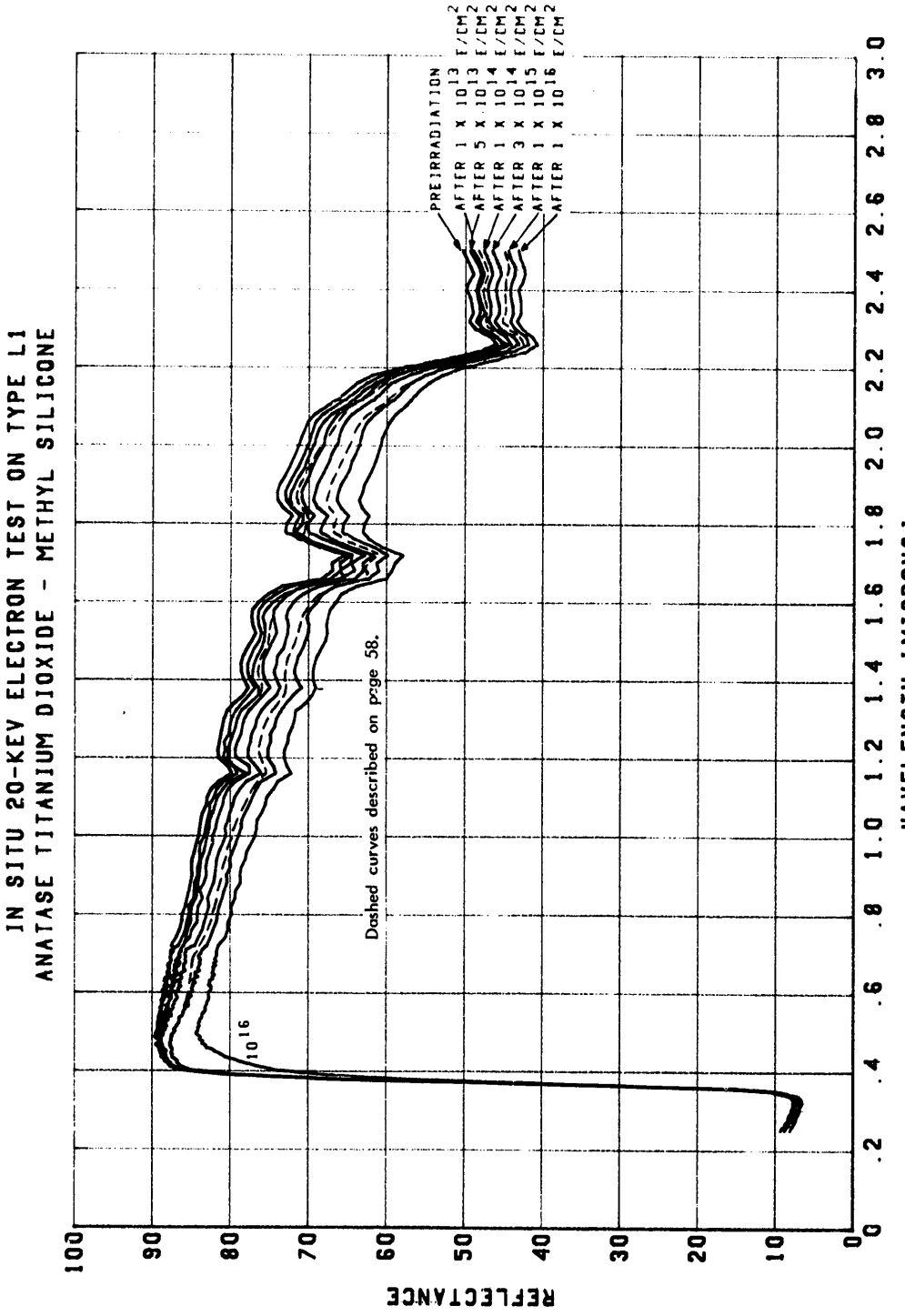

Figure 4. Effects of 20-keV Electrons on Anatase TiO_2—Methyl Silicone (Type L_1)

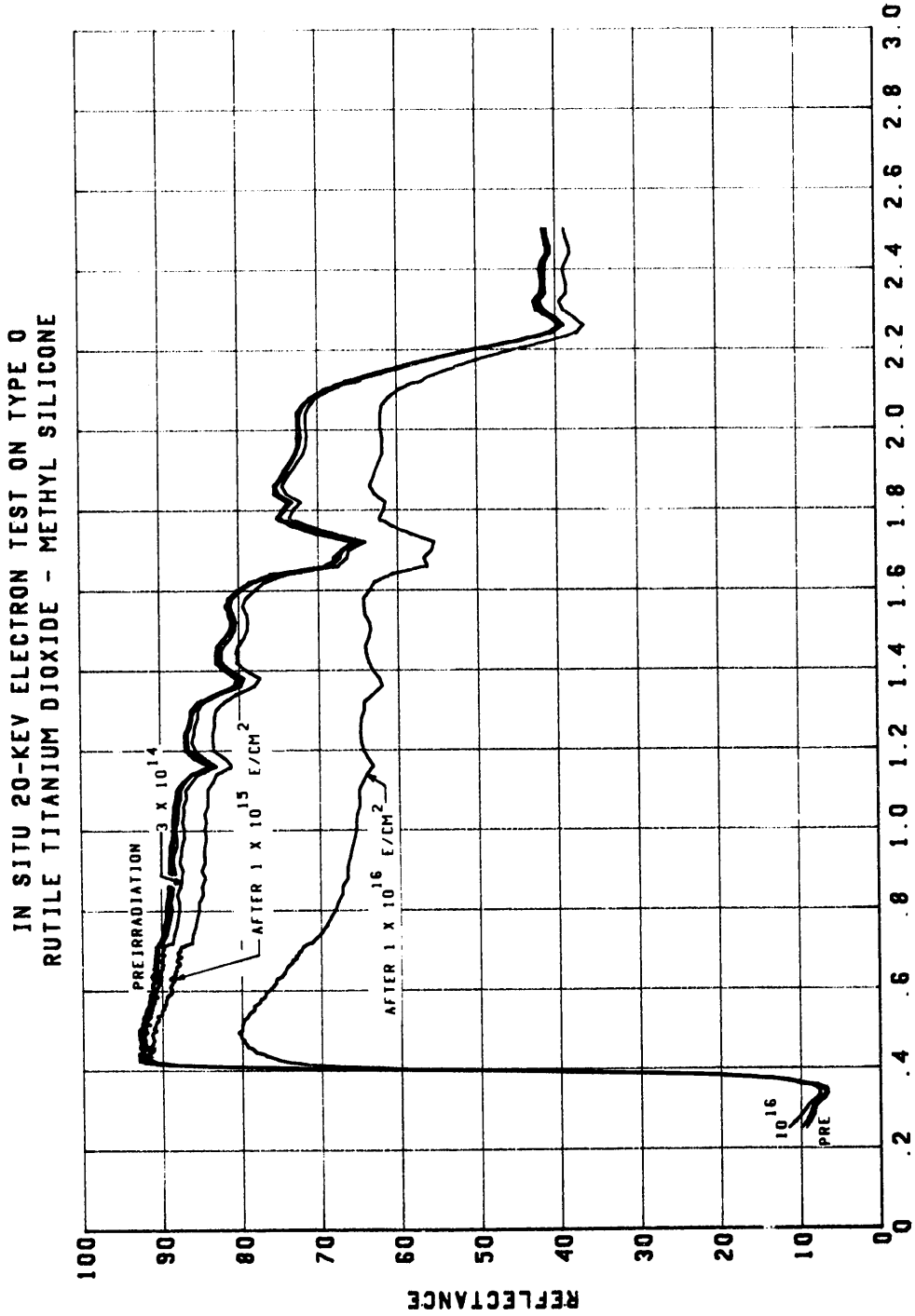

Figure 5. Effects of 20-keV Electrons on Rutile TiO_2—Methyl Silicone (Type O)

Figures 1 through 5 reveal that exposure to 20-keV electrons weakens, but does not eradicate, infrared-region structure (such as the methyl silicone absorption doublet at 1.7 microns), even at fluences as high as 10^{16} electrons/cm^2. Especially for the case of type M, this behavior contrasts markedly with that observed in earlier tests at 50 keV for Contract NAS5-9650. In those tests, and in the higher-energy test results reported in Sections 2.3 and 2.4, infrared absorption structure in type M and other silicone paints was found to disappear for electron fluences in the 10^{14} - 10^{15} ranges.

Results for the three types of coatings with potassium silicate (K_2SiO_3) binders exposed to 20-keV electrons are shown in Figures 6, 7, and 8. In aluminum oxide—potassium silicate (type D_3), significant reflectance changes occur only at wavelengths less than about 0.7 micron—in the so-called silicate band (Figure 6). The combined effect of the presence of other pigment materials in types E_3 and F_3 is apparent when reflectance changes shown in Figures 7 and 8 are compared with changes in Figure 6. The coatings with titanium dioxide (type E_3, Figure 7) and zinc oxide (type F_3, Figure 8) degrade throughout the visible and infrared wavelength regions; the damage is superimposed upon the induced silicate-band absorption. To 10^{14} 20-keV electrons/cm^2, E_3 and F_3 are quite comparable for reflectance; beyond 10^{14}, type F_3 exhibits the better performance.

Three types of Alzak coatings were exposed to 20-keV electrons. In our designations, type Z_3 has a 0.15-mil overcoating, type Z_4 a 0.22-mil overcoating, and type Z_5 a 0.34-mil overcoating. All three types degrade moderately, especially in the ultraviolet wavelength region. Changes in reflectance as fractions of initial or in-vacuum, preirradiation reflectance (that is, $\Delta R/R_i = [R_i - R_f]/R_i$) are shown for the three Alzak types in Figures 9, 10, and 11. Numbers in the upward direction from zero along the vertical axis are reflectance decreases. The test results for the three Alzak types are plotted by hand (as opposed to computer-processing) throughout most of the 0.25- to 2.5-micron wavelength region. The interference structure in the Alzak samples—the adjacent maxima and minima—occur frequently enough with wavelength that the wavelength shifts which occur during exposure,

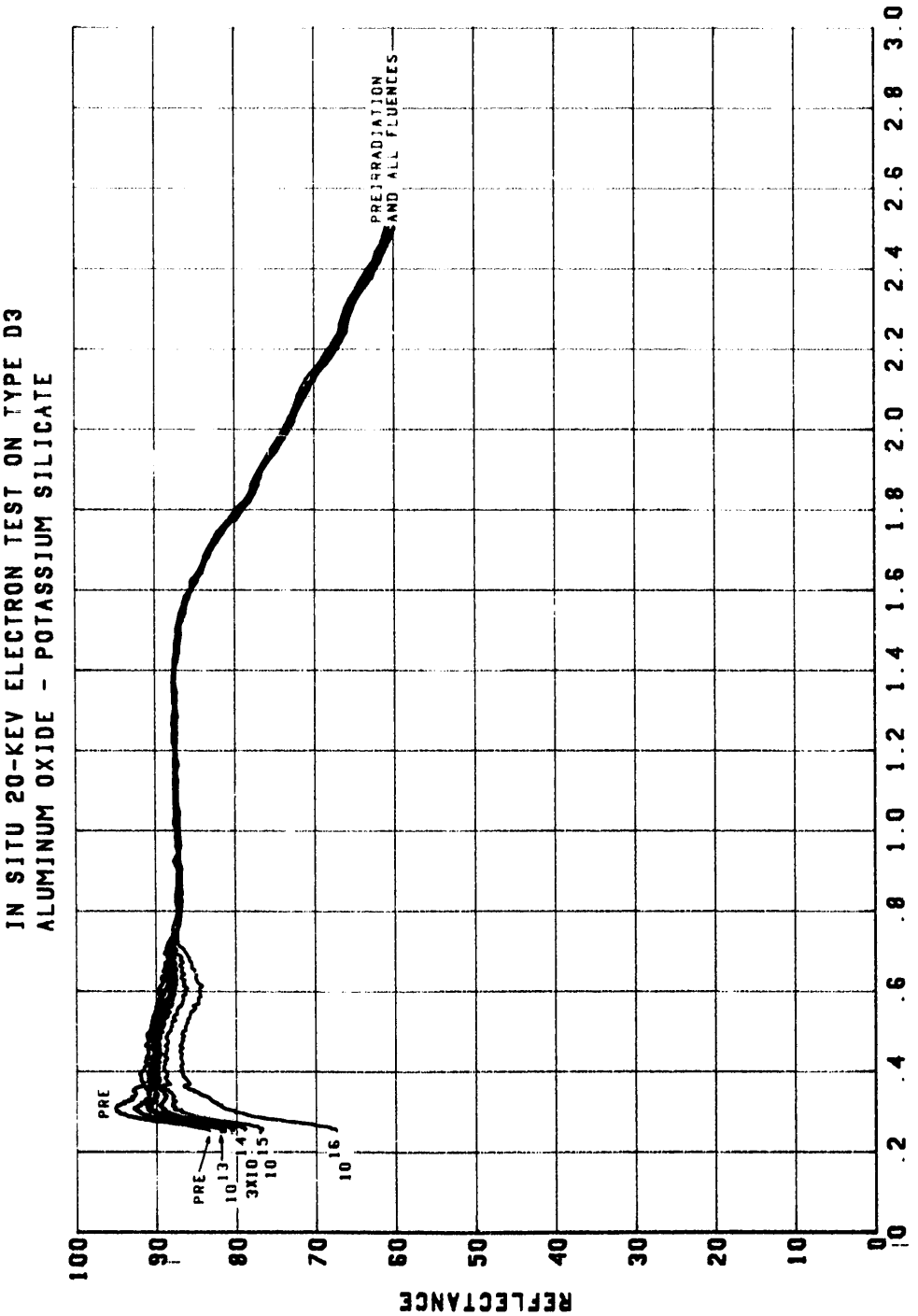

Figure 6. Effects of 20-keV Electrons on Al_2O_3—K_2SiO_3 (Type D_3)

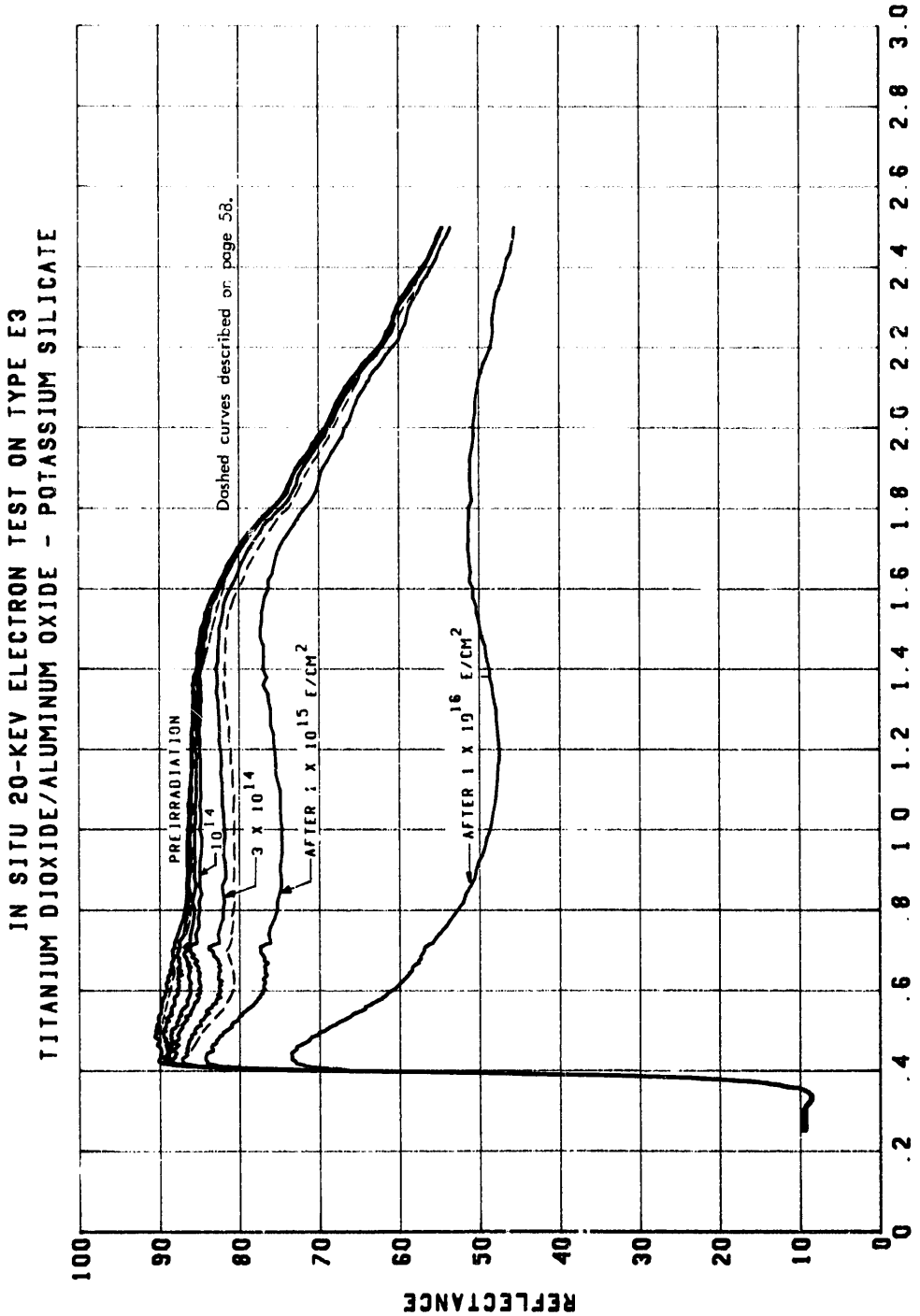

Figure 7. Effects of 20-keV Electrons on TiO_2/Al_2O_3—K_2SiO_3 (Type E_3)

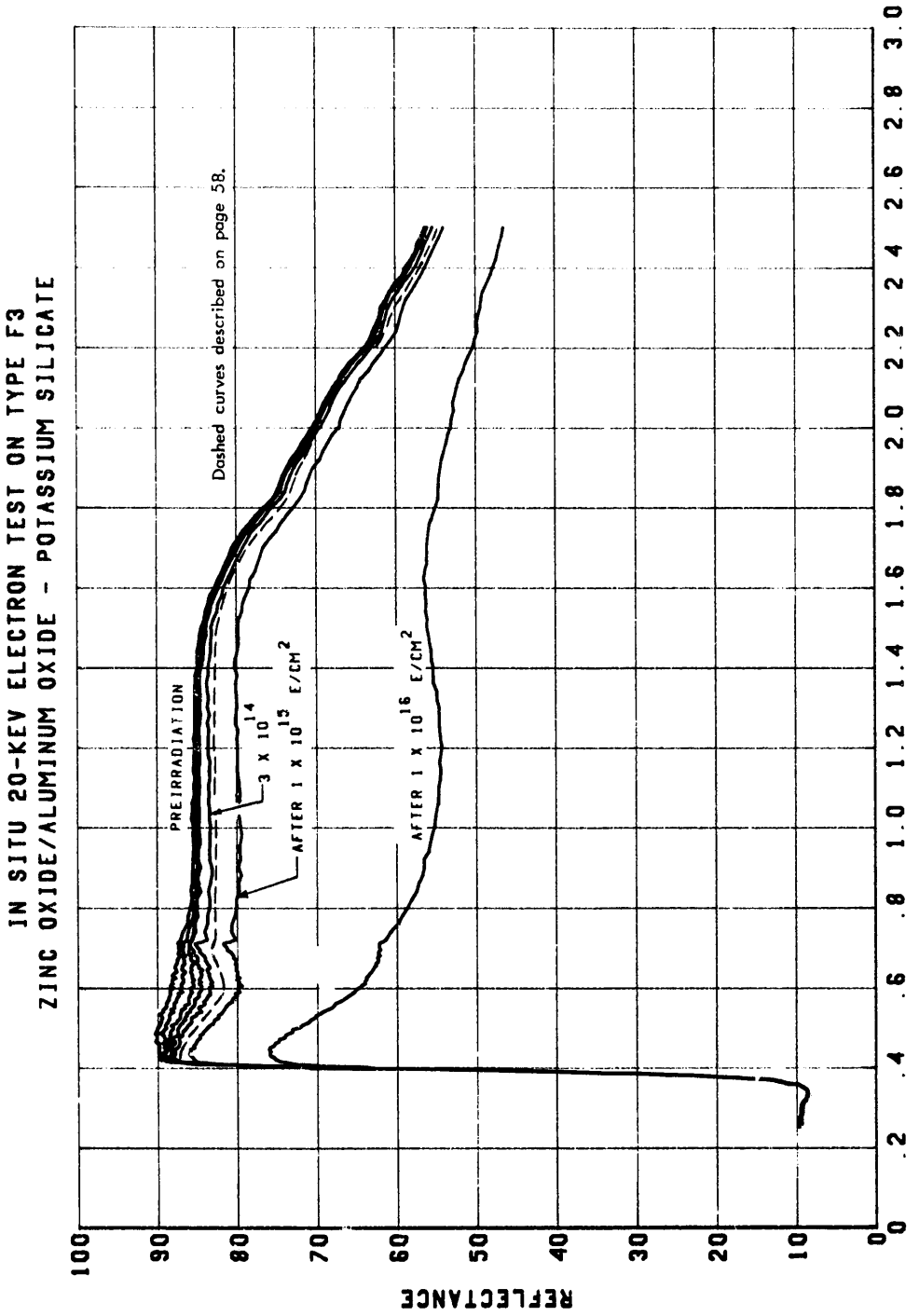

Figure 8. Effects of 20-keV Electrons on ZnO/Al_2O_3—K_2SiO_3 (Type F_3)

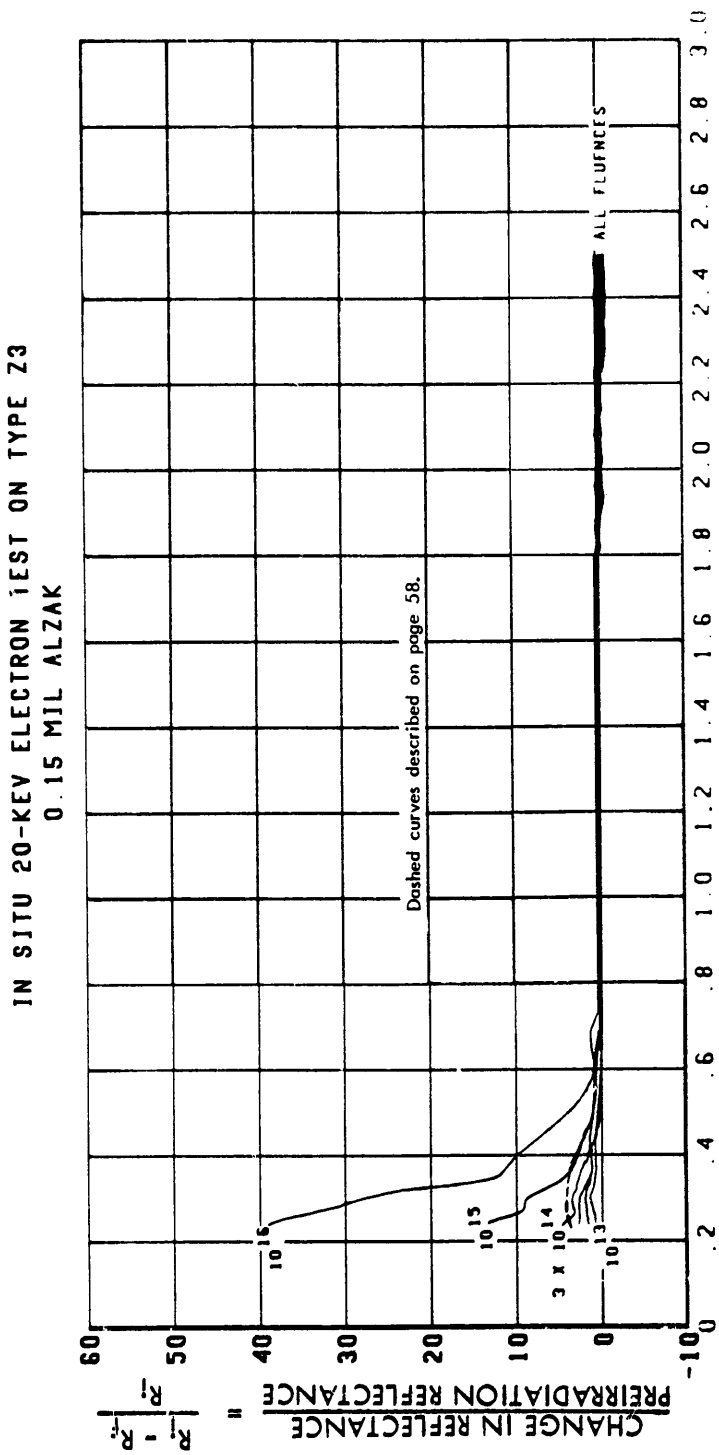

Figure 9. Reflectance Changes in 0.15-mil Alzak (Type Z_3) Due to 20-keV Electron Exposure

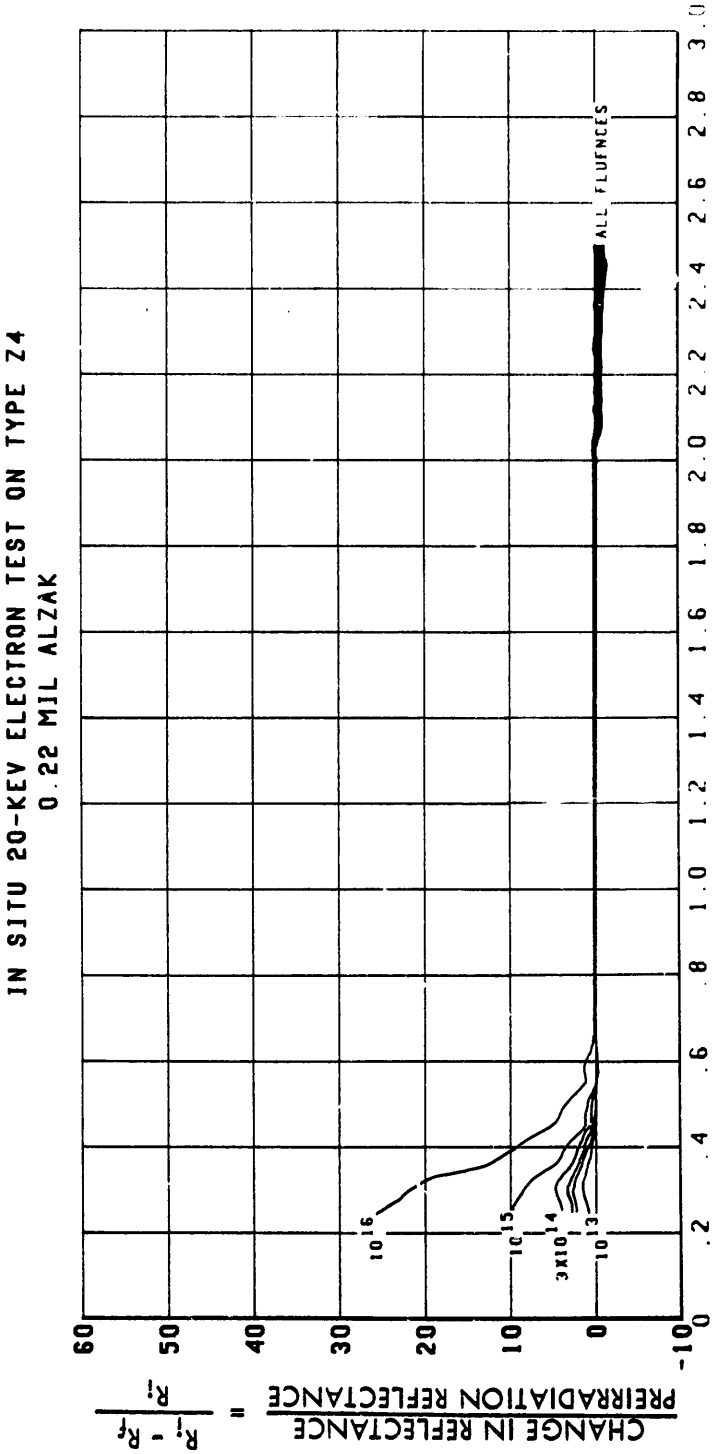

Figure 10. Reflectance Changes in 0.22-mil Alzak (Type Z_4) Due to 20-keV Electron Exposure

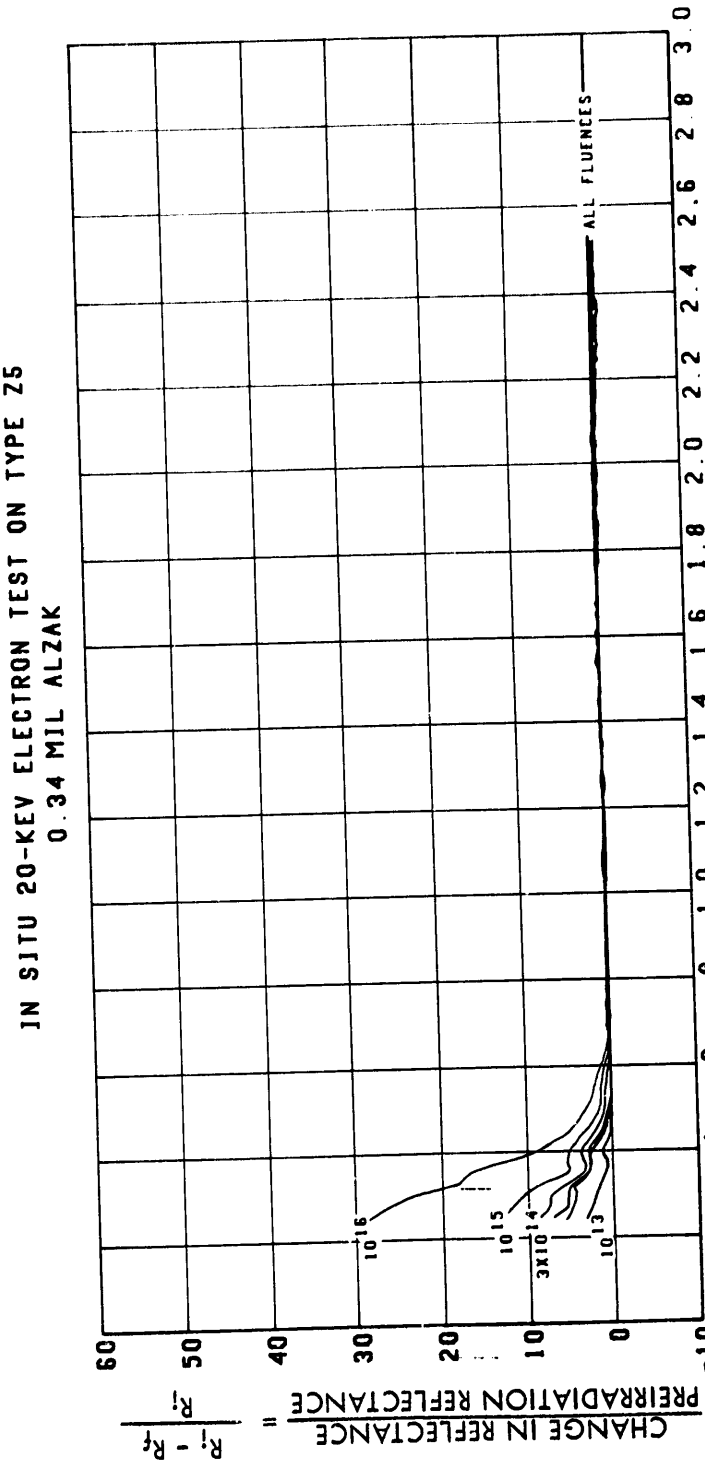

Figure 11. Reflectance Changes in 0.34-mil Alzak (Type Z_5) Due to 20-keV Electron Exposure

would result in the appearance of oscillating increases and decreases in reflectance, were the data processed and plotted via computer without averaging the local maxima and minima. (See also Section 2.6.5).

Values of solar absorptance may readily be determined by multiplying the $\Delta R/R_i$ data by R_i values obtained with a bench-type absolute reflectance instrument.

Similarly, reflectance changes due to exposure of Kapton H film (type N) to 20-keV electrons are indicated in Figure 12. The changes are seen to be minimal at fluences below 10^{15} electrons/cm^2, and negligible beyond one micron wavelength at all fluences. The largest reflectance changes at 10^{16} electrons/cm^2 are in the ultraviolet and at wavelengths just longer than the visible-region absorption band. Reflectance gains in the 0.4-micron region appear "noisy" due to the fact that both ΔR and R_i are small values.

Sample types G, H, I, J, and K strongly resist reflectance changes from 20-keV electrons. Only very small changes in reflectance occur in these types, even at 10^{16} electrons/cm^2. Figures 13 through 17 show the results. For types G and H, which have overcoatings resulting in interference structure, the values of adjacent minima and maxima have been averaged and hand-plotted throughout wavelength regions in which computer processing without averaging would have resulted in plots with oscillating decreases and increases in reflectance with wavelength.

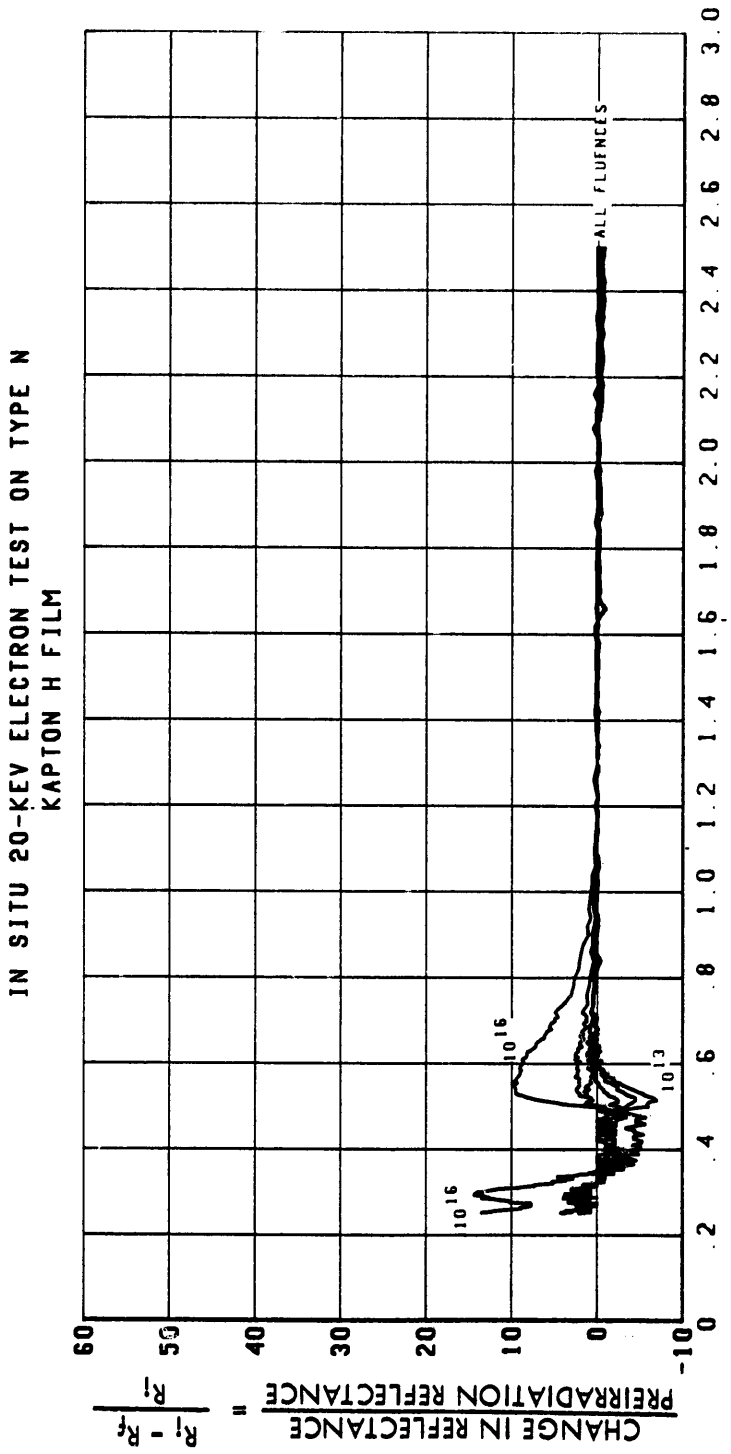

Figure 12. Reflectance Changes in Kapton H Film (Type N) Due to 20-keV Electron Exposure

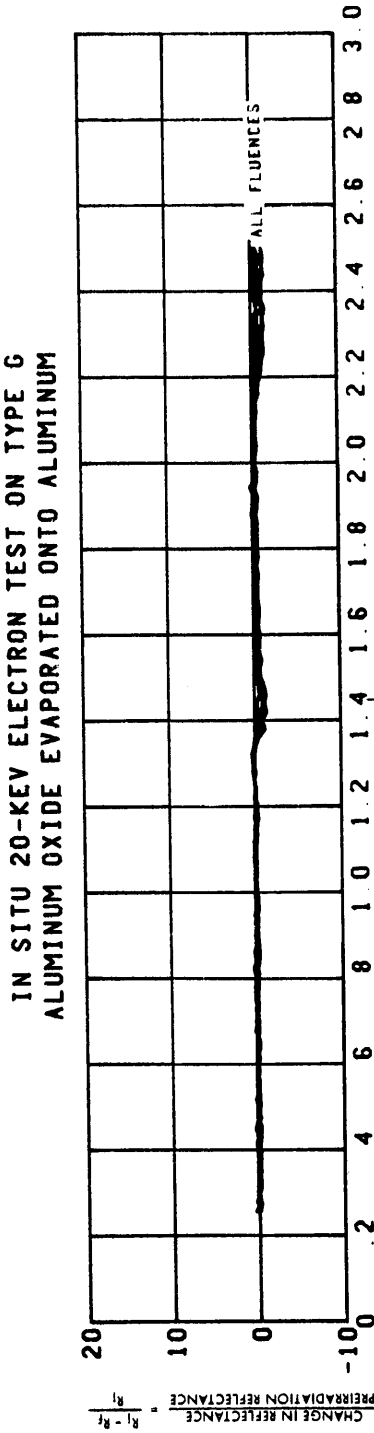

Figure 13. Reflectance Changes in Al_2O_3 Over Al (Type G) Due to 20-keV Electron Exposure

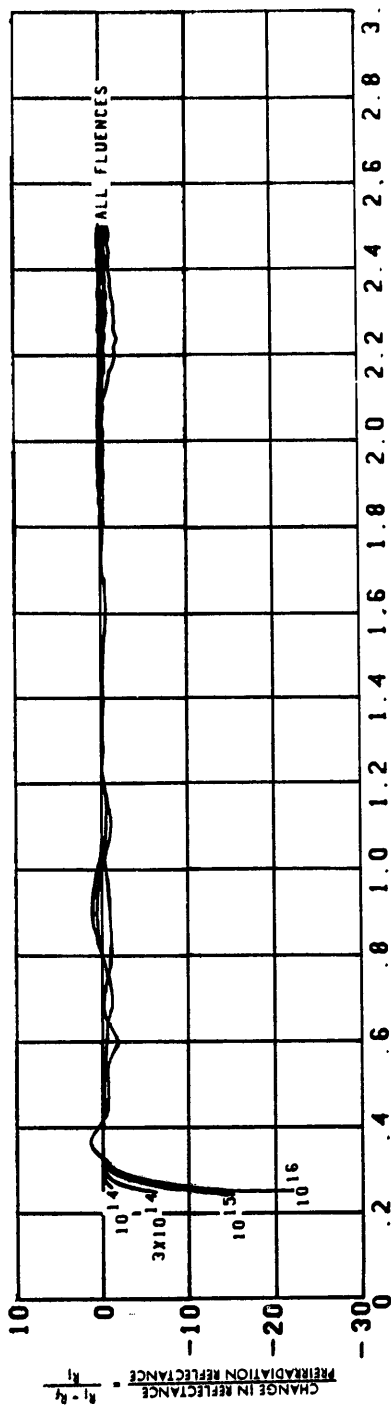

Figure 14. Reflectance Changes in SiO_2 Over Al (Type H) Due to 20-keV Electron Exposure

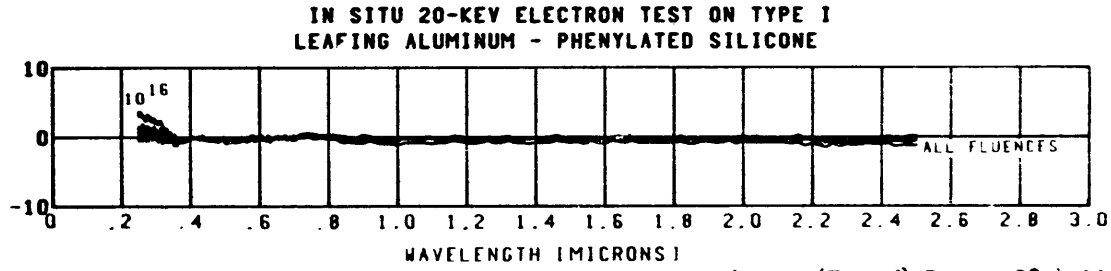

Figure 15. Reflectance Changes in Leafing Aluminum—Silicone (Type I) Due to 20-keV Electron Exposure

$$\frac{\text{CHANGE IN REFLECTANCE}}{\text{PREIRRADIATION REFLECTANCE}} = \frac{R_i - R_f}{R_i}$$

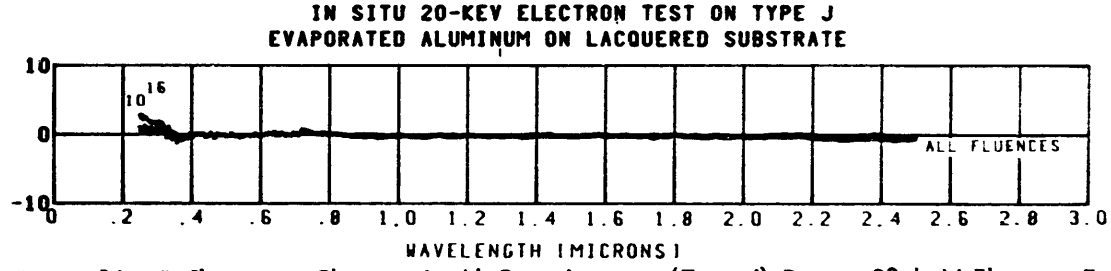

Figure 16. Reflectance Changes in Al Over Lacquer (Type J) Due to 20-keV Electron Exposure

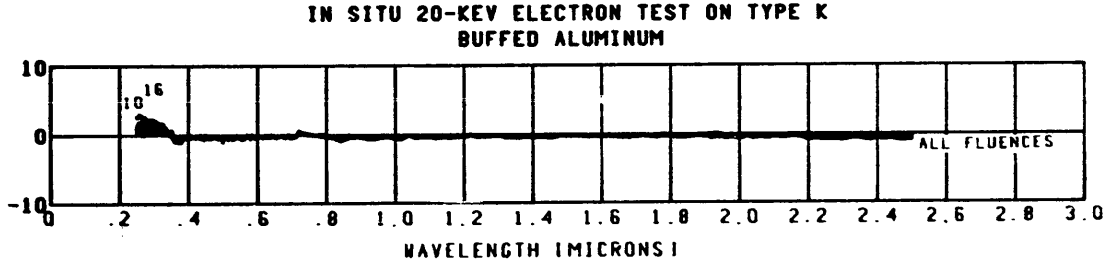

Figure 17. Reflectance Changes in Buffed Al Surface (Type K) Due to 20-keV Electron Exposure

2.3 80-KEV ELECTRON TEST

The test with 80-keV electrons involved exposure of 23 types of surfaces, as indicated in Table 1. Table 3 exhibits the electron fluences or exposure levels at which spectral reflectance measurements were made on each test specimen, and the electron flux or rate used to achieve each exposure level. During each exposure segment the electron flux was controlled to within ±5 percent of the value stated in Table 3. Each exposure time is known to within one percent.

Table 3. 80-keV Test Points and Exposure Rates

Electron Fluences for measurements	Electron Flux
Pre-irradiation	- - - -
1.0×10^{13} e/cm^2	1.0×10^{10} e/cm^2-sec
5.0×10^{13}	1.1×10^{10}
1.0×10^{14}	1.1×10^{10}
3.0×10^{14}	2.0×10^{10}
1.0×10^{15}	3.9×10^{10}
1×10^{16}	5×10^{11}

The effects of 80-keV electrons in zinc oxide—methyl silicone coatings are seen in Figures 18, 19, and 20. Figure 18 shows S-13 (type B) reflectance before exposure and at six electron fluences to and including 10^{16} 80-keV electrons/cm^2. S-13 in this test, as well as when exposed to 20-keV electrons, had the most degradation of all coatings at the first electron fluence measurement point, 10^{13} electrons/cm^2. Each "unit" of each successive exposure is seen from Figure 18 to have less and less degrading effect, and saturation is approached, beginning in the 10^{14} fluence range. Degradation in the visible wavelength region becomes substantial only after 10^{15} electrons/cm^2. Structure in the infrared absorption bands is nearly lost after 10^{16} electrons/cm^2.

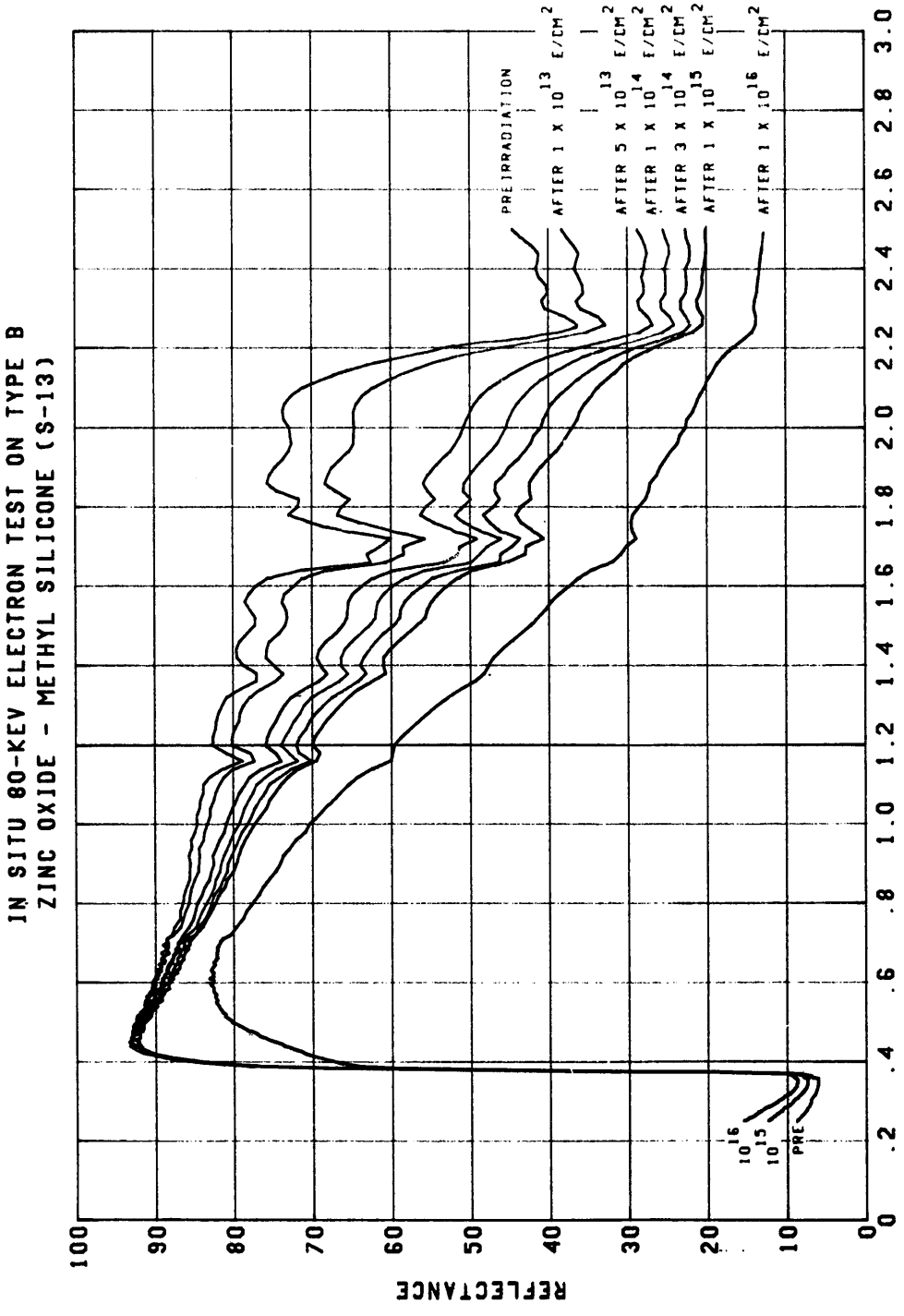

Figure 18. Effects of 80-keV Electrons on S-13 (Type B)

By contrast, 80-keV electron degradation in S-13G (type M), which has different charge acceptance characteristics than S-13, proceeds in a different manner. Compared to S-13 (Figure 18), S-13G (Figure 19) shows less damage at 10^{13} electrons/cm^2, and more degradation at higher electron fluences. Even at 10^{14} infrared structure is considerably weakened, and is masked after a fluence of 3×10^{14} 80-keV electrons/cm^2. Degradation is also substantial in the visible wavelength region at this fluence. Visible region damage may be characterized as severe at 10^{16} electrons/cm^2. Infrared damage is virtually saturated at 10^{16}.

Figure 20 shows the degradation which occurs in type R, treated zinc oxide—methyl silicone (Goddard Series 101-7-1 follow-on to S-13) after exposure to 80-keV electrons. Upon comparison of Figure 20 with Figure 19, type R is seen to be somewhat harder than type M against electron damage. Before exposure, the reflectance of type R in the 0.4- to 0.5-micron portion of the visible wavelengths is depressed some 2-3 percent below that of the 0.5- to 0.6-micron portion. A discernible improvement in the reflectance of the type R test specimens takes place in the 0.4- to 0.5-micron region at the lower 80-keV fluences. Even at a fluence of 10^{15} electrons/cm^2 the reflectance in this wavelength region is higher than before exposure. Visible-region reflectance at 10^{16} 80-keV electrons/cm^2 is degraded to an extent somewhat worse than in S-13, but not as much as in S-13G.

In the infrared wavelength region the buildup of damage in type R occurs at a slower rate than in S-13G. At 3×10^{14} 80-keV electrons/cm^2 some infrared absorption structure remains (in contrast with the situation for S-13G). A fluence of 10^{15} produces significantly more degradation, but saturation then occurs rapidly, with 10^{16} electrons/cm^2 causing little additional infrared damage.

The two titanium dioxide—methyl silicone coatings tested exhibit decidedly different behavior under 80-keV electron exposure. Degradation in type L_1 (with anatase titanium dioxide pigment) builds up in a very orderly progression, as Figure 21 shows. Type O (with rutile titanium dioxide pigment) resists degradation from electrons until the 10^{14} fluence range is reached. Then, as Figure 22 shows, type O damages so rapidly that at 10^{16} 80-keV electrons/cm^2, it has a significantly

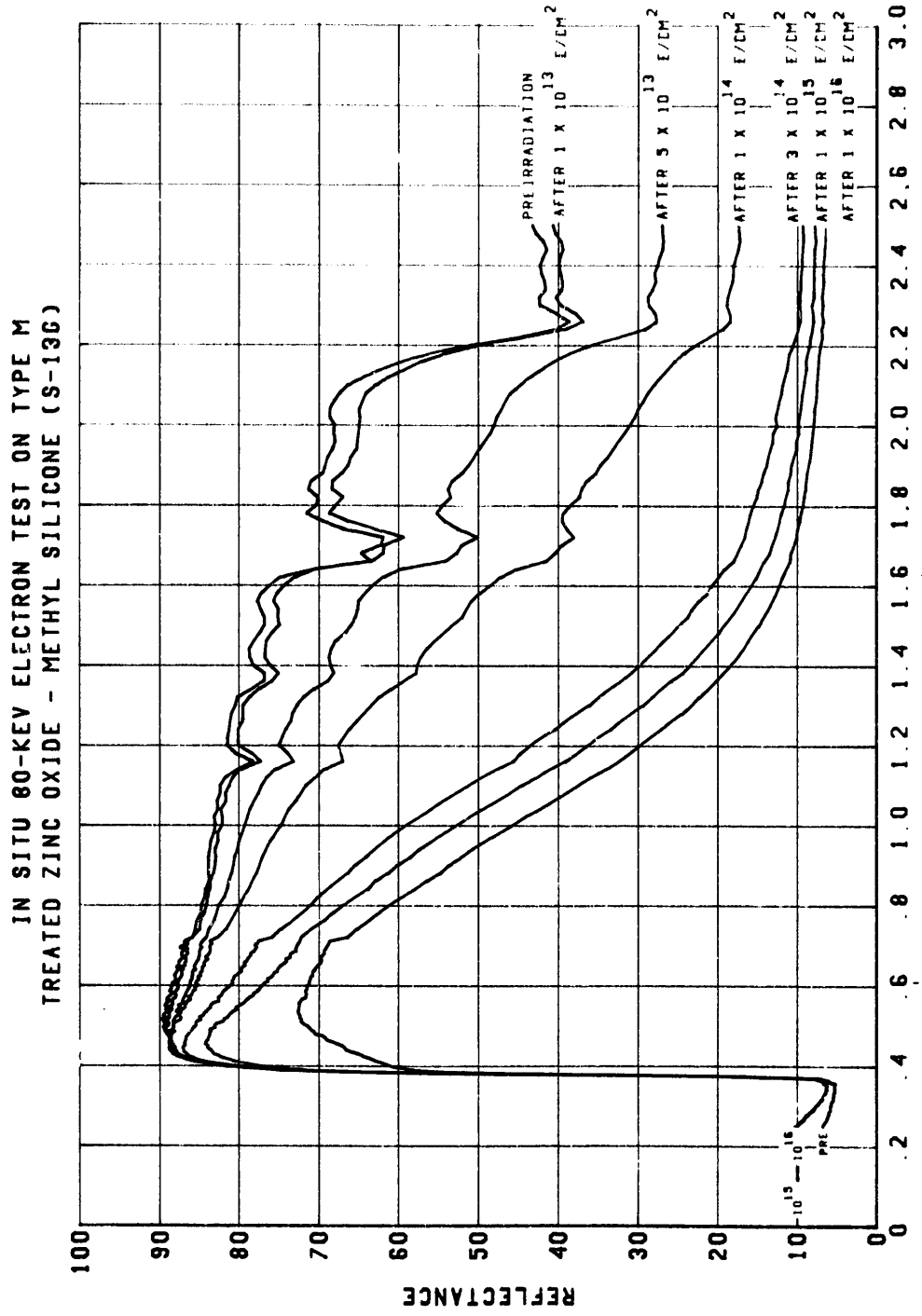

Figure 19. Effects of 80-keV Electrons on S-13G (Type M)

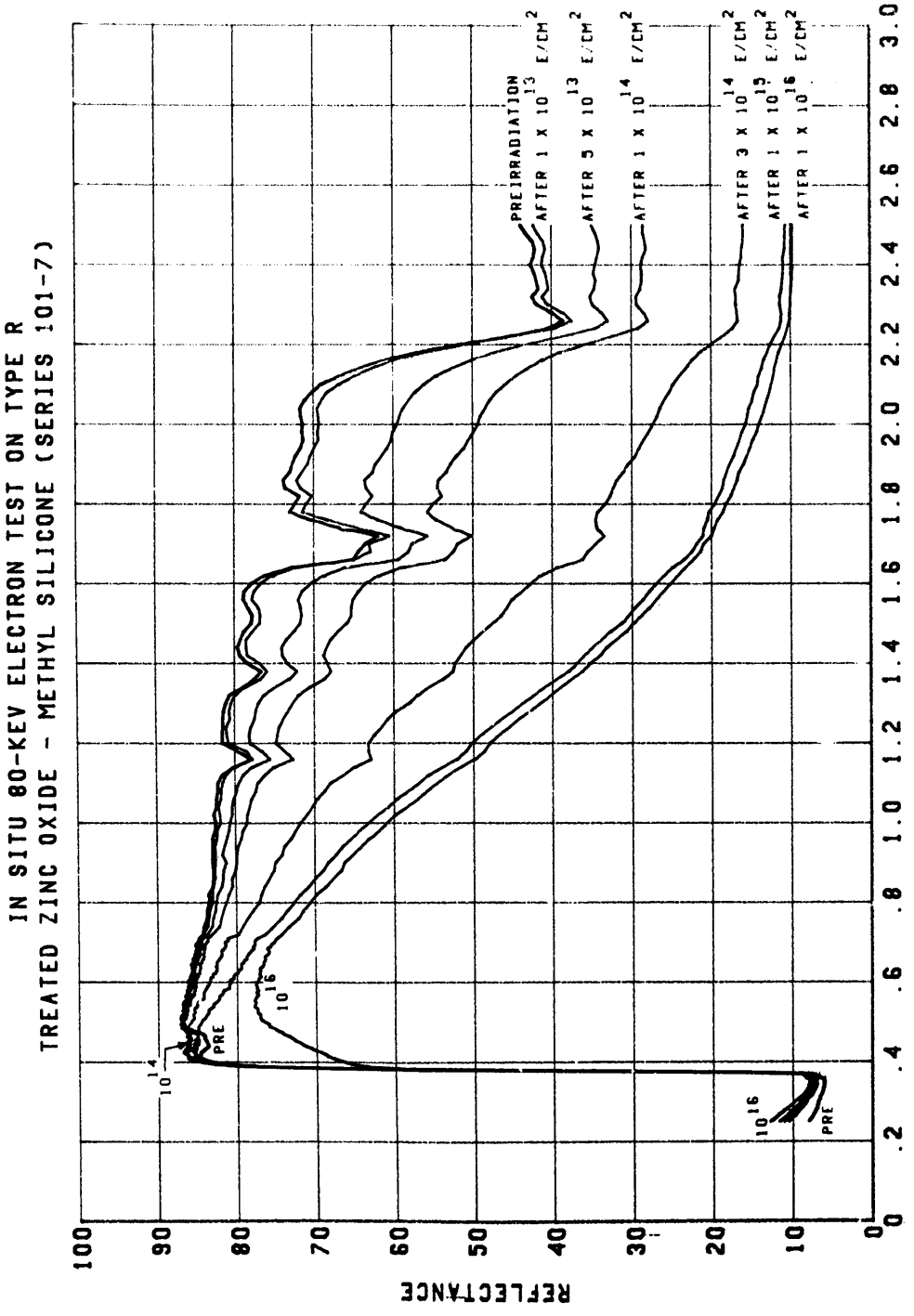

Figure 20. Effects of 80-keV Electrons on Series 101 (Type R)

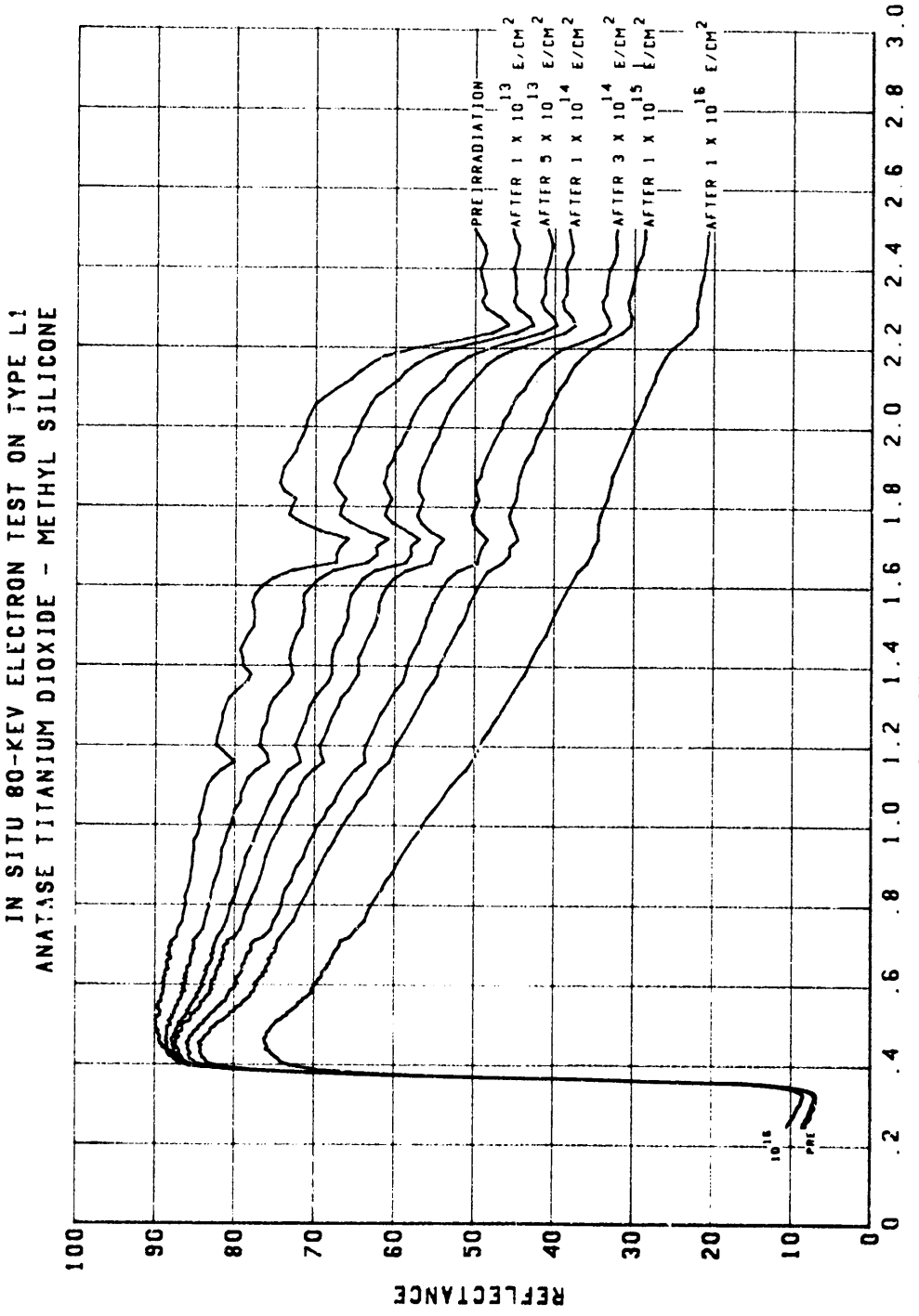

Figure 21. Effects of 80-keV Electrons on Anatase TiO_2—Methyl Silicone (Type L_1)

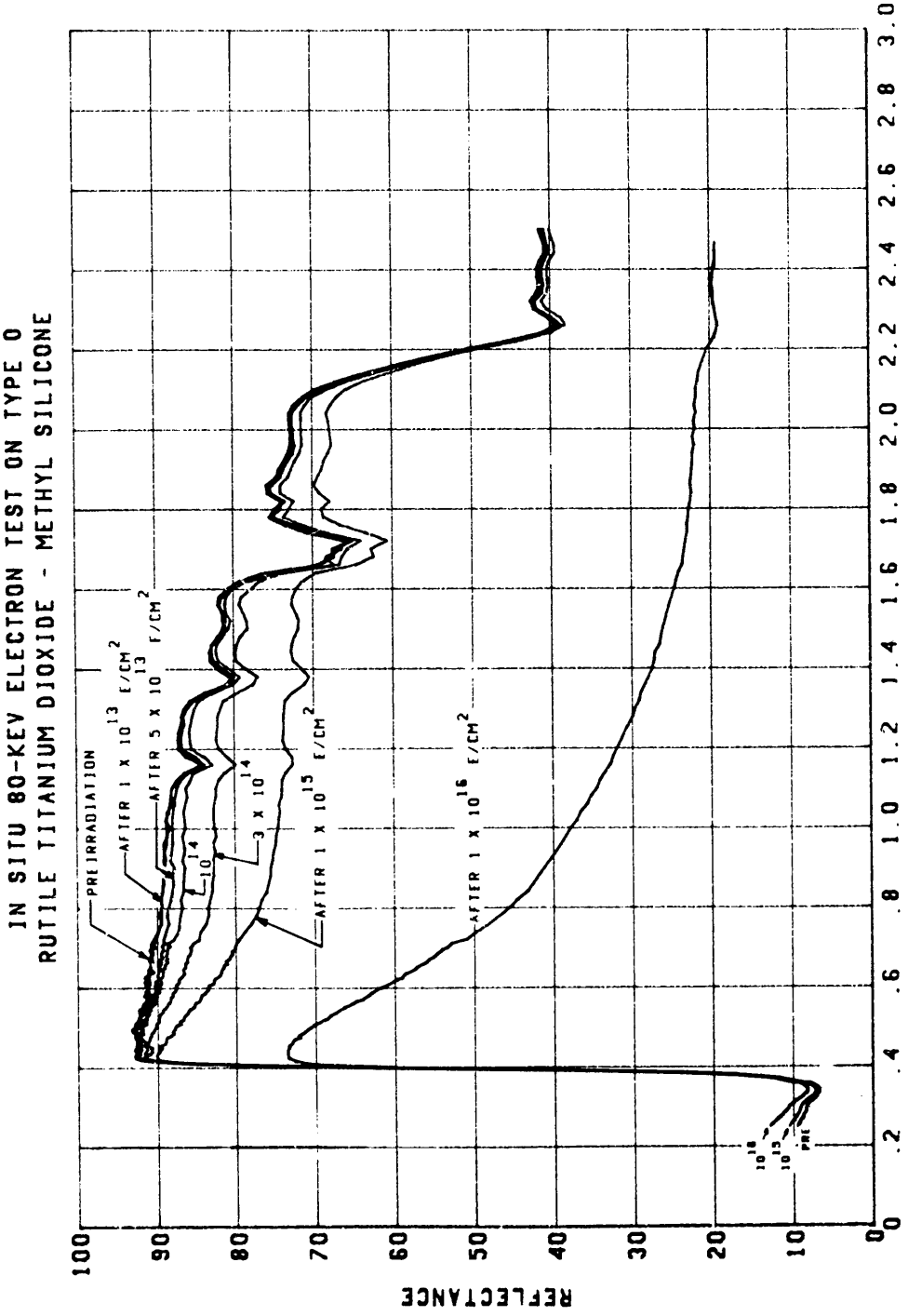

Figure 22. Effects of 80-keV Electrons on Rutile TiO_2—Methyl Silicone (Type O)

higher solar absorptance than type L_1 has at 10^{16}. There is little infrared structure in either type following exposure to 10^{16} 80-keV electrons/cm^2.

As in the 20-keV electron test, a speckled or spotted appearance was observed in type O at the higher fluences (10^{15} and 10^{16} electrons/cm^2). In the 80-keV test, the spots were discernible in both test specimens, though they appeared more subdued in one than in the other. The size, number, and density of spots was similar to that observed during the 20-keV test. After the 80-keV test, these spots all but disappeared upon re-exposure of the test samples to dry air.

Results on three types of coatings with potassium silicate binder (D_3, E_3, and F_3) are shown in Figures 23, 24, and 25. Type D_3, aluminum oxide—potassium silicate, shows the least 80-keV electron damage of the three types. Decrease in reflectance is confined to the so-called "silicate band" at wavelengths shorter than about 0.7 micron.

Coating types E_3 and F_3 (Figures 24 and 25, respectively) exhibit much greater degradation. The presence of other pigment constituents (see Table 1 and Figures 24 and 25) results in a superposition of longer wavelength damage upon the "silicate band" degradation. Type F_3 is able to maintain reasonably high reflectance until a fluence of about 10^{15} 80-keV electrons/cm^2 is reached; then degradation occurs rapidly. Type E_3 possesses reasonably high reflectance only until 3×10^{14} fluence is reached. At higher 80-keV electron fluences damage builds to severe amounts. Of the two, type E_3 has higher solar absorptance above 10^{14} 80-keV electrons/cm^2.

Alzak types Z_3 (0.15-mil), Z_4 (0.22-mil), and Z_5 (0.34-mil) were included in the 80-keV electron test. Reflectance degradation is confined to the smallest values in 0.22-mil Alzak (type Z_4). Test results are shown in Figures 26, 27, and 28. As with the 20-keV Alzak results (Figures 9, 10, and 11), data treatment by hand has been done for those wavelengths where interference effects would distort the meaning of the $\Delta R/R_i$ data.

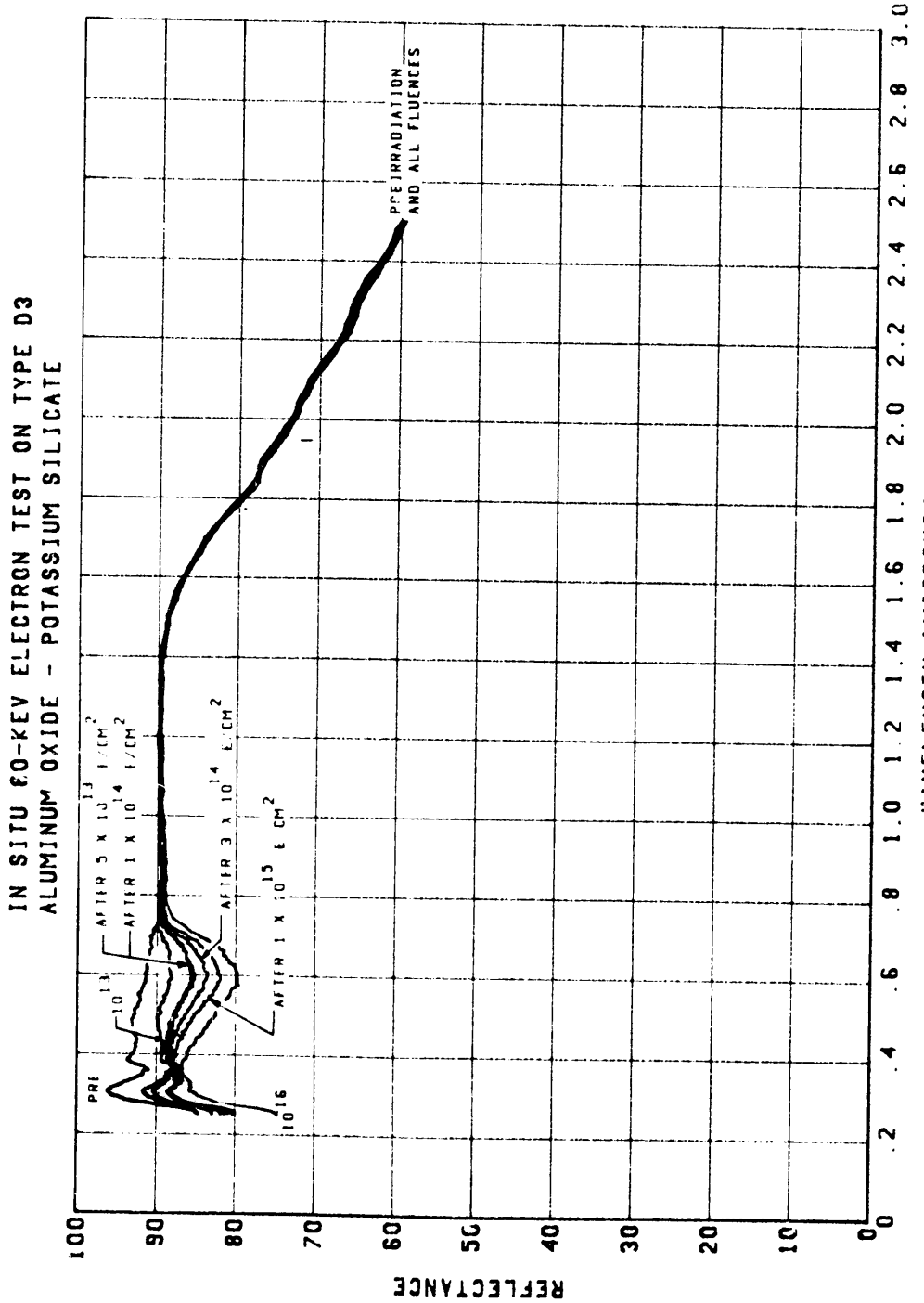

Figure 23. Effects of 80-keV Electrons on Al_2O_3—K_2SiO_3 (Type D_3)

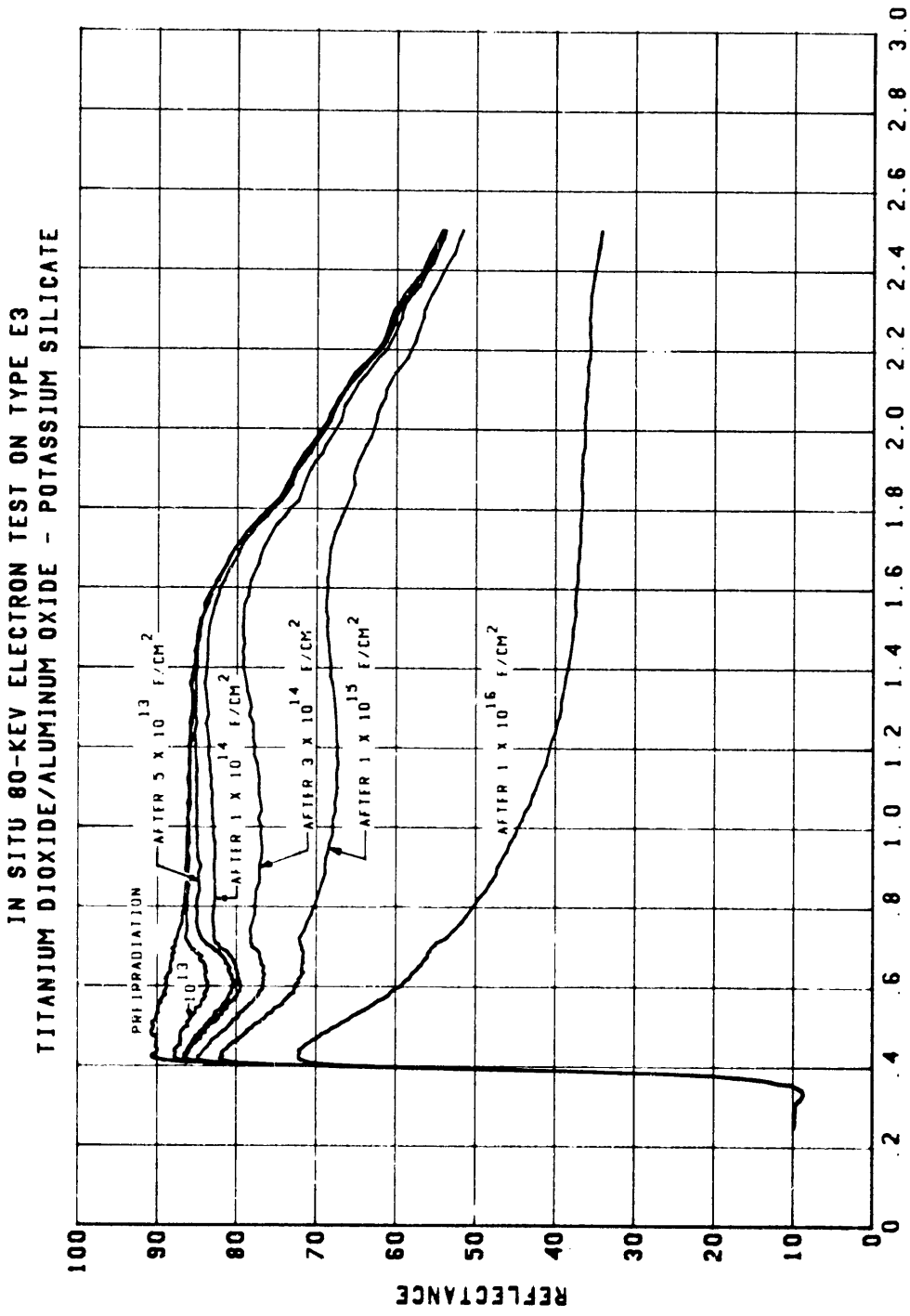

Figure 24. Effects of 80-keV Electrons on $TiO_2/Al_2O_3—K_2SiO_3$ (Type E_3)

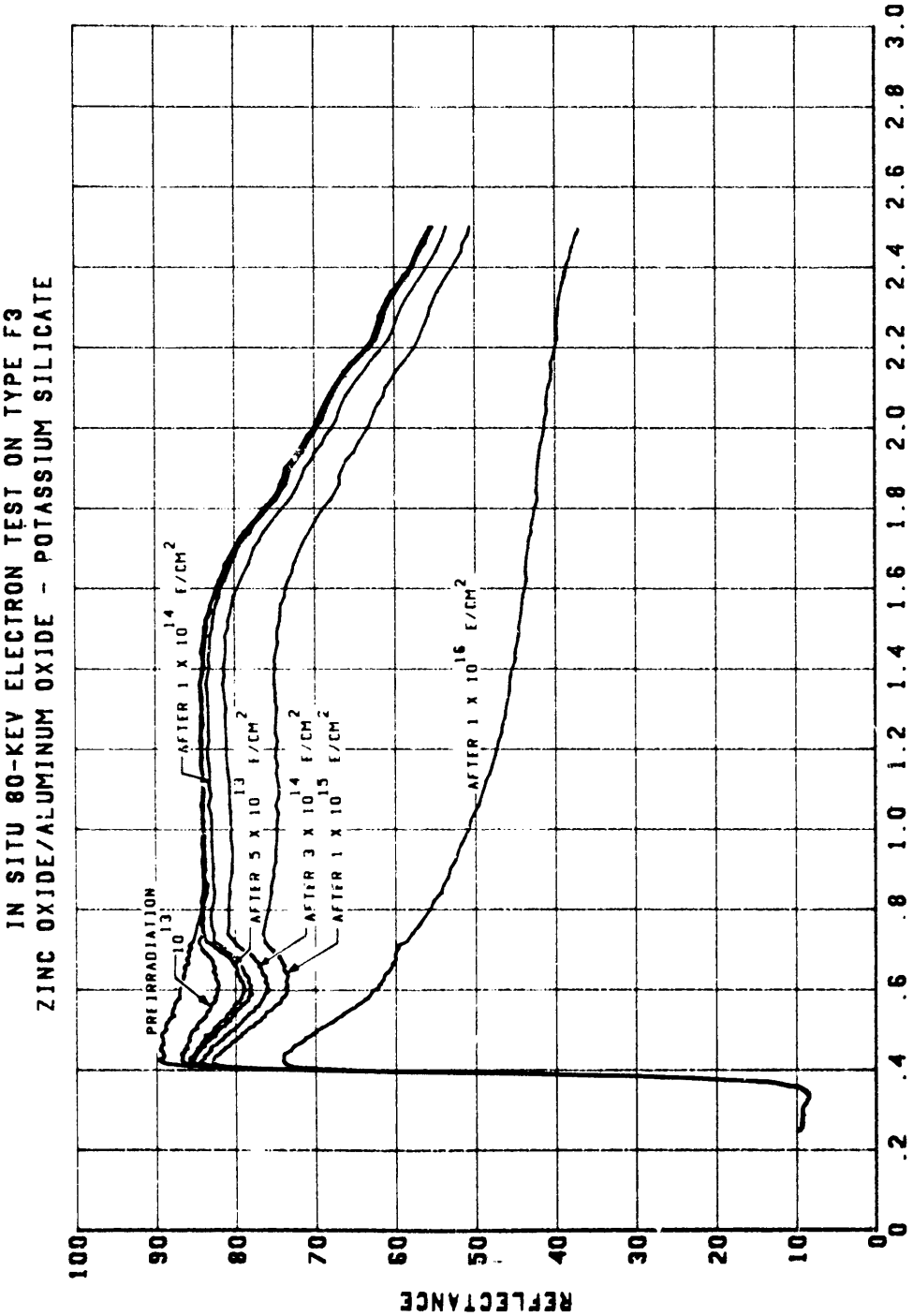

Figure 25. Effects of 80-keV Electrons on $ZnO/Al_2O_3—K_2SiO_3$ (Type F_3)

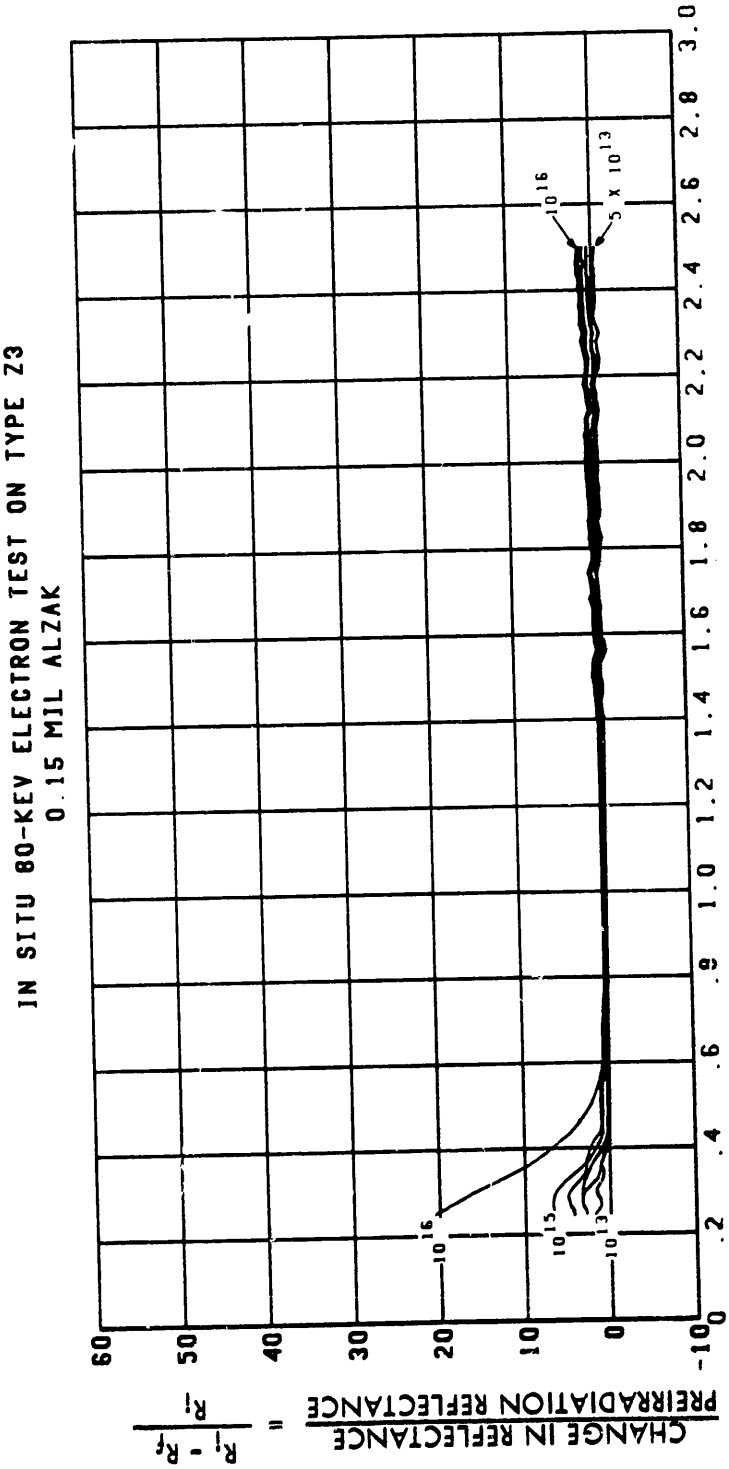

Figure 26. Reflectance Changes in 0.15-mil Alzak (Type Z_3) Due to 80-keV Electron Exposure

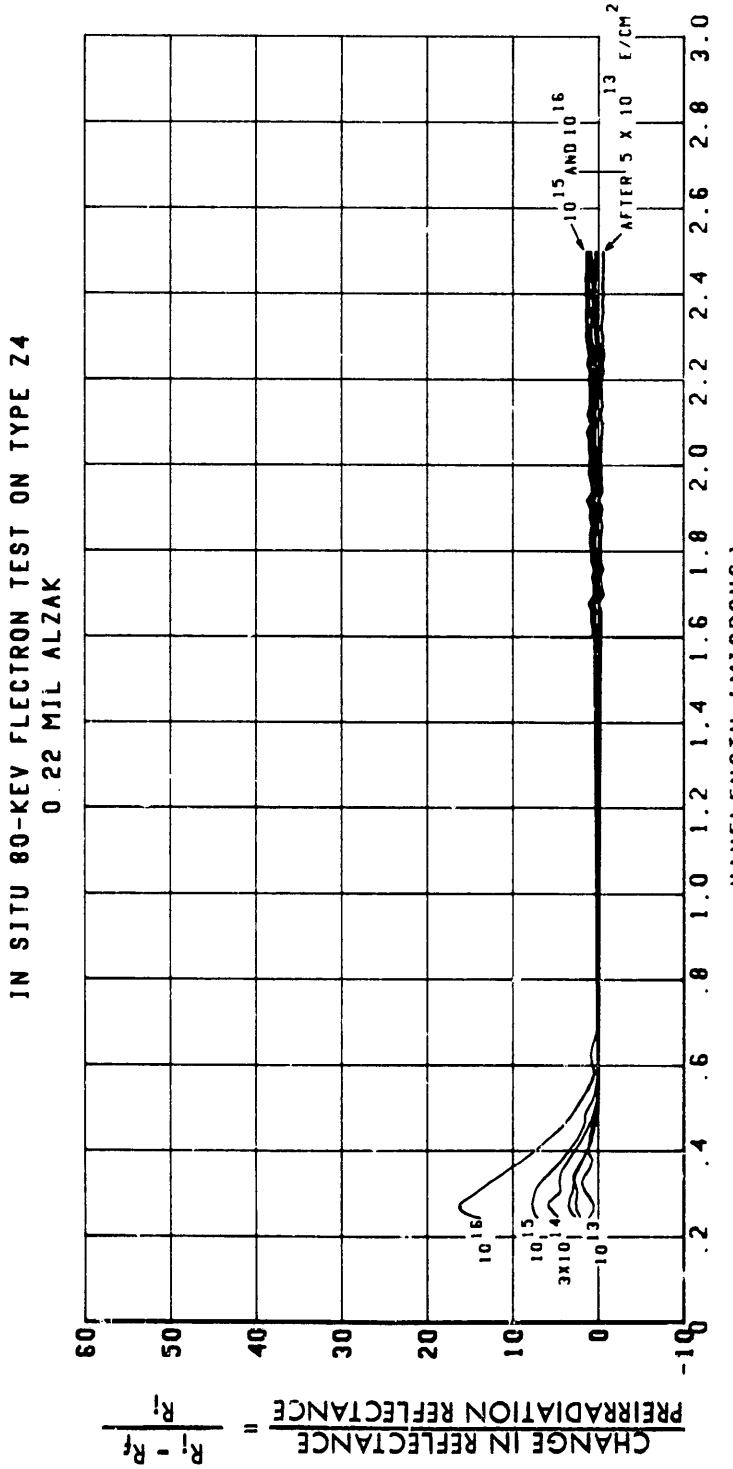

Figure 27. Reflectance Changes in 0.22-mil Alzak (Type Z_4) Due to 80-keV Electron Exposure

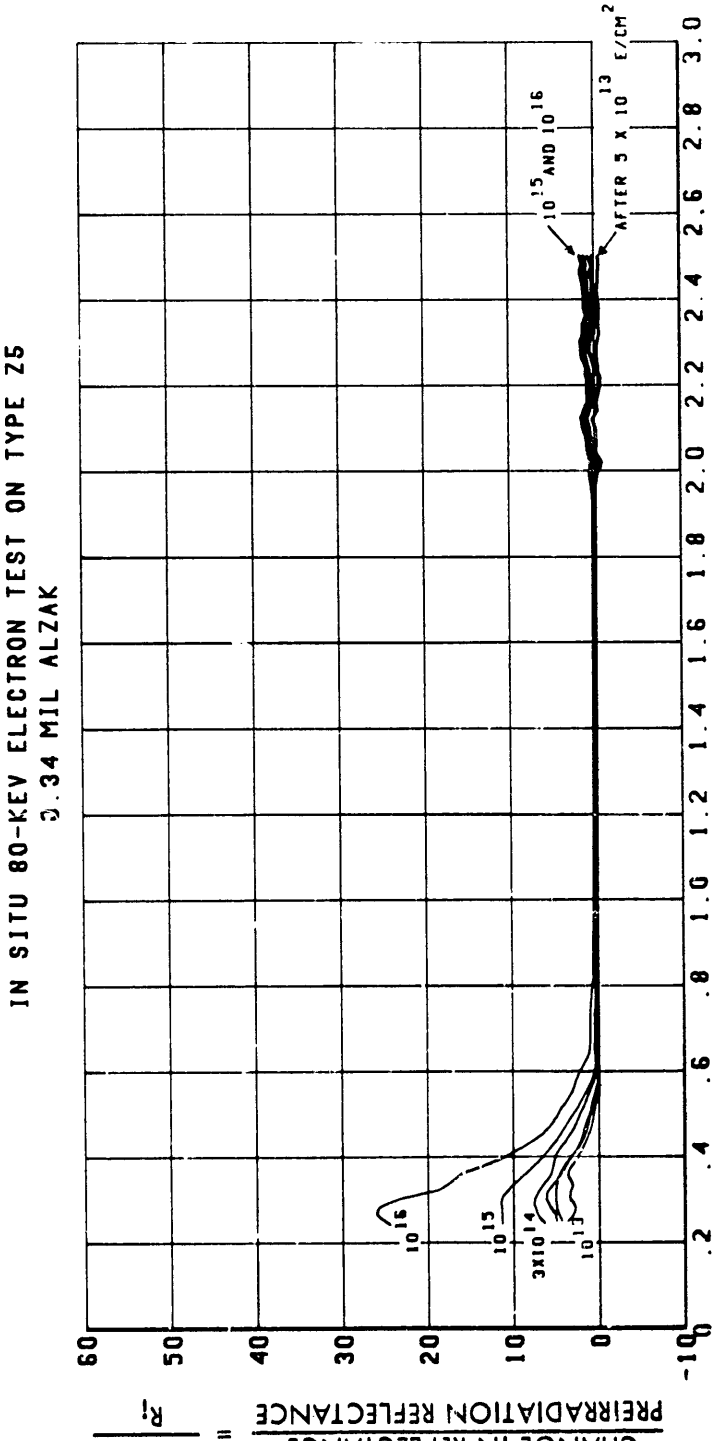

Figure 28. Reflectance Changes in 0.34-mil Alzak (Type Z_5) Due to 80-keV Electron Exposure

Effects of 80-keV electrons in Kapton H film (type N) are presented in Figure 29. Decreases in reflectance are seen to be much more severe than after exposure to 20-keV electrons (Figure 12).

As in the 20-keV electron test, types G, H, I, J, and K strongly resist reflectance degradation due to 80-keV electron exposure. Figures 30 through 34 are presentations of the limited amounts of reflectance changes measured. As has also been observed in past exposures to ultraviolet radiation (Reference 2), type H undergoes significant improvement in reflectance in the 0.25- to 0.3-micron wavelength region during electron irradiation.

Figures 35 through 40 show results obtained on six Teflon-based coatings received during this program and added to the 80-keV electron test. The results deserve the following description, which applies to all six types, 2-mil, 5-mil, and 10-mil aluminized Teflon; and 2-mil, 5-mil, and 10-mil silvered Teflon: After the samples had been exposed to 10^{15} 80-keV electrons/cm^2, the exposed surfaces still retained a specular appearance and, except at the shortest wavelengths measured, had sustained only minor reflectance degradation. The exposure to 10^{16} electrons/cm^2, however, left each Teflon coating significantly altered. The Teflon assumed a light gray appearance, so that the vapor-deposited metal was masked. Some crazing and a considerable amount of mottling of each Teflon surface was also evident. The question may be raised as to whether this is an effect of fluence or flux. Reference 5 reports the thermal conductivity (K) of polytetrafluoroethylene to be 2.9×10^{-6} BTU/(sec-in-°F) at room temperature. Based upon the assumption that the Teflon primarily limits heat transfer to the specimen substrate via a uniform temperature gradient, and using the above value of K, the maximum temperature rise expected at the Teflon surface which faces the electron beam may be determined using

$$\Delta T = T - T_s = Qd/KA\,t$$

where T_s is the specimen substrate temperature, Q the energy transported by the electron beam, A the specimen area, d the coating thickness, and t is time. The variables are conveniently grouped as follows:

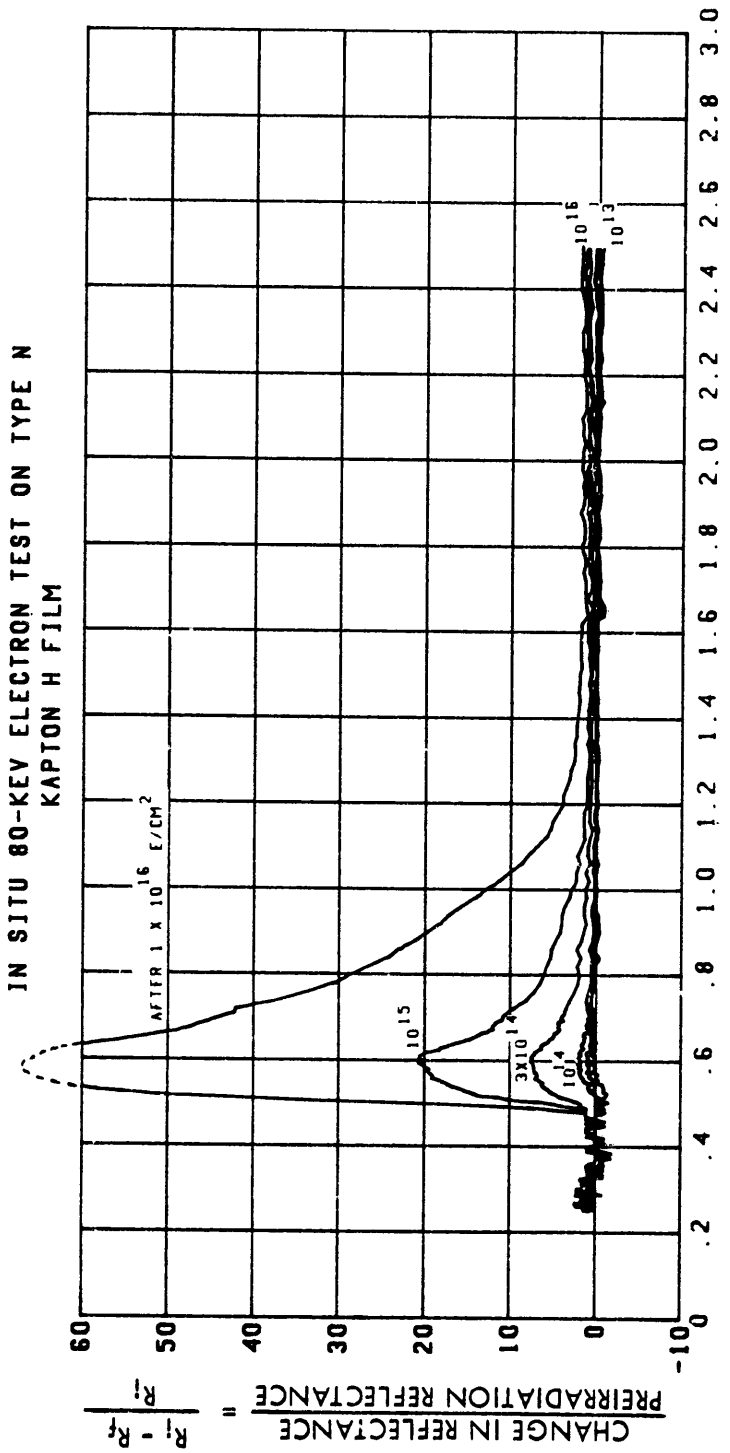

Figure 29. Reflectance Changes in Kapton H Film (Type N) Due to 80-keV Electron Exposure

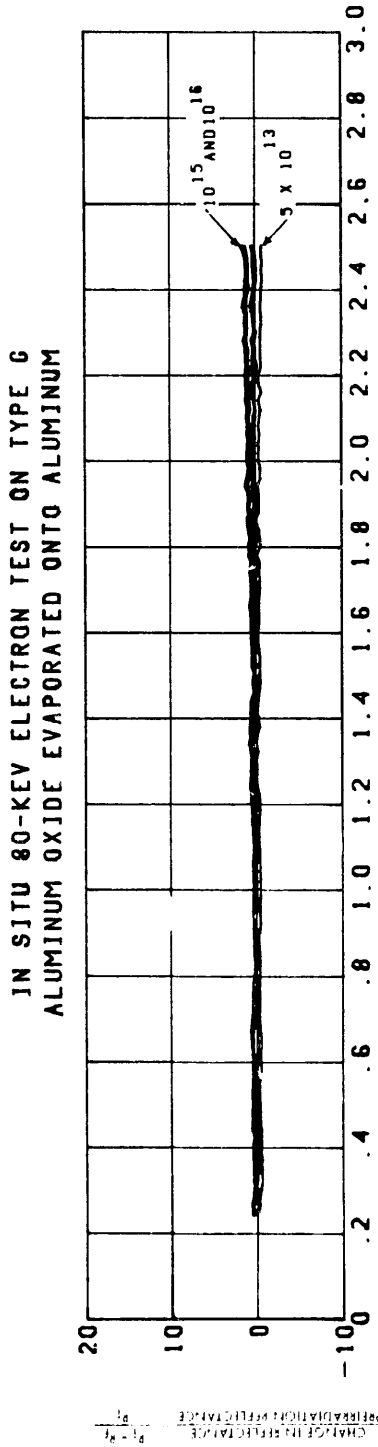

Figure 30. Reflectance Changes in Al_2O_3 Over Al (Type G) Due to 80-keV Electron Exposure

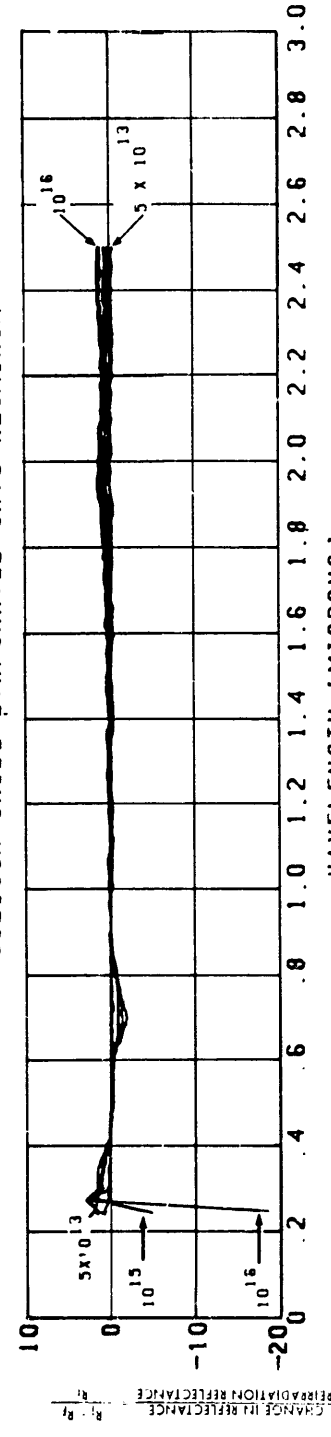

Figure 31. Reflectance Changes in SiO_2 Over Al (Type H) Due to 80-keV Electron Exposure

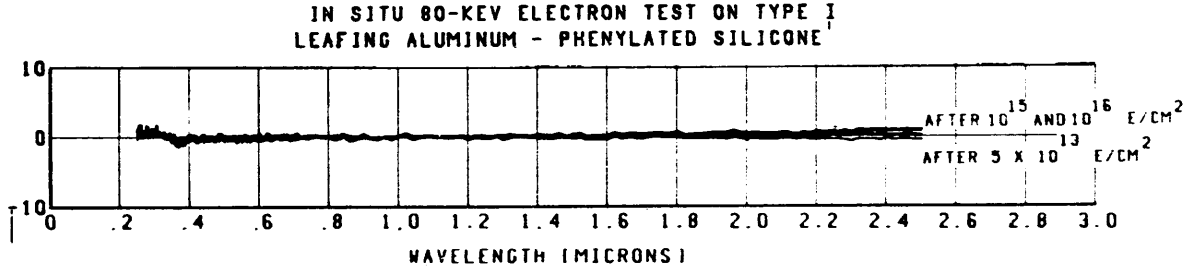

Figure 32. Reflectance Changes in Leafing Aluminum—Silicone (Type I) Due to 80-keV Electron Exposure

$$\frac{\text{CHANGE IN REFLECTANCE}}{\text{PREIRRADIATION REFLECTANCE}} = \frac{R_i - R_f}{R_i}$$

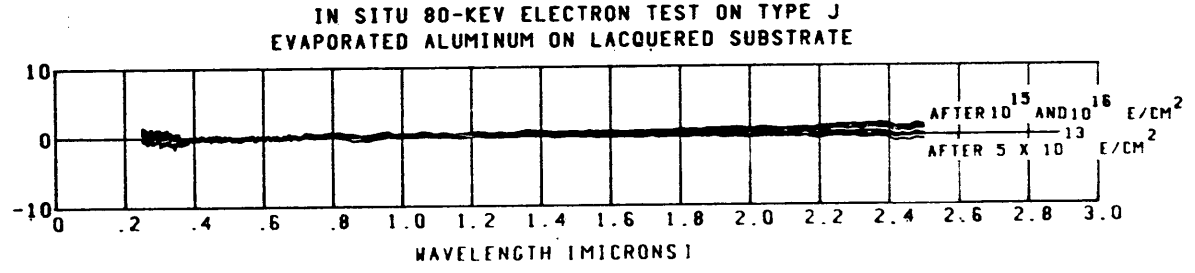

Figure 33. Reflectance Changes in Al Over Lacquer (Type J) Due to 80-keV Electron Exposure

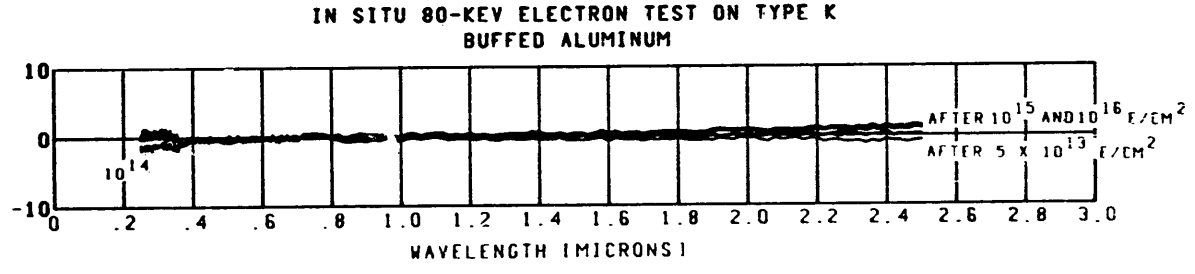

Figure 34. Reflectance Changes in Buffed Al Surface (Type K) Due to 80-keV Electron Exposure

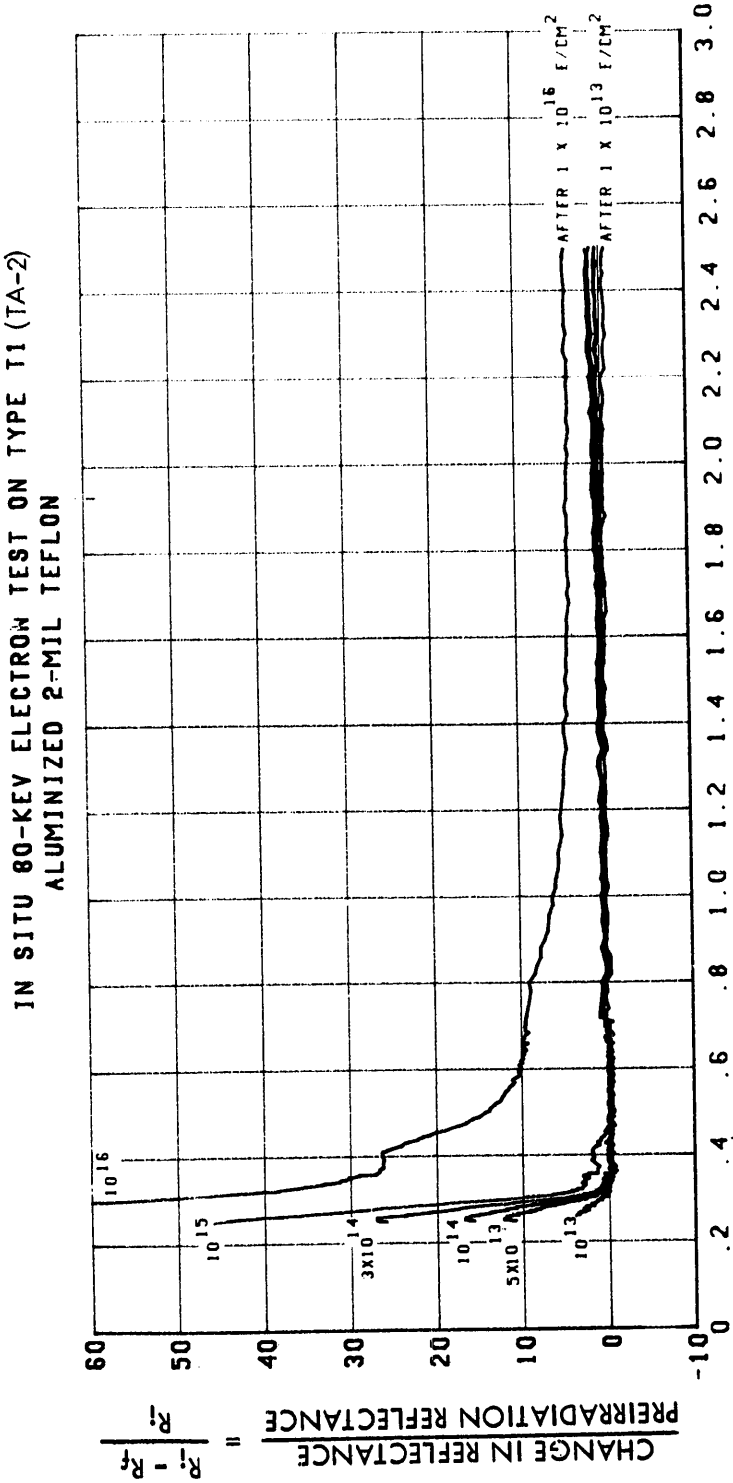

Figure 35. Reflectance Changes in Aluminized 2-mil Teflon (Type TA-2) Due to 80-keV Electron Exposure

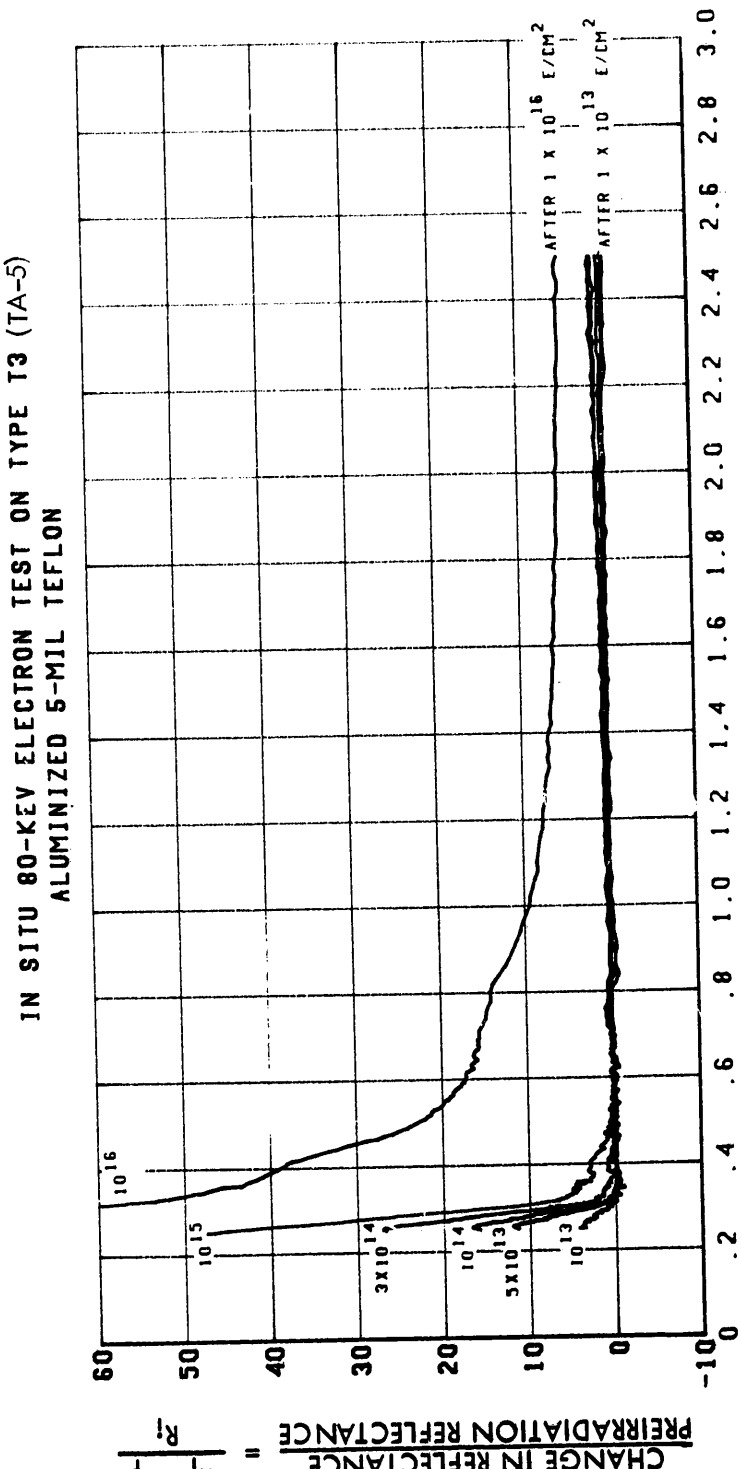

Figure 36. Reflectance Changes in Aluminized 5-mil Teflon (Type TA-5) Due to 80-keV Electron Exposure

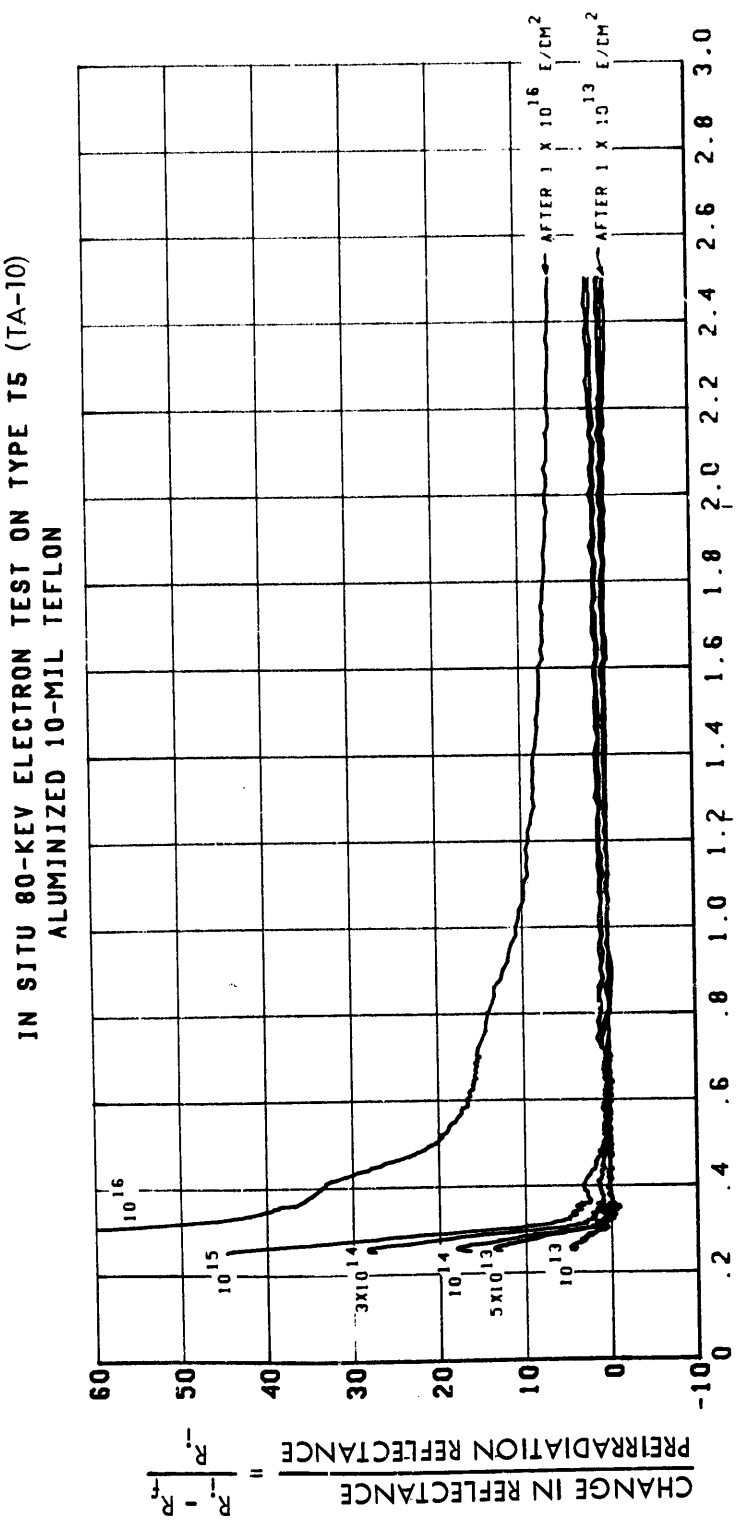

Figure 37. Reflectance Changes in Aluminized 10-mil Teflon (Type TA-10) Due to 80-keV Electron Exposure

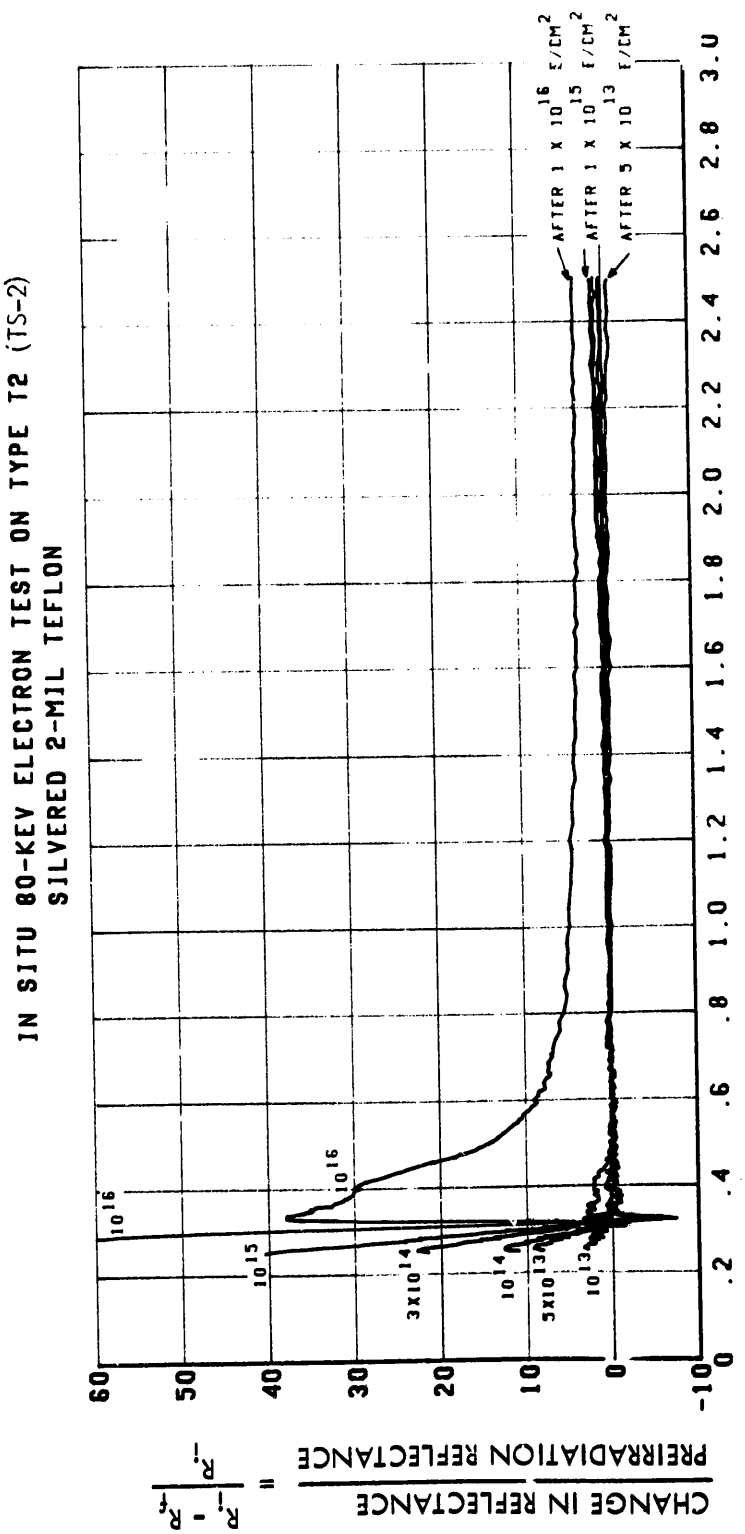

Figure 38. Reflectance Changes in Silvered 2-mil Teflon (Type TS-2) Due to 80-keV Electron Exposure

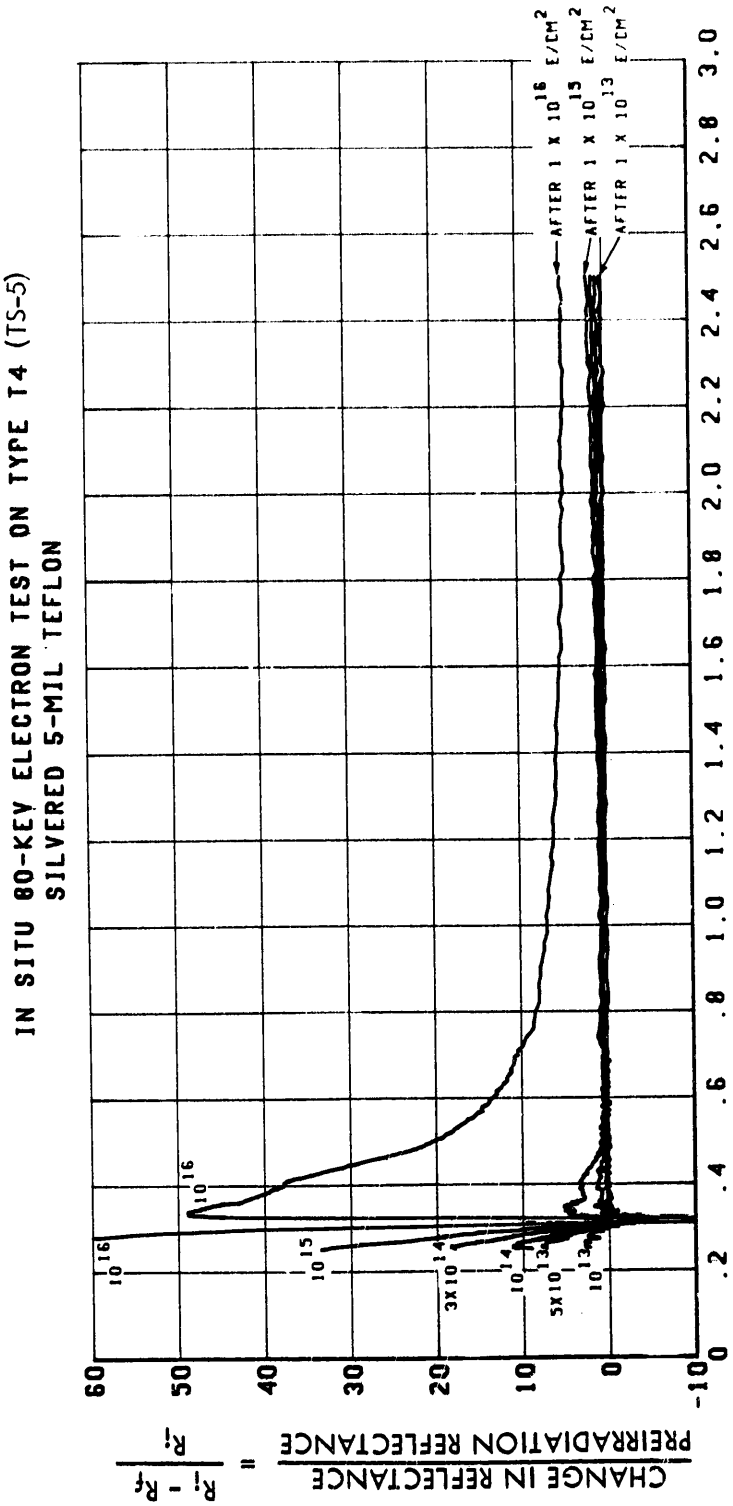

Figure 39. Reflectance Changes in Silvered 5-mil Teflon (Type TS-5) Due to 80-keV Electron Exposure

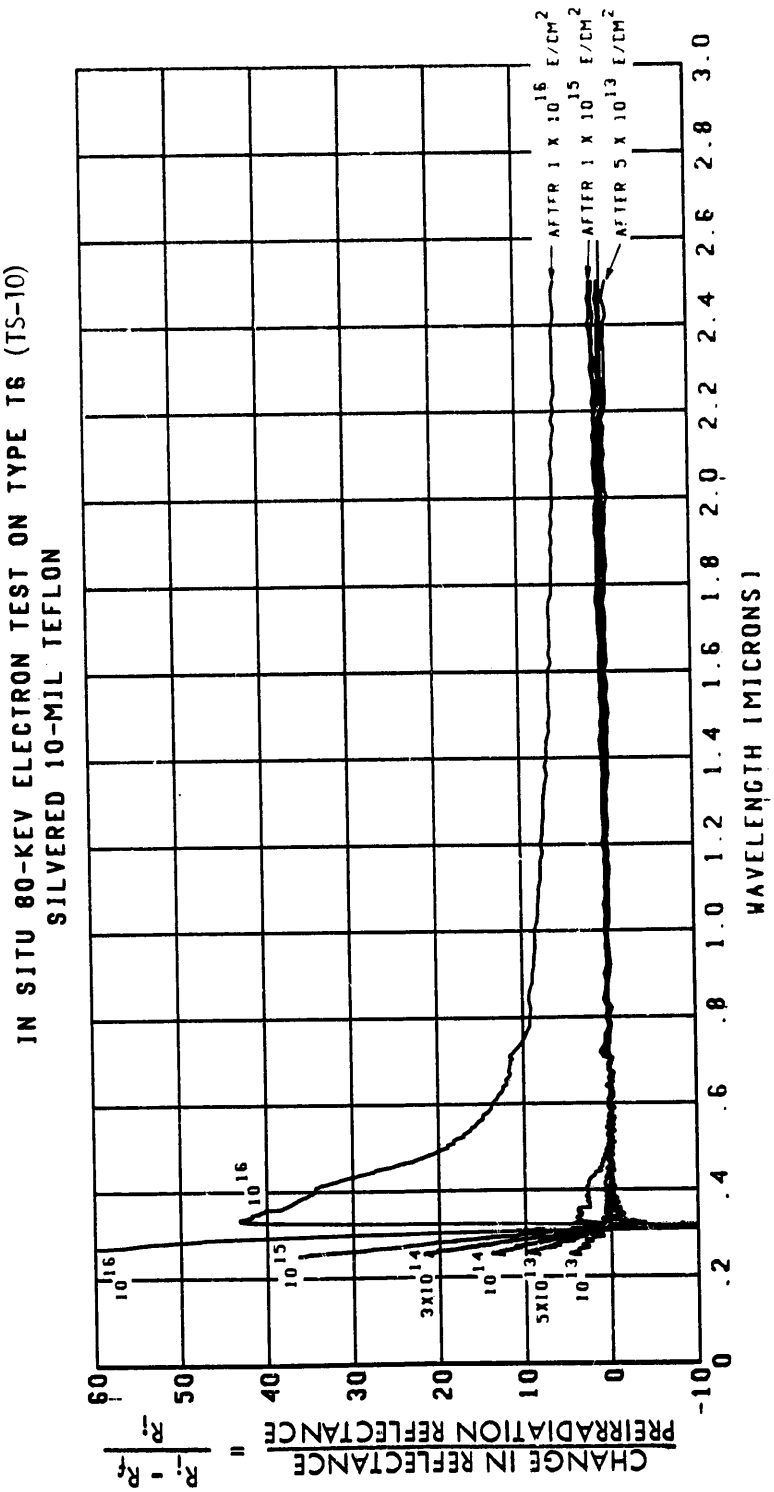

Figure 40. Reflectance Changes in Silvered 10-mil Teflon (Type TS-10) Due to 80-keV Electron Exposure

$$T - T_s = \left(\frac{Q}{At}\right)\left(\frac{d}{K}\right)$$

Q/At is readily derived from the electron flux of 5×10^{11} electrons/cm^2-second used for the 80-keV exposure from 10^{15} to 10^{16} electrons/cm^2. Thus it is found that

$$5 \times 10^{11}\ e/(cm^2\text{-sec}) \times 8 \times 10^4\ eV/e = 4 \times 10^{16}\ eV/(cm^2\text{-sec})$$

and that

$$4 \times 10^{16}\ eV/(cm^2\text{-sec}) \times 1.6 \times 10^{-19}\ \text{joule/eV} = 6.4 \times 10^{-3}\ \text{watt/cm}^2 = Q/At.$$

This is approximately 0.04 times the solar "constant" of 0.15-0.16 watt/cm^2 or 1.9-2.0 calories/cm^2-minute. For a specimen area of 5 cm^2, this means that each sample receives beam energy at the rate of only 0.032 watt, or 0.0076 calorie/second. Using 1 BTU = 1055 joules, the units of K become consistent by setting

$$2.9 \times 10^{-6}\ \text{BTU/(sec-in-°F)} \times 1055\ \text{watts/(BTU/sec)} = 3.1 \times 10^{-3}\ \text{watt/(in-°F)}$$

and

$$3.1 \times 10^{-3}\ \text{watt/(in-°F)} \times (9°\text{F}/5°\text{C}) \times (1\ \text{in}/2.54\ \text{cm}) = 2.2 \times 10^{-3}\ \text{watt/(cm-°C)}.$$

The greatest temperature rise occurs in the 10-mil (0.025-cm) Teflon. The temperature difference between front and back surfaces is

$$T - T_s = (6.4 \times 10^{-3}\ \text{watt/cm}^2) \times (0.025\ \text{cm})/(2.2 \times 10^{-3}\ \text{watt/cm-°C}) = 0.073\text{C°}.$$

The calculated temperature at the Teflon-surface exposed to radiation is virtually the same as that at the Teflon-substrate interface. This appears to eliminate the uncertainty regarding an electron flux effect at 5×10^{11} electrons/cm^2-second, and thus the change in each Teflon surface is attributed to electron fluence.

The calculated amount of temperature rise during electron exposure differs markedly with the situation which is encountered when the emittance of samples with low thermal conductivity is measured using a heated cavity. Past experience

with Teflon includes an instance in which a 10-mil thick specimen ignited shortly after insertion into a Hohlraum at 1500°F. Similar to the calculation above for Teflon in an electron beam, a calculation for the case of Teflon in a heated cavity shows a temperature rise on the order of 100°C, an amount insufficient to ignite the material. Both temperature-rise results assume that a uniform temperature gradient (dT/dx) exists through the Teflon. Existence of a non-uniform gradient in a material would be expected to alter the calculated temperature rise in the direction of a higher temperature for the surface exposed to the incident energy (electron beam, heated cavity, etc.). Both experimental results cited — the alteration of the aluminized and silvered Teflon, and the ignition of Teflon following insertion into a Hohlraum — support the hypothesis of a higher-than-expected temperature rise due to a non-uniform temperature gradient.

2.4 ADDITIONAL EXPERIMENTS

As mentioned in Section 1.1, the need to conduct additional tests beyond those originally planned became apparent as the first electron test (at 20 keV) was underway.

2.4.1 In-Vacuum Reflectance Recovery Effects

After reaching an exposure of 5×10^{13} electrons/cm^2 and after completing subsequent reflectance measurements, the 20-keV electron test schedule entered a 96-hour standby period. During this time interval no exposures or measurements were undertaken, but specimens remained in the dark, and vacuum was maintained such that chamber pressure dropped from an initial value of 1×10^{-8} torr to a final value of 6×10^{-9} torr. Prior to resuming exposure to the next fluence level, reflectance measurements were repeated on selected types of coatings. The following in situ changes were revealed:

1. Type B(S-13), which had lost 7 percent reflectance at 2050 mμ, recovered some 3 percent during the 96 hours. Type M (S-13G), which had lost 6 percent reflectance at 2050 mμ, recovered 3 percent during the 96 hours.
2. Type D_3 in the ultraviolet, and type E_3 in the visible region, did not recover from their reflectance losses of a few percent.
3. Type Z_5 (0.34-mil Alzak) recovered about 1 percent from its loss of about 3 percent in the ultraviolet. Type Z_4 (0.22-mil Alzak) recovered between 1 and 2 percent from its ultraviolet reflectance losses of about 3 percent.

In proceeding to the next fluence of 10^{14} 20-keV electrons/cm^2, a pause was made at 6×10^{13}, and type 3 measured in the infrared wavelength region. Its reflectance at 2050 mμ dropped some 3 percent, matching the original 5×10^{13} value closely. This 3 percent reflectance loss for an incremental fluence of 1×10^{13} (=$6 - 5 \times 10^{13}$), it may be pointed out, is more than type B's first loss at 1×10^{13} electrons/cm^2.

When sufficiently long times (~ days) elapsed between measurements, similar in-vacuum reflectance recovery effects continued to be observed in some types at higher electron fluences also. In addition, an extensive set of measurements taken to learn more about this phenomenon, was made on type M (an early formulation of S-13G) in the infrared wavelength region after 10^{15} electrons/cm^2. Reflectance data are displayed 3 different ways in Figures 41, 42, and 43. Figure 41 shows preirradiation reflectance, the initial reflectance of type M following 10^{15} electrons/cm^2, and improvement in this reflectance with time. The initial measurement scan was begun as close to the end of the exposure time as was practical—3.8 minutes. Reflectance improvement in type M with time after exposure to 10^{15} 20-keV electrons/cm^2 is seen to be appreciable after 6 hours.

Figure 41 suggests that reflectance recovery is most extensive in the 1.2- to 1.6-micron wavelength region. This is indeed the case, as Figures 42 and 43 portray more directly. The baseline in Figure 42 is preirradiation reflectance. In Figure 43 the graph baseline is the initial reflectance measurement following exposure to 10^{15} 20-keV electrons/cm^2. Figures 41 and 42 show clearly that more recovery toward preirradiation values is possible in the 1.8- to 2.1-micron region, yet the peak recovery (exhibited most clearly in Figure 43) is in the 1.2- to 1.65-micron region.

2.4.2 Unsegmented 20-keV Electron Test

The phenomenon of in-vacuum reflectance recovery during in-vacuum testing brings out the question of the validity to be expected from a segmented test—that is, a test in which the exposures take place in segments separated by measurement periods. If a hypothetical segmented test were found to result in spectral reflectance changes like those shown by the solid/dot curve of Figure 44, the question arises as to what reflectance would be observed after an unsegmented exposure. The short-dashed curve in Figure 44 is one potential case—the one case in which identical results are obtained for both segmented and unsegmented exposures. Another possibility, shown by the long-dashed curve in Figure 44, is that the results from segmented and unsegmented exposures are different, perhaps by the amount of in-vacuum reflectance recovery observed.

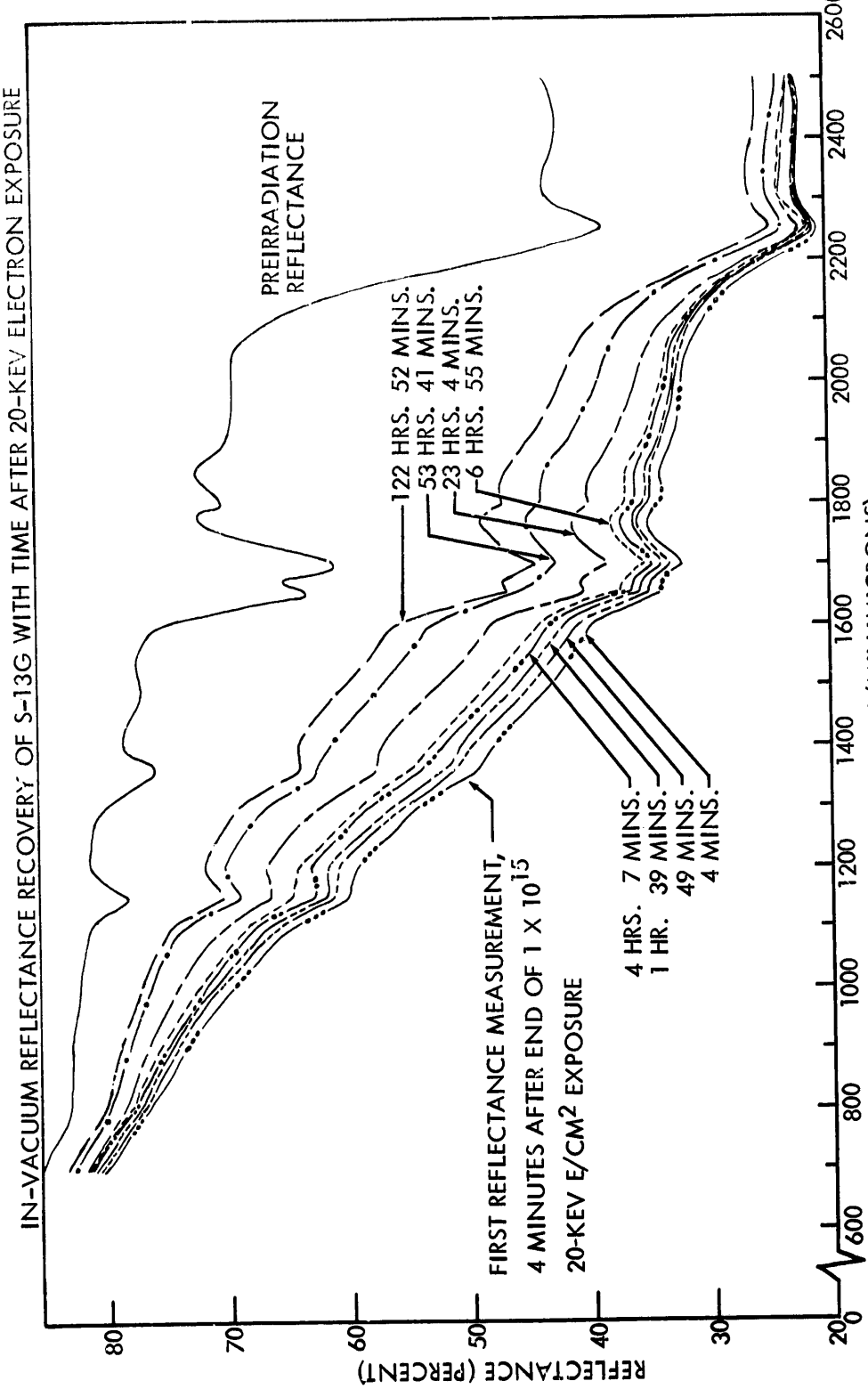

Figure 41. In-vacuum Reflectance Recovery of S-13G (Type M) With Time Following Exposure to 10^{15} 20-keV Electrons/cm^2

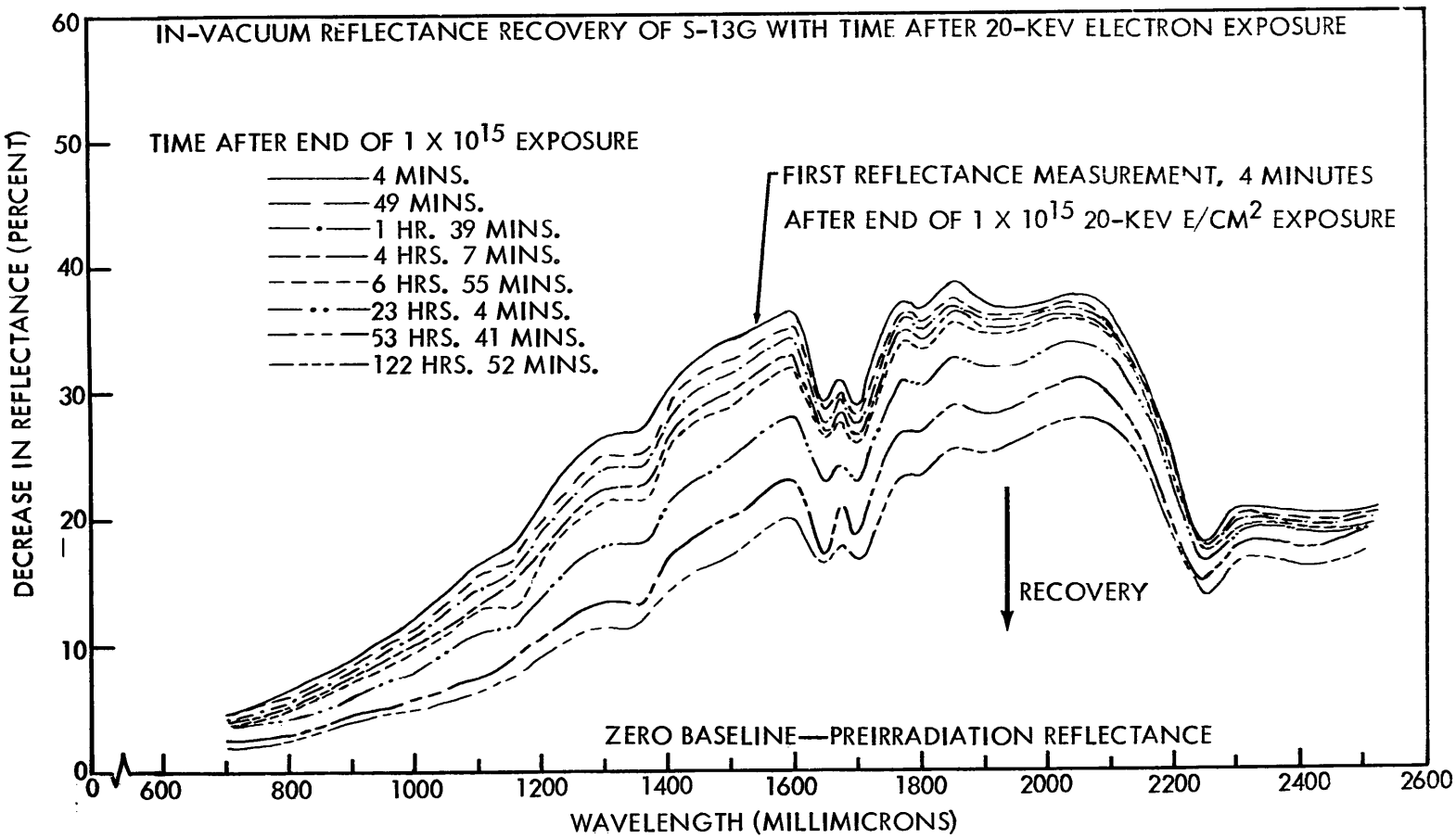

Figure 42. In-vacuum Reflectance Recovery of S-13G (Type M) as a Function of Wavelength, Using Baseline of Preirradiation Reflectance

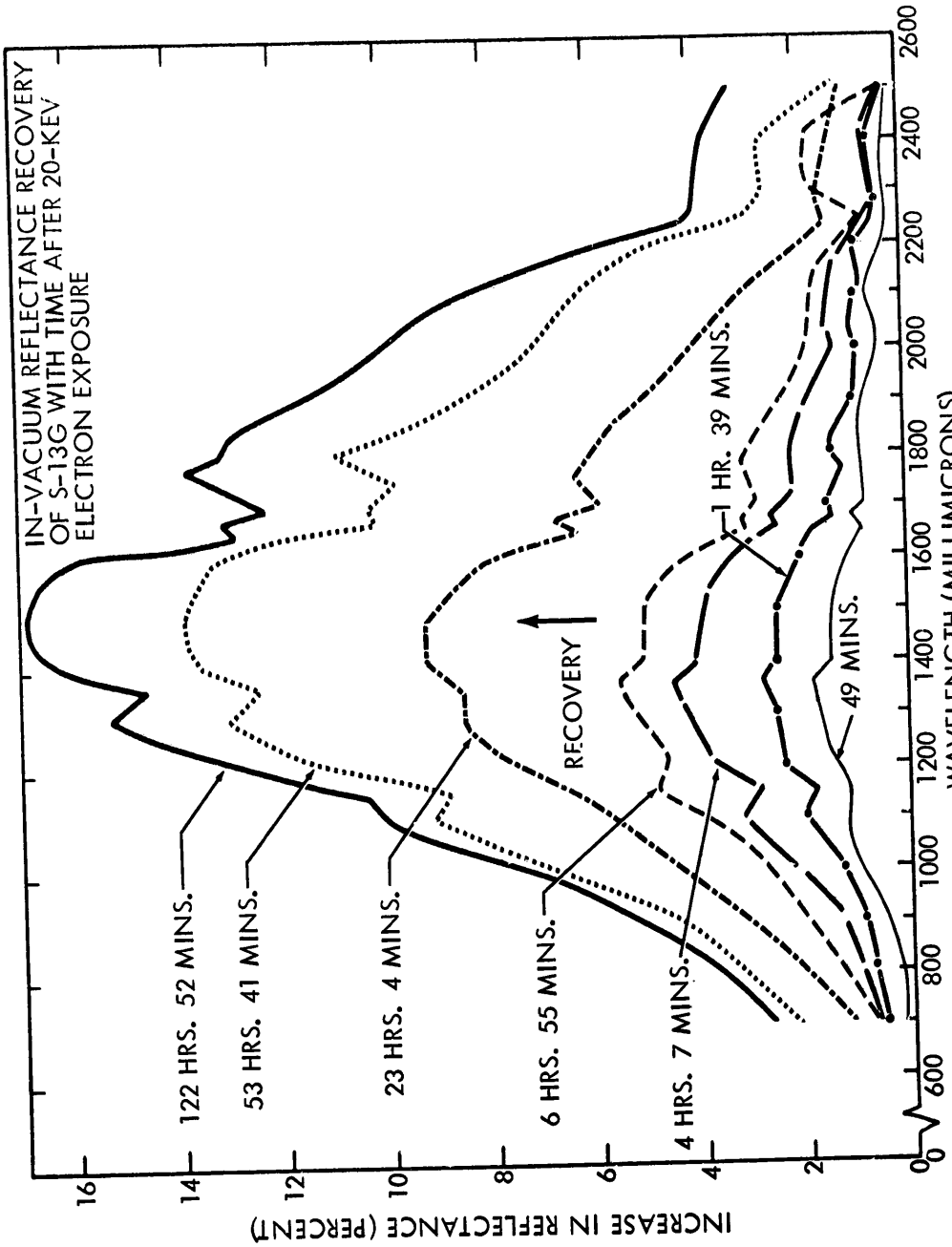

Figure 43. Near Infrared Peaking of In-vacuum Reflectance Recovery in S-13G (Type M)

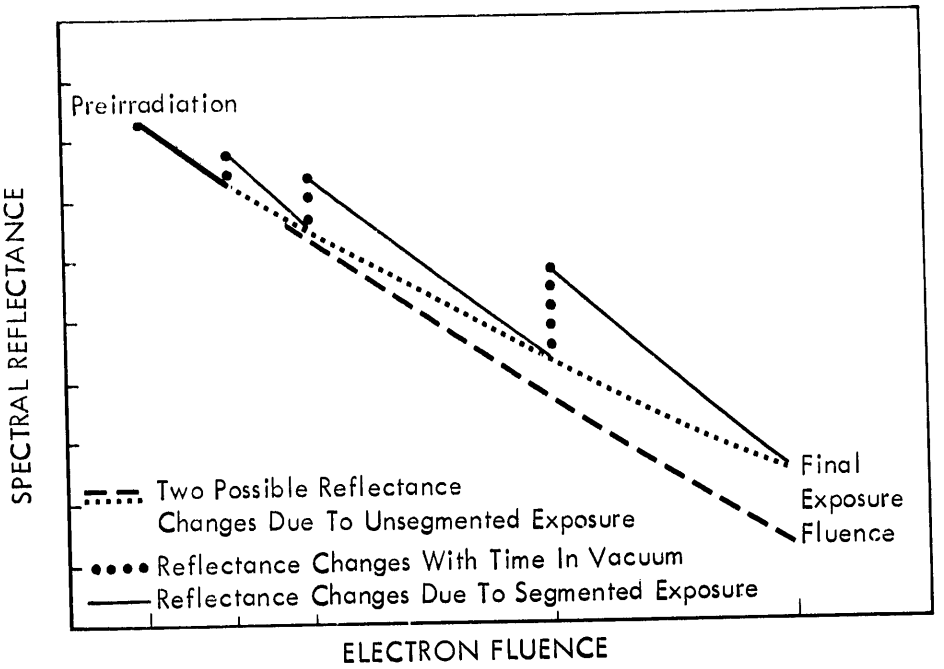

Figure 44. Possible Spectral Reflectance Changes Resulting From Segmented and Unsegmented Exposures

To test the validity of the 20-keV electron test data from segmented exposures, a separate, unsegmented exposure to 3×10^{14} electrons/cm^2 was made using control samples. Types B, M, R, L_1, E_3, F_3, and Z_3 were measured just before and just after exposure to 20-keV electrons at a rate of 1.0×10^{10} electrons/cm^2-second (the same flux used in the main 20-keV test). Results from these measurements are shown as dashed curves (not computer-processed) in Figures 1, 2, 3, 4, 7, 8, and 9 (respectively). Reflectance changes measured in types B and L_1 after this 3×10^{14} unsegmented exposure were about 2 percent less than the changes measured following 3×10^{14} fluence in the segmented-exposure (main) test. On the other hand, reflectance changes in type M were about 2 percent greater after the unsegmented exposure; in types R, E_3, F_3, and Z_3 the measured changes were about one percent greater following the unsegmented exposure. Considering the overall degradation, these are small differences, and it should be noted from the dashed curves that sample-to-sample differences are as great as any differences

between segmented-exposure results and unsegmented-exposure results. Thus, the results from the unsegmented-exposure test are felt to validate the reflectance data obtained from segmented-exposure testing with 20-keV electrons.

The question can well be raised as to why reflectance changes arising from unsegmented-exposure testing agree so well with net changes (alternating degradation and recovery) resulting from exposures broken into segments by measurement periods. A clue is provided by observations made in Section 2.2 (Figure 1) and Section 2.4.1 for the case of type B zinc oxide—methyl silicone (S-13). At a wavelength of 2050 mμ, type B degrades about 2 percent after exposure to 1×10^{13} 20-keV electrons/cm^2, and about 7 percent after exposure to 5×10^{13} 20-keV electrons/cm^2. Then, over the next 96 hours following the end of exposure to 5×10^{13}, type B recovers about 3 percent in reflectance at 2050 mμ, while remaining in the dark and in vacuum. Thereafter, exposure to 6×10^{13} from 5×10^{13} 20-keV electrons/cm^2 causes the 2050-mμ reflectance of type B to degrade 3 percent, which for this incremental fluence of 1×10^{13} ($=6 - 5 \times 10^{13}$) is greater than the reflectance decrease for a total fluence of 1×10^{13} 20-keV electrons/cm^2. This suggests that type B has something of a "memory" for previous damage, as has been observed previously for zinc oxide pigment (Reference 6). In other words, as exposure to radiation begins again after an interruption during which some reflectance recovery has taken place, sample reflectance evidently has an initial rate of decrease which is greater than rates of decrease later on during the exposure. Somewhat in contrast, this result with type B differs from that which was observed at this laboratory during Contract NAS5-9650. Then it was found that a brief exposure ($\sim 10^{14}$ 50-keV electrons/cm^2) following a second pumpdown to vacuum did not "trigger" a zinc oxide—methyl silicone sample's return to a degraded state which was caused by exposure to 10^{16} 50-keV electrons/cm^2 during the first pumpdown to vacuum.

2.4.3 Recovery/Temperature Study After 80-keV Test

Following the 80-keV electron test, an experimental study was conducted to determine whether the extent of or rate of in-vacuum reflectance recovery has a dependence upon electron energy or upon specimen temperature during the recovery time period. Sample substrate temperature during the 80-keV test was $6 \pm 1°C$.

After the final test exposure (10^{16} electrons/cm^2), this temperature was maintained for two days while two sets of reflectance measurements were made on seven selected types of coatings (B, M, R, L_1, O, E_3, and F_3). Then, two days after the final test exposure was completed, the temperature of each specimen substrate was gradually raised to 20 ± 1°C, as the sample wheel water flow was stopped and the sample wheel rose to room temperature. After this temperature change four more sets of reflectance data were obtained for each of the seven types of coatings over a period of 16 days, while the samples remained in vacuum and in the dark.

Figures 45 through 51 show the results obtained on these coatings. The most degraded reflectance curves in these figures are the initial measurements made following exposure to 10^{16} 80-keV electrons/cm^2, which are the same as the most degraded reflectance curves indicated in Figures 18, 19, 20, 21, 22, 24, and 25. The next-to-most-degraded reflectance curves are the second set of measurements made with specimen substrate temperatures of 6°C. The other four sets of reflectance measurements, obtained while the specimens remained at 20°C in the 10^{-8} torr vacuum environment, lie above the 6°C curves. The uppermost in-vacuum reflectance curves in Figures 45 through 51, showing the least degradation from preirradiation reflectance, and showing the most reflectance improvement with time after exposure to 10^{16} electrons/cm^2, are those obtained some 18 days following the end of the 10^{16} exposure.

Figures 45 through 51 allow a comparison of reflectance recovery properties at 6°C and at 20°C. It is apparent that reflectance recovery proceeds—slowly at either temperature—to significant amounts of reflectance improvement with time in vacuum. This in-vacuum reflectance improvement with time after end of exposure is measurable in type B (S-13) and type L_1, quite significant in type M (S-13G) and type R (Goddard series 101-7-1), and dramatically large in types O, E_3, and F_3 (Figures 49, 50, and 51).

Finally, Figures 45 through 51 allow a comparison of each sample's preirradiation reflectance with that measured some five days after return of the test chamber to a dry air atmosphere. Nearly full restoration of original reflectance

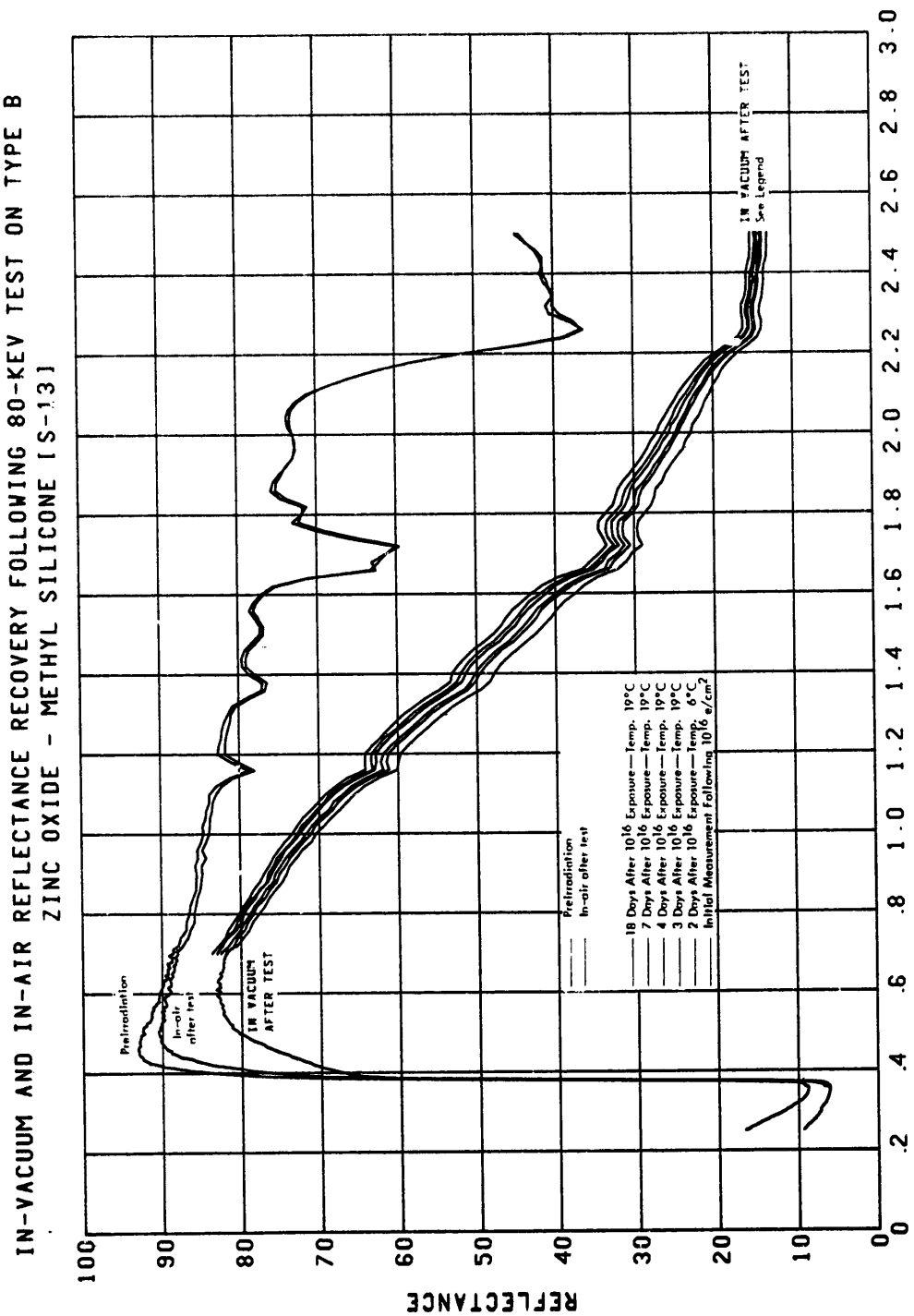

Figure 45. Reflectance Recovery in Type B (S-13) Following 80-keV Electron Test

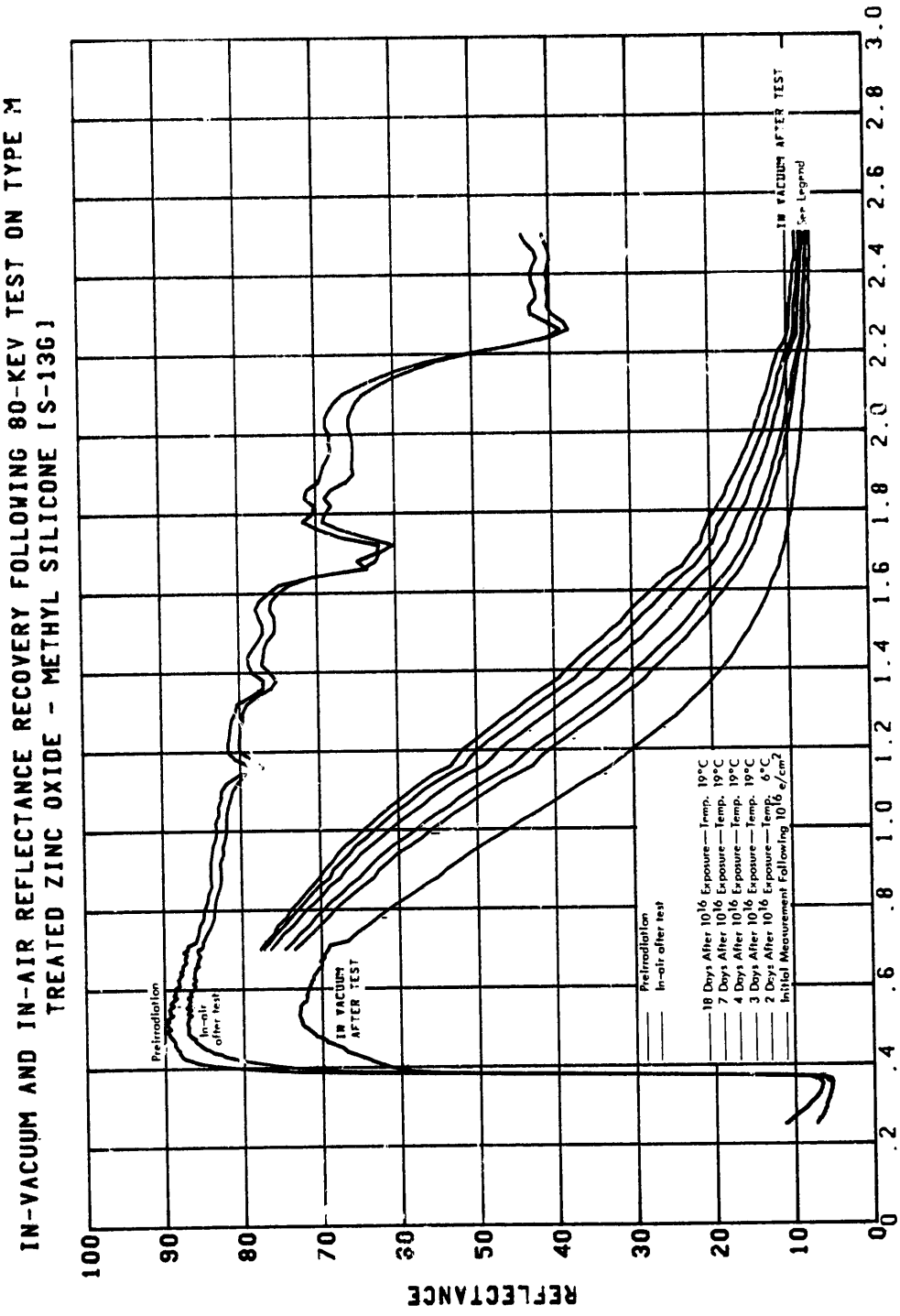

Figure 46. Reflectance Recovery in Type M (S-13G) Following 80-keV Electron Test

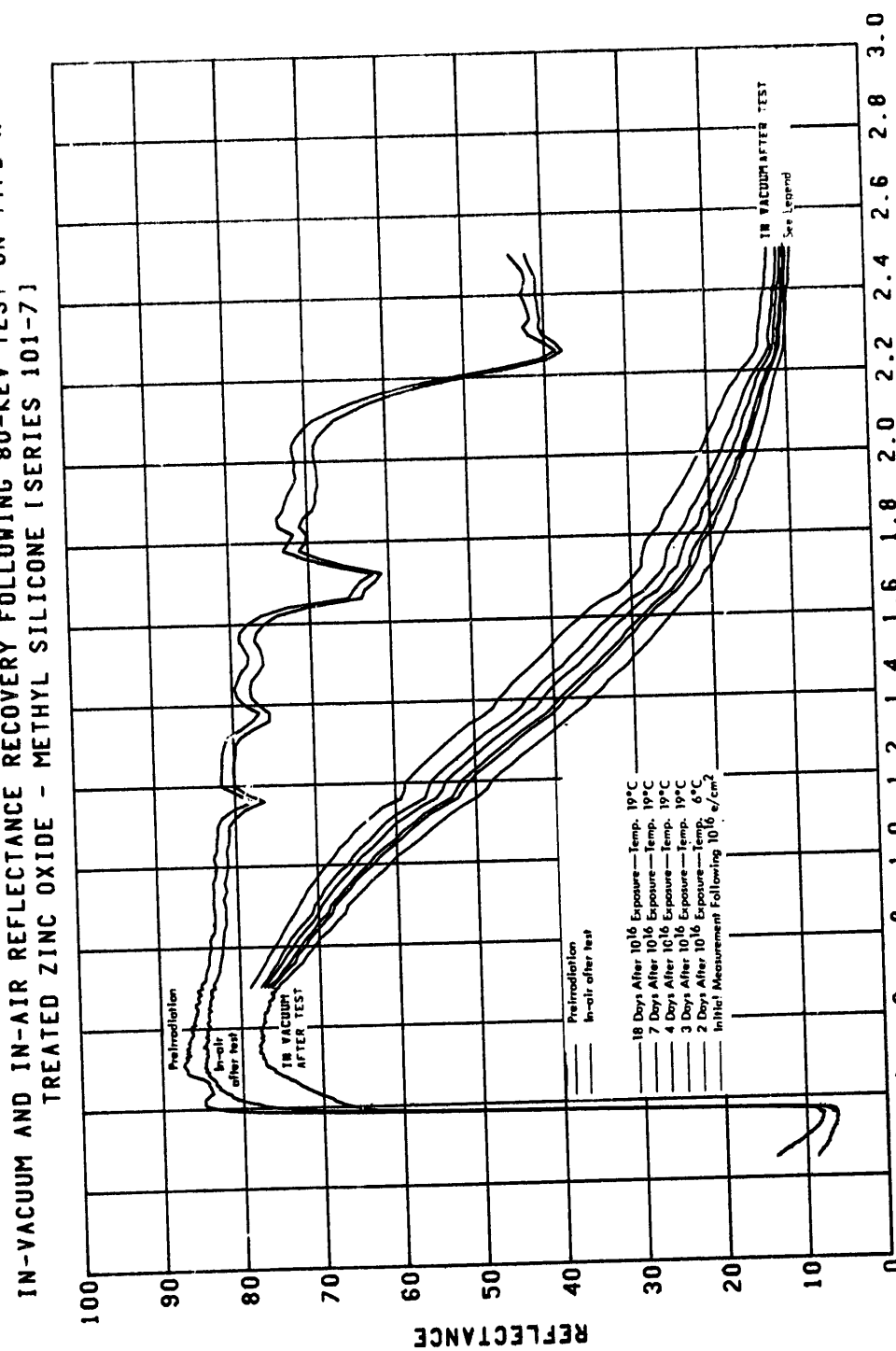

Figure 47. Reflectance Recovery in Type R (Series 101-7) Following 80-keV Electron Test

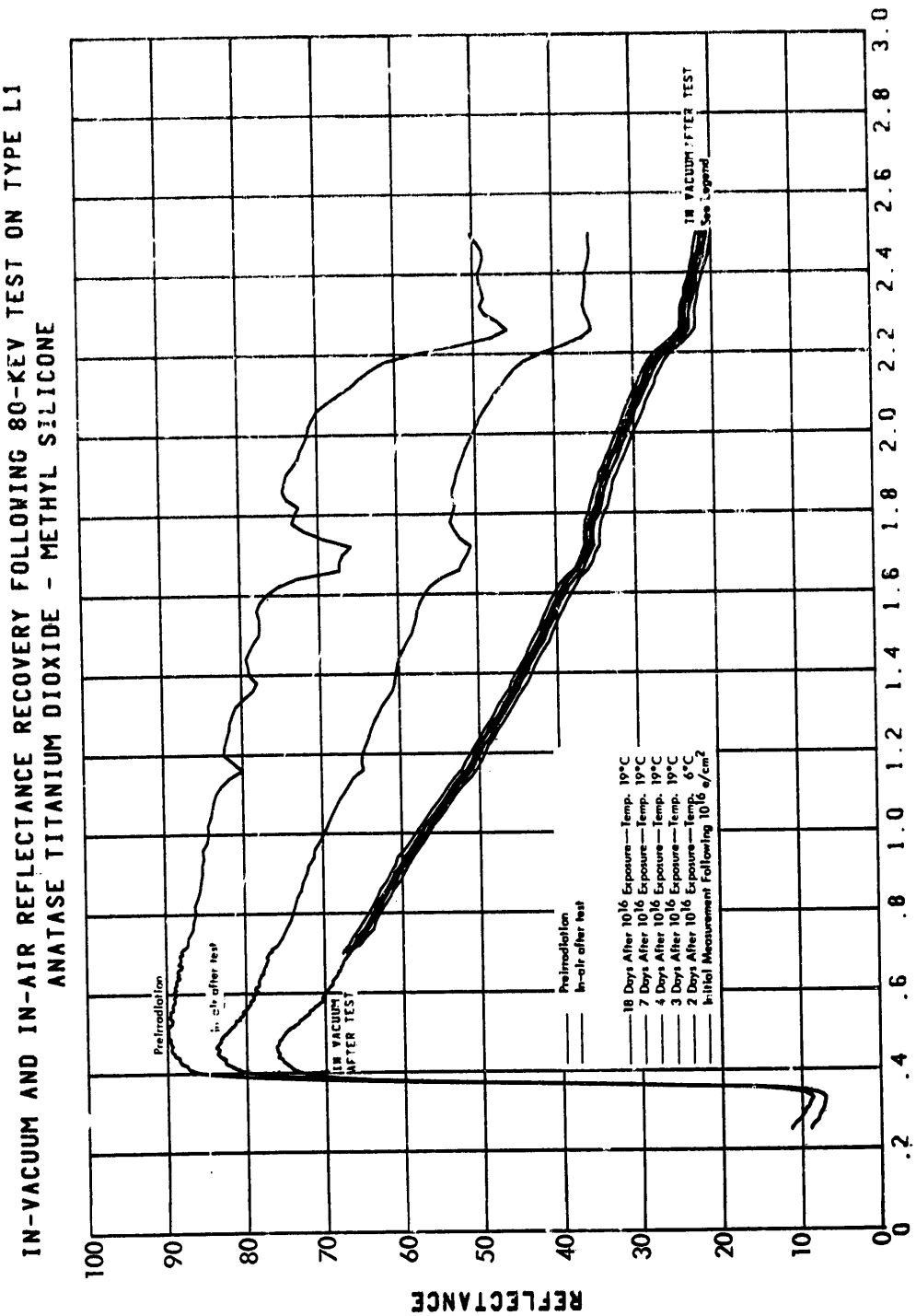

Figure 48. Reflectance Recovery in Type L_1 Following 80-keV Electron Test

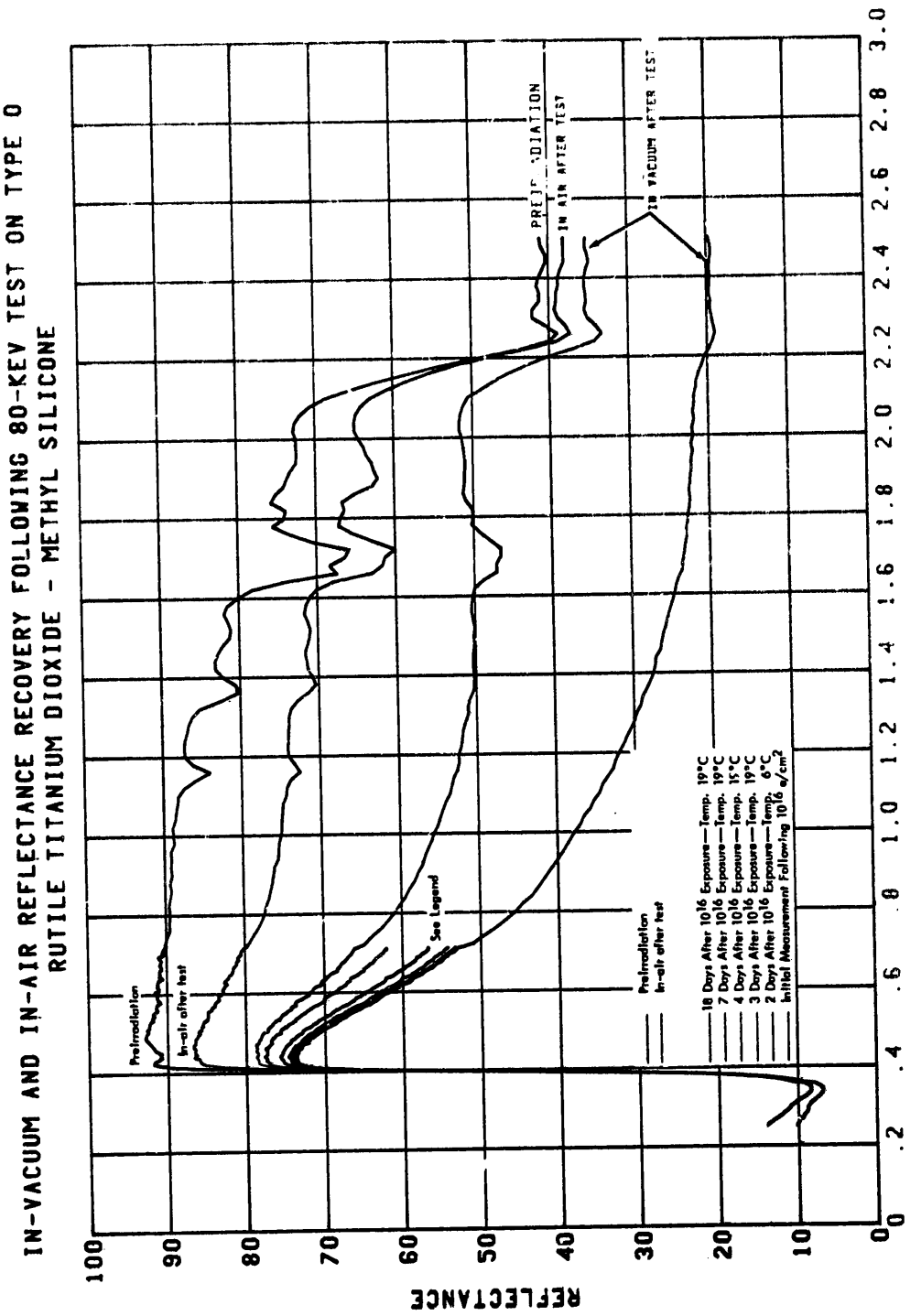

Figure 49. Reflectance Recovery in Type O Following 80-keV Electron Test

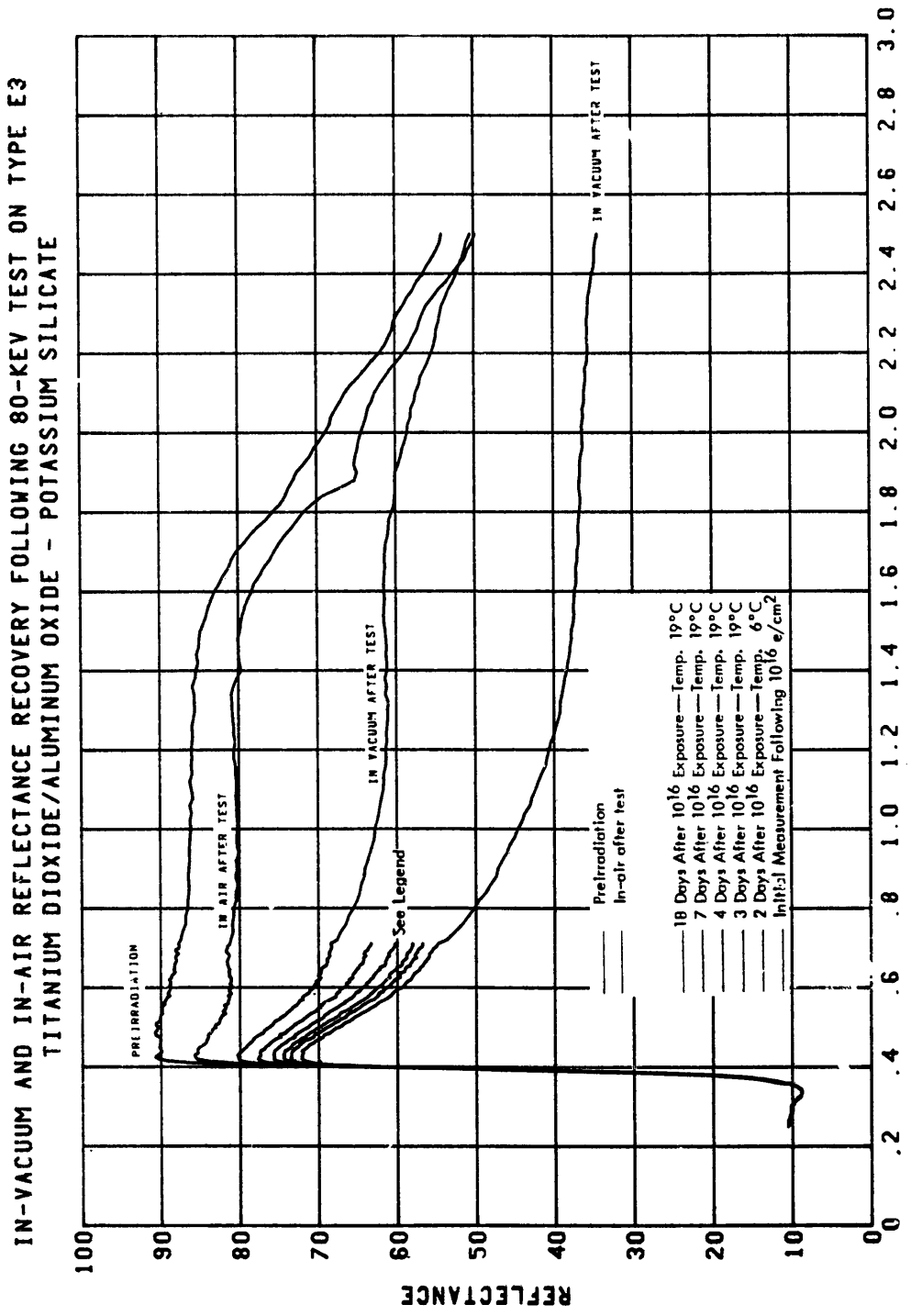

Figure 50. Reflectance Recovery in Type E_3 Following 80-keV Electron Test

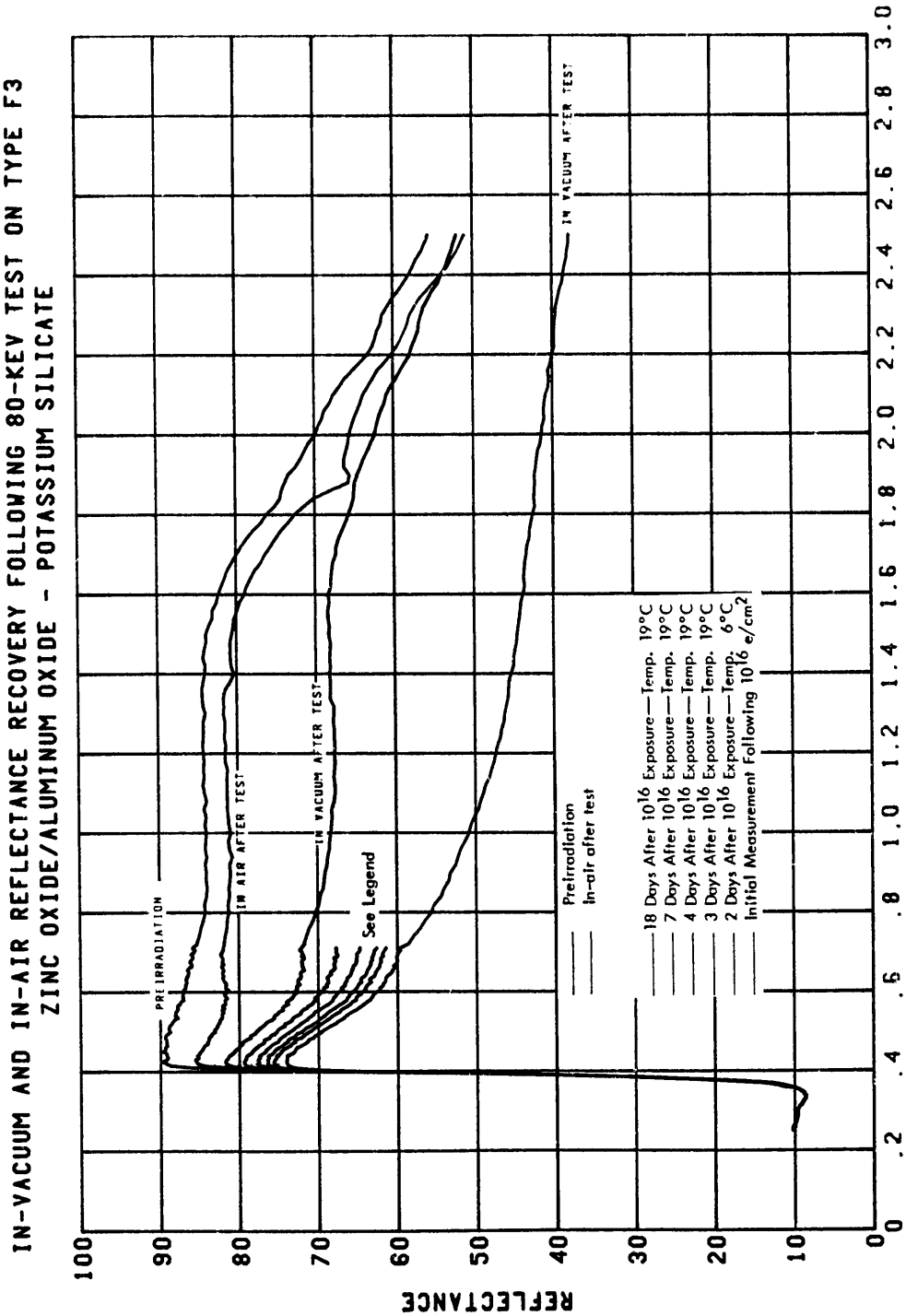

Figure 51. Reflectance Recovery in Type F_3 Following 80-keV Electron Test

occurs in the zinc oxide—methyl silicone samples (types B, M, and R; Figures 45, 46, and 47). On the other hand, types L_1, O, E_3, and F_3 exhibit significant departures in their post-test, in-air reflectance values from those measured before 80-keV electron exposure (Figures 48, 49, 50, and 51).

2.4.4 50-keV Electron Test

As detailed in Section 2.5, an energy dependence determination is a principal output from this program. Test results from the 20-keV (Section 2.2) and the 80-keV (Section 2.3) electron exposures conducted for this program are to be related to 50-keV electron test results. A limited amount of 50-keV data is readily accessible from an earlier program, NAS5-9650. More detailed 50-keV data—data which is in the same form as the 20-keV and 80-keV data—has been made available by performing a new 50-keV electron test on types B, M, R, L_1, E_3, and F_3. Reflectance data after exposures to 5×10^{13}, 1×10^{14}, 3×10^{14}, 5.5×10^{14}, and 1×10^{15} 50-keV electrons/cm^2 are shown in Figures 52 through 57 for these six sample types, respectively.

2.4.5 Reflectance Recovery After 50-keV Test

Information about reflectance recovery properties following exposure to 50-keV electrons was obtained on coating types B, M, R, L_1, E_3, and F_3. The results are shown in Figures 58 through 63. The reflectance curves showing the greatest amounts of degradation are the initial reflectance measurements made following exposure to 10^{15} 50-keV electrons/cm^2. In Figures 58 through 63, the reflectance curves second from the bottom show the extent of reflectance improvement in each type of coating after four days in the dark in a 10^{-8} torr vacuum.

Following these two sets of in-vacuum reflectance measurements, the chamber was backfilled with dry air. After nearly five days in this dry air environment the post-test, in-air reflectance curves shown in Figures 58 through 63 were obtained. In types B, M, and R the post-test, in-air reflectance nearly duplicates pre-irradiation reflectance. In types L_1, E_3, and F_3 significant differences between pre-test and in-air, post-test reflectance values remain even after the five days of sample exposure to dry air.

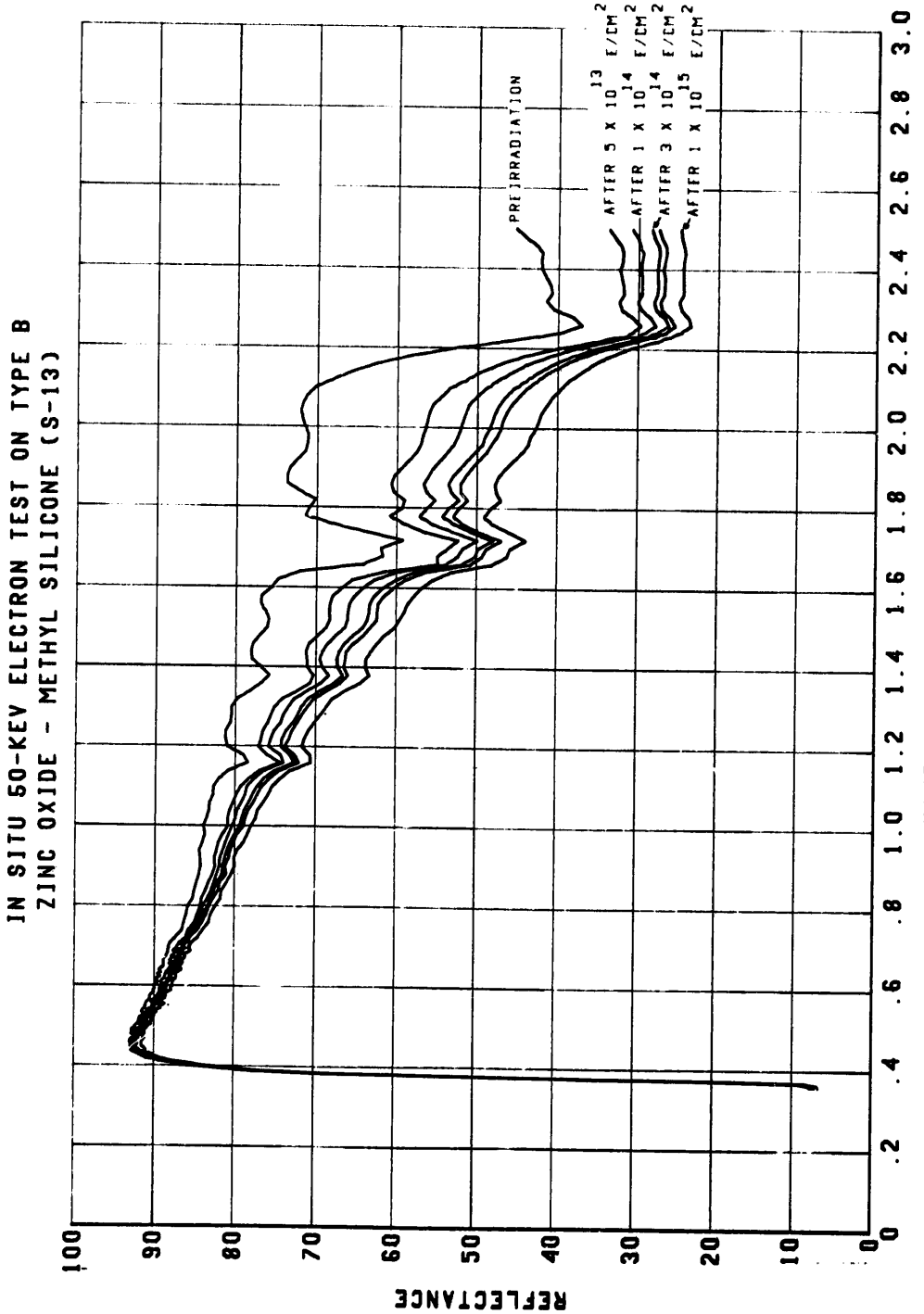

Figure 52. Effects of 50-keV Electrons on S-13 (Type B)

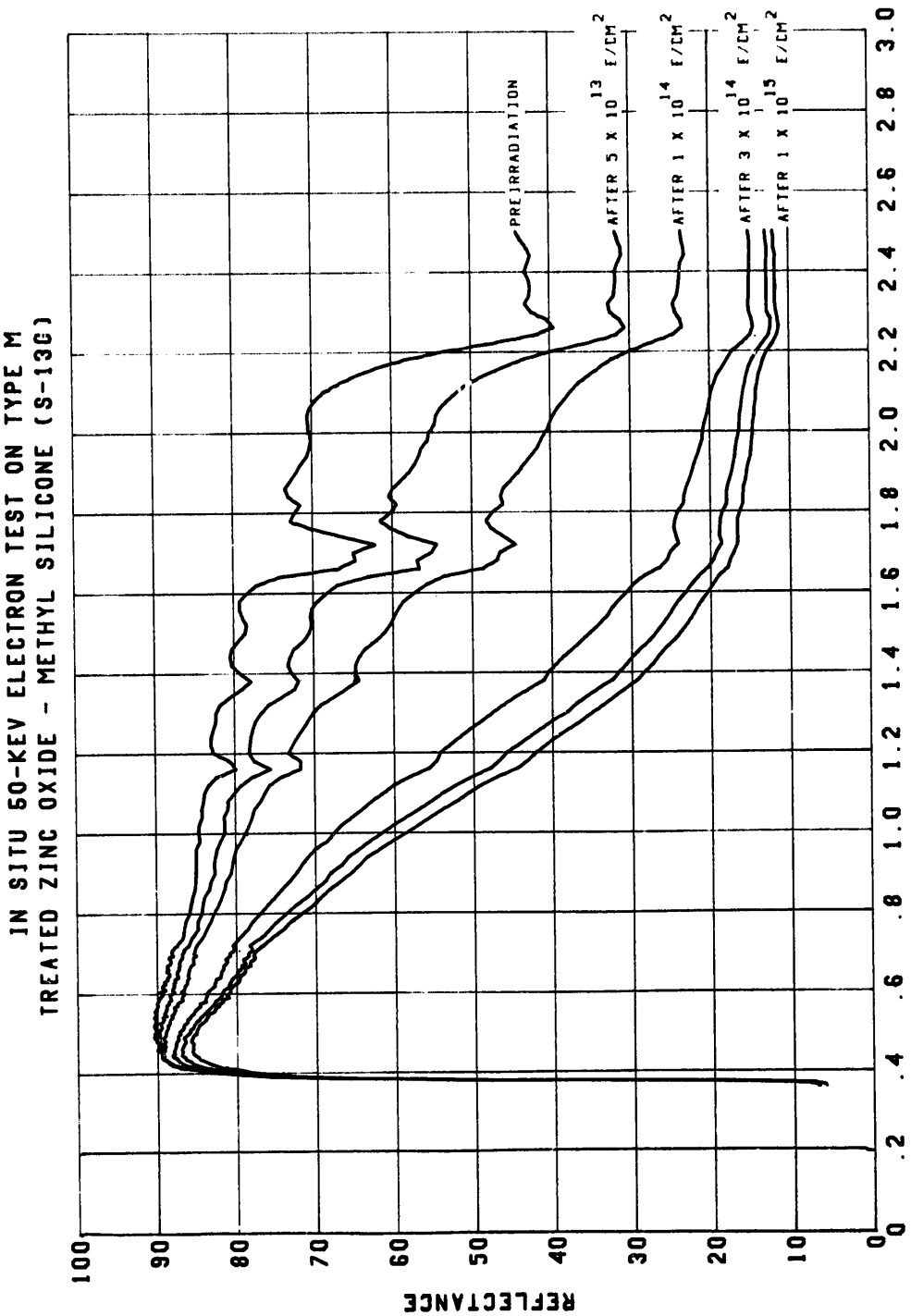

Figure 53. Effects of 50-keV Electrons on S-13G (Type M)

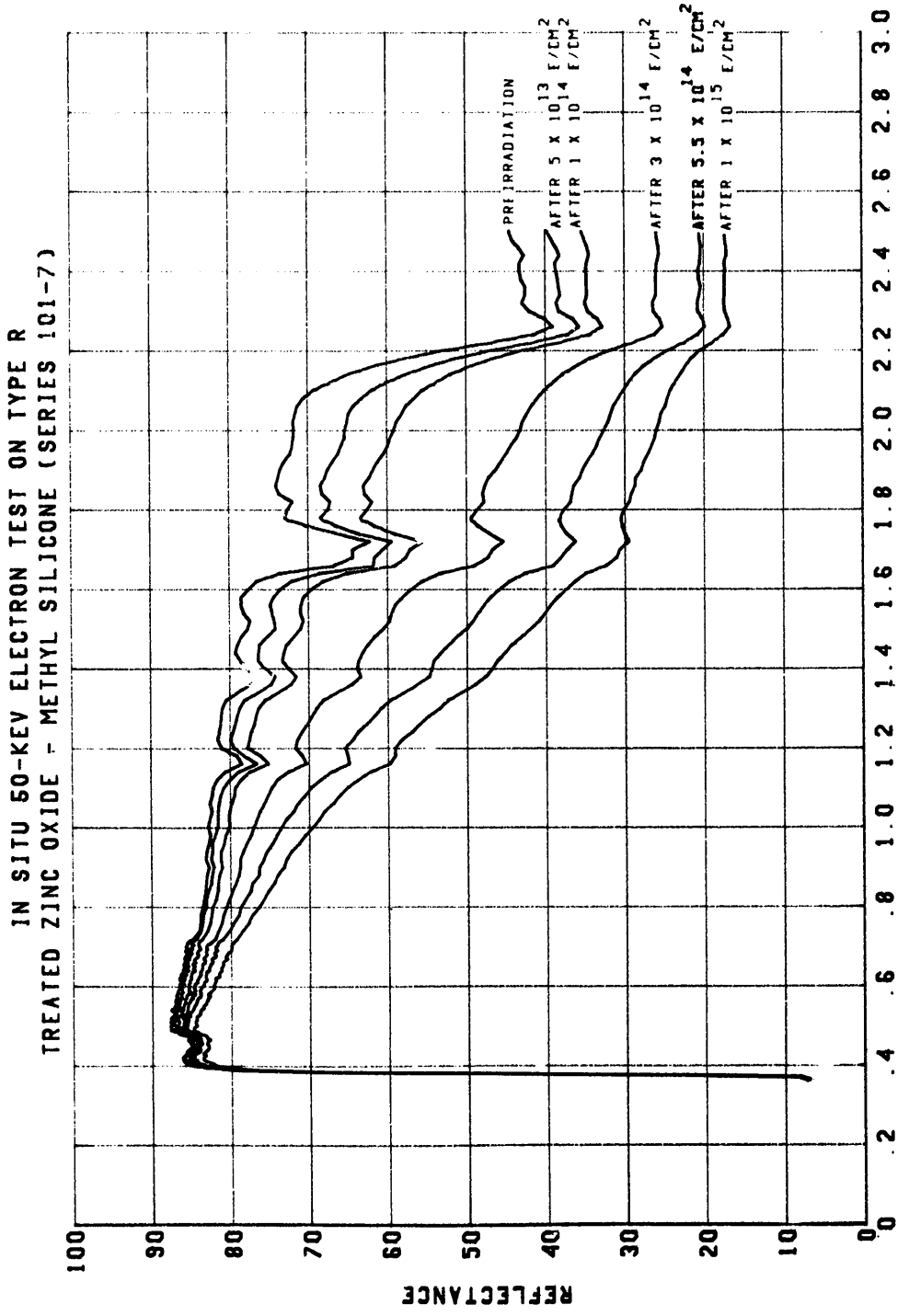

Figure 54. Effects of 50-keV Electrons on Series 101 (Type R)

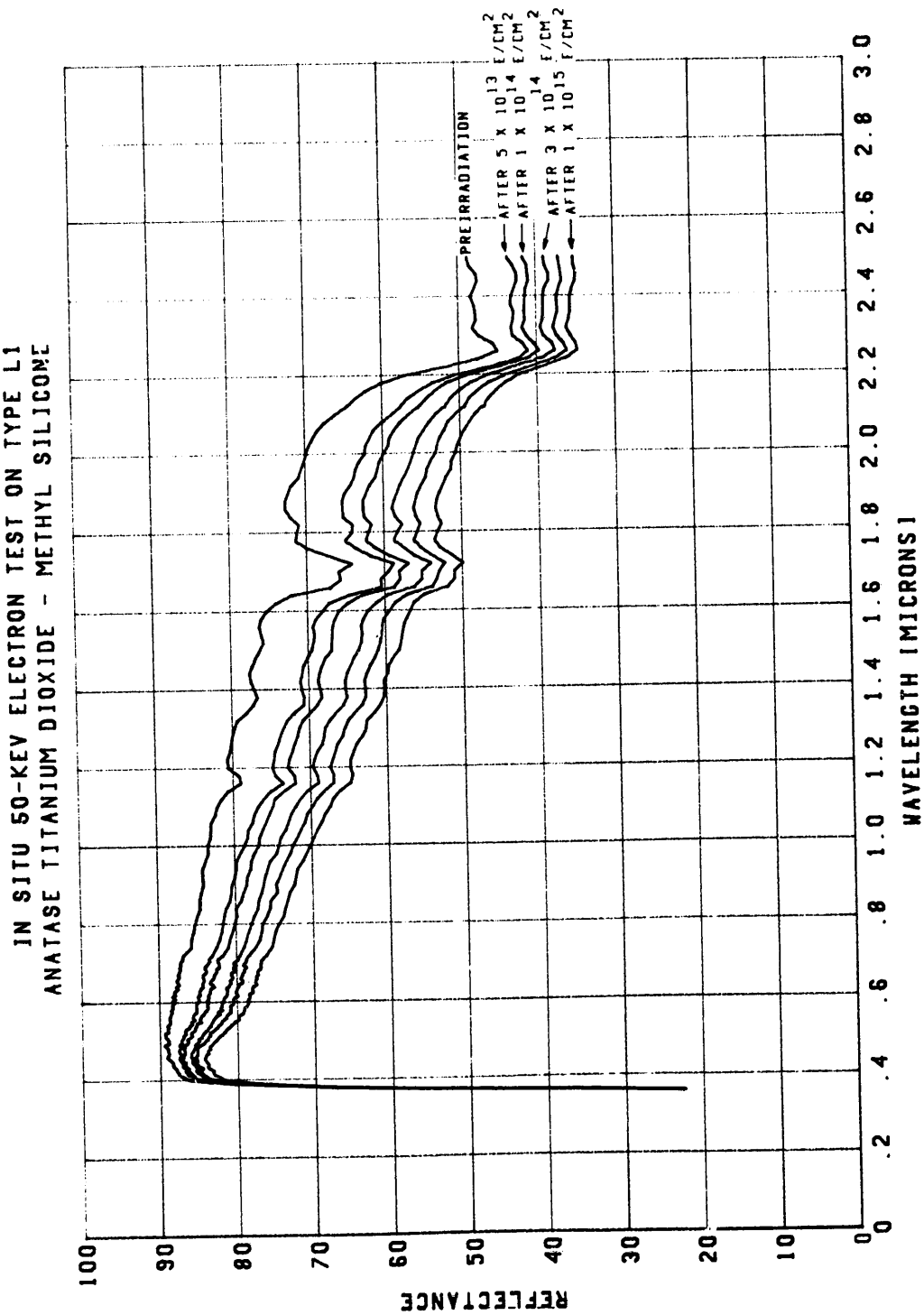

Figure 55. Effects of 50-keV Electrons on Anatase TiO_2—Methyl Silicone (Type L_1)

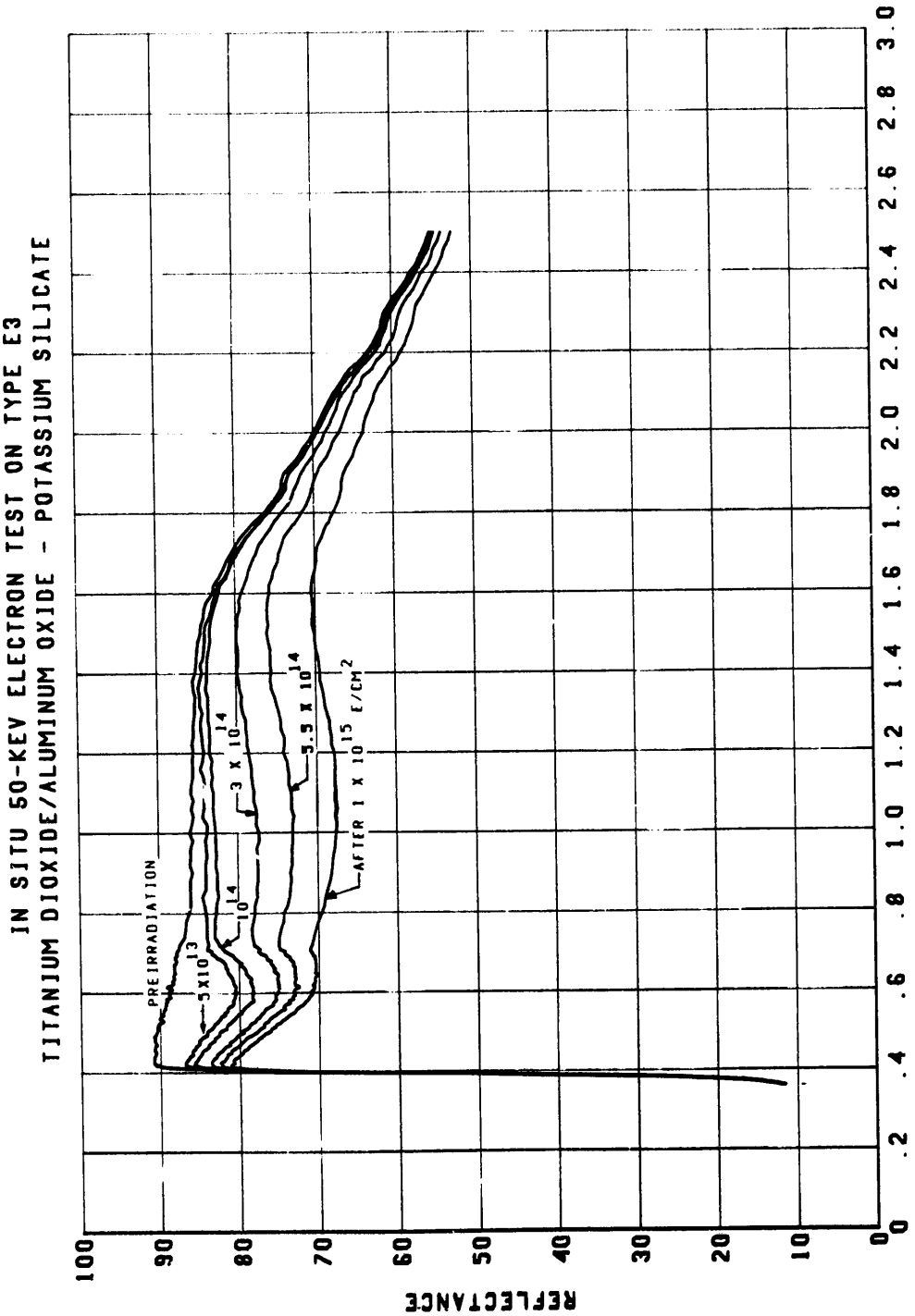

Figure 56. Effects of 50-keV Electrons on $TiO_2/Al_2O_3—K_2SiO_3$ (Type E_3)

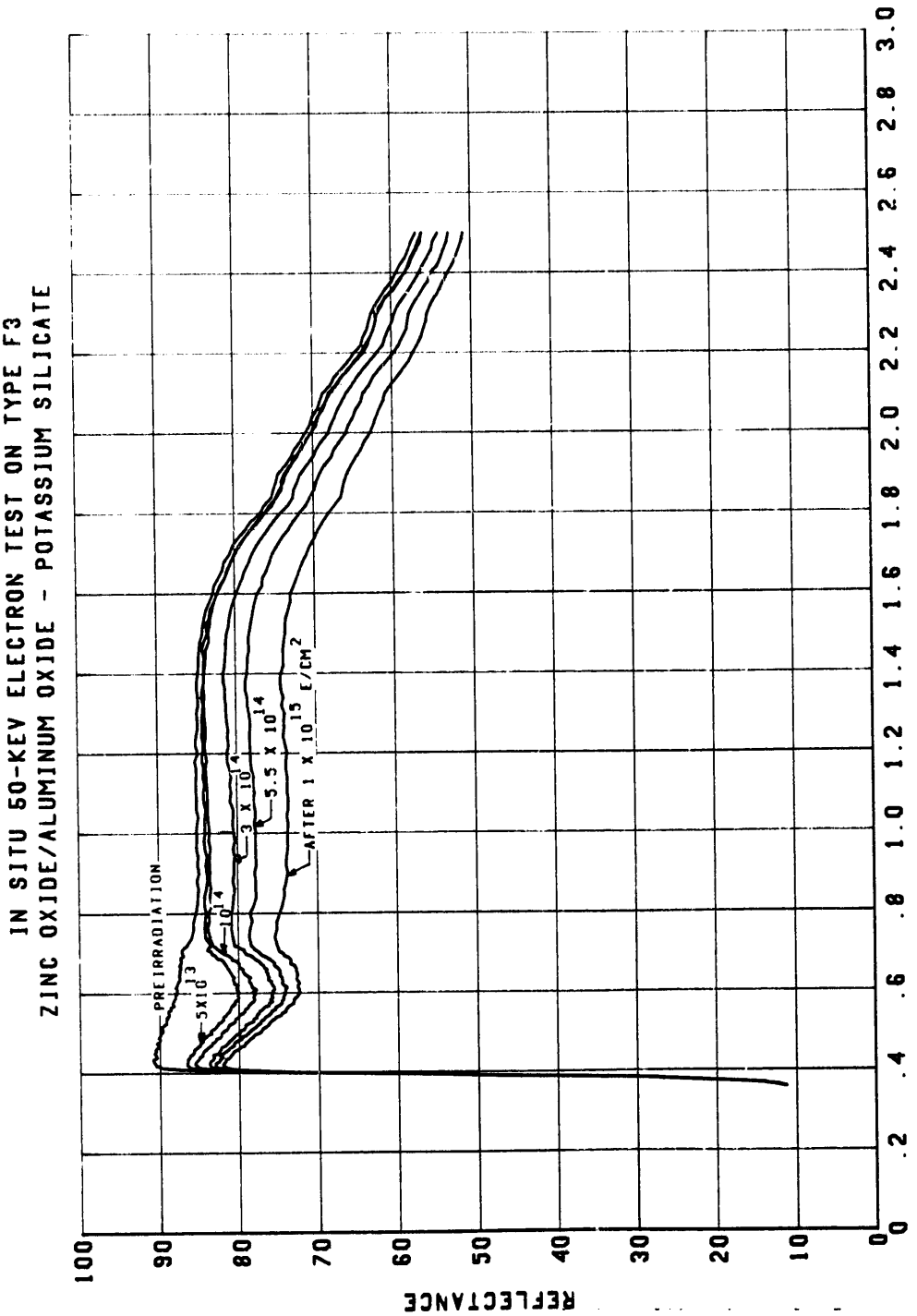

Figure 57. Effects of 50-keV Electrons on $ZnO/Al_2O_3—K_2SiO_3$ (Type F_3)

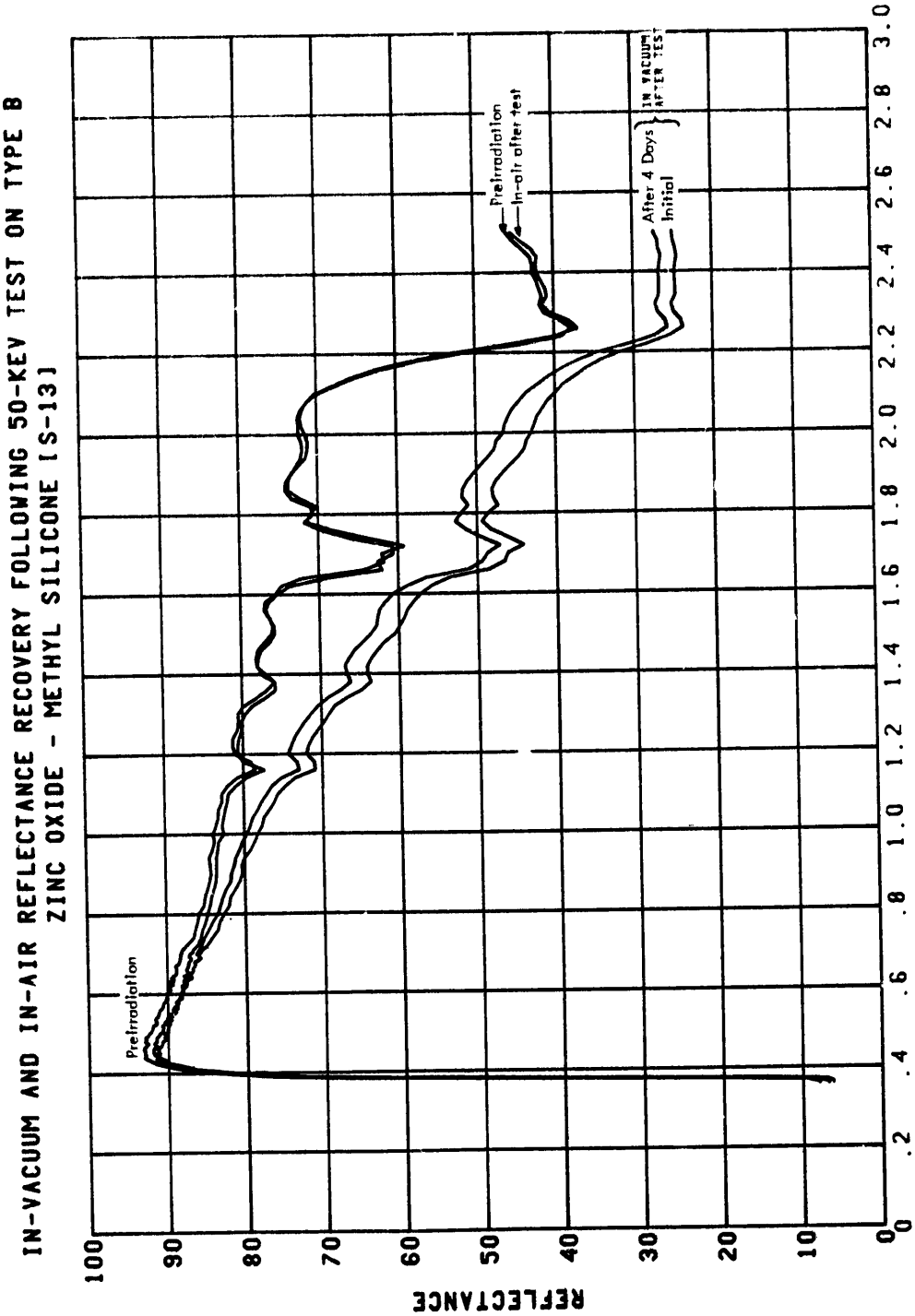

Figure 58. Reflectance Recovery in Type B (S-13) Following 50-keV Electron Test

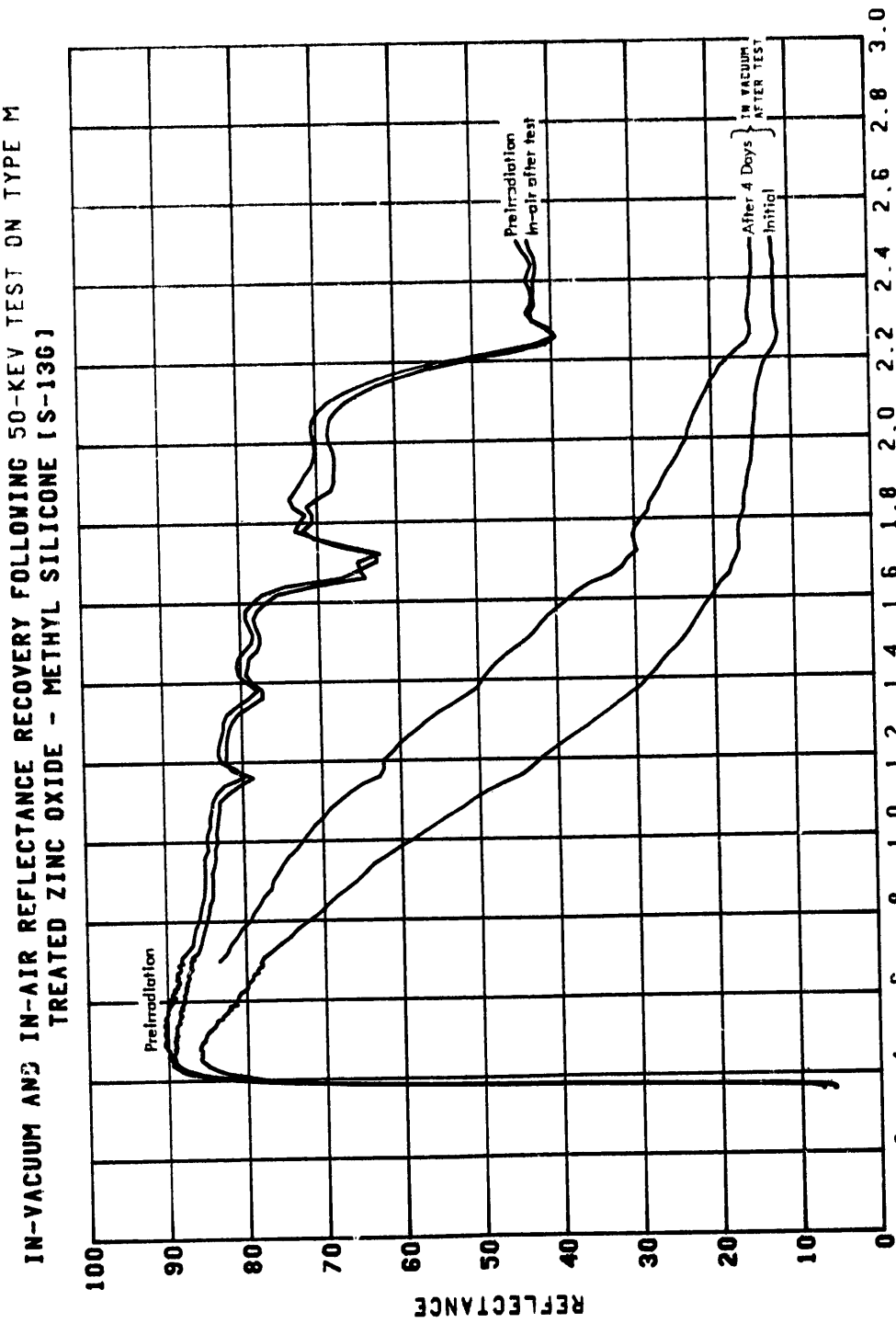

Figure 59. Reflectance Recovery in Type M (S-13G) Following 50-keV Electron Test

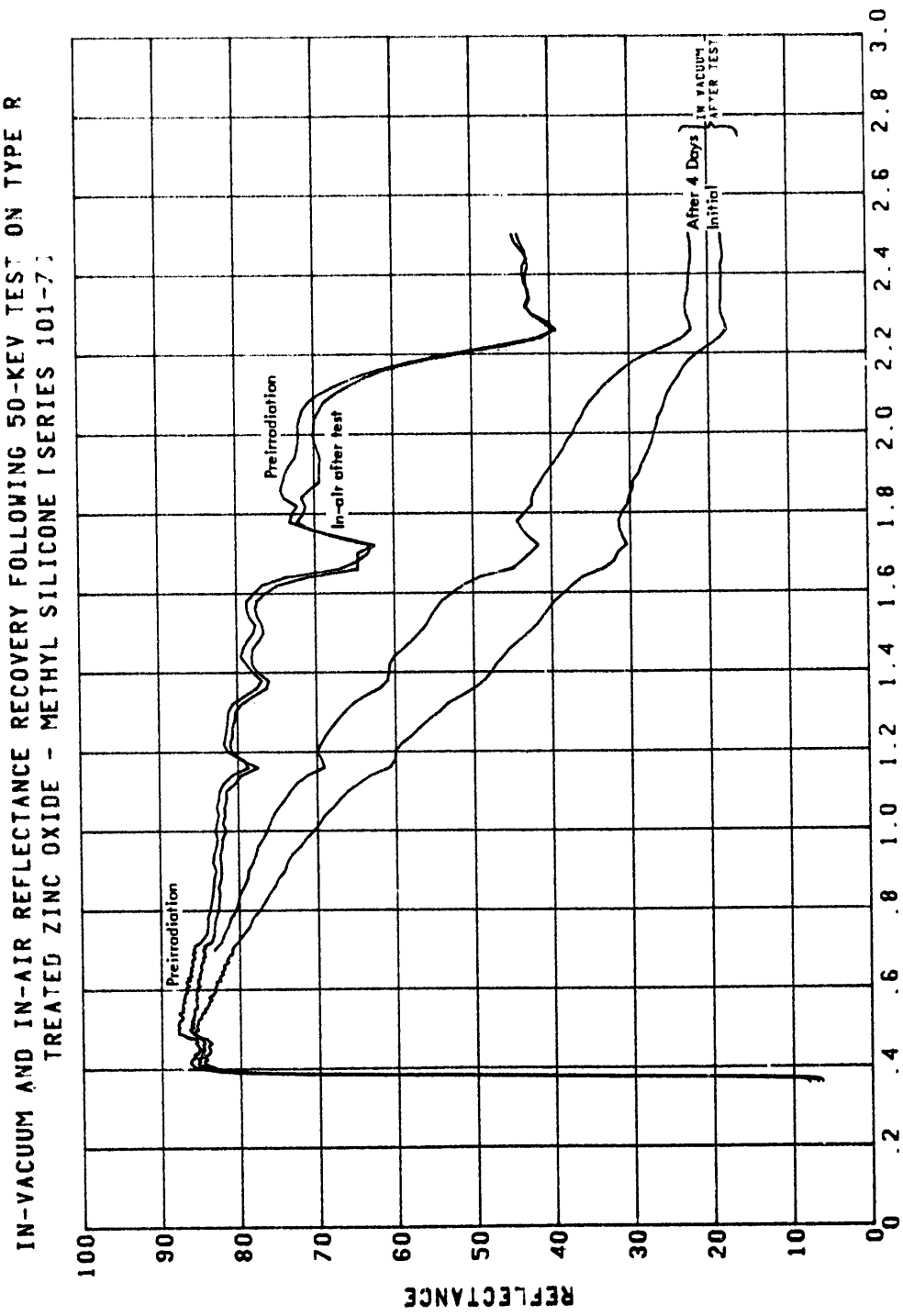

Figure 60. Reflectance Recovery in Type R (Series 101-7) Following 50-keV Electron Test

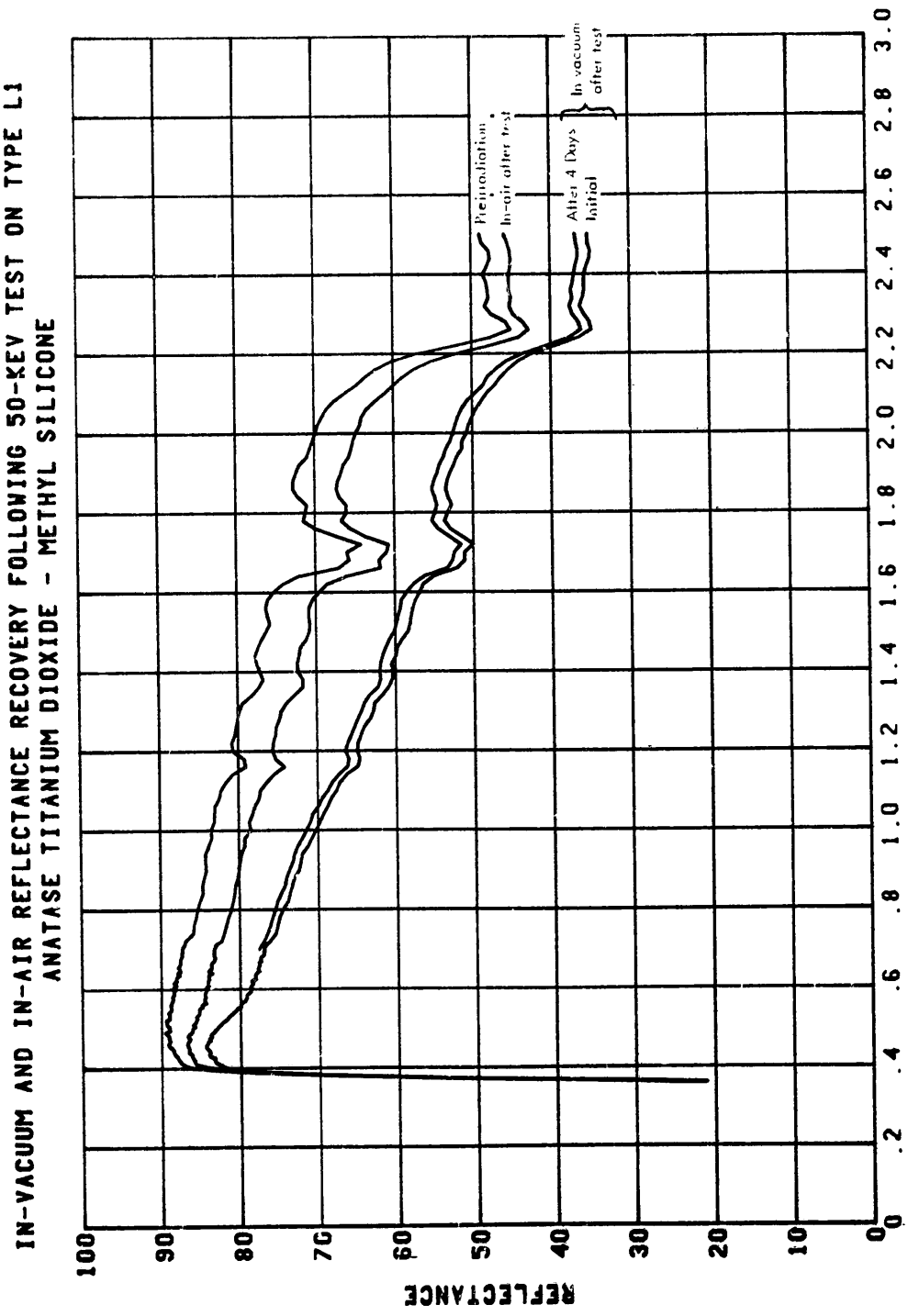

Figure 61. Reflectance Recovery in Type L_1 Following 50-keV Electron Test

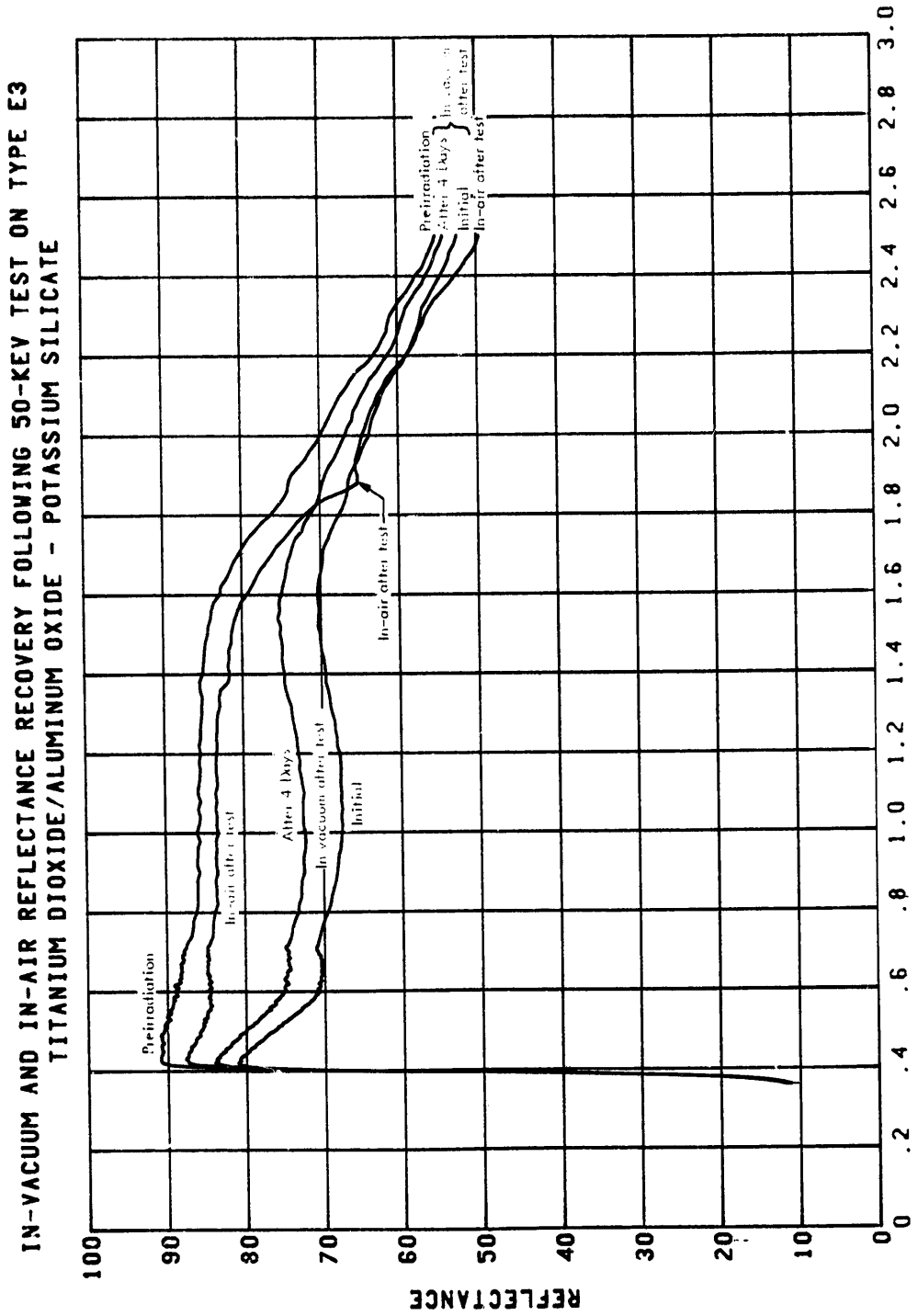

Figure 62. Reflectance Recovery in Type E_3 Following 50-keV Electron Test

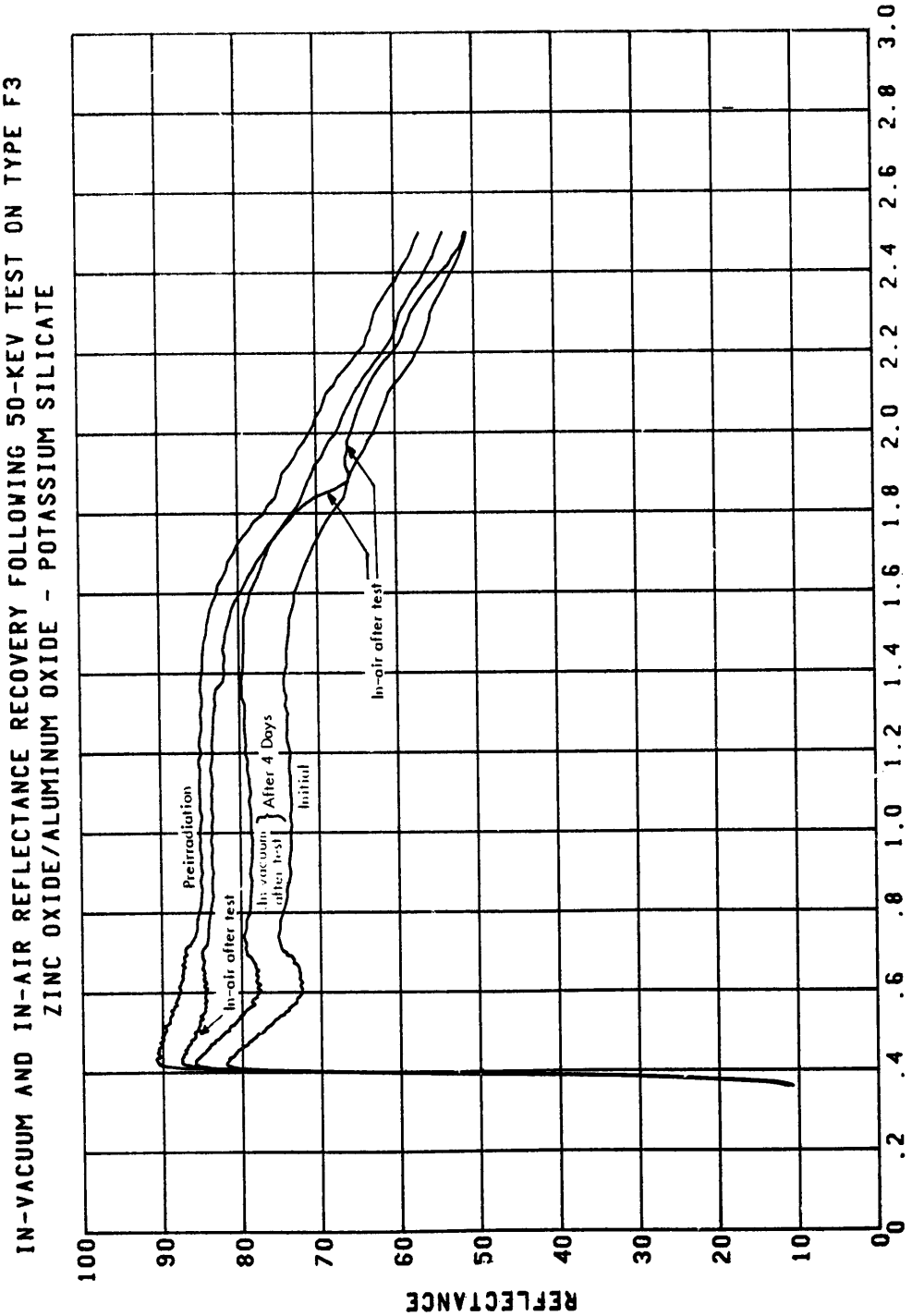

Figure 63. Reflectance Recovery in Type F_3 Following 50-keV Electron Test

2.4.6 Significance in Solving Thermal Control Coating Problems

There remain many unanswered questions concerning the effects of in-vacuum reflectance recovery on current testing practices and interpretation of exposure data.

Since the mechanisms of damage recovery are not understood, it is impossible to identify those test environmental parameters that affect it. One might attempt to explain in-vacuum recovery as an extrapolation of in-air recovery. While this may indeed be a factor, it becomes less attractive when considering the 10^{-8} and 10^{-9} torr pressure ranges wherein it is observed. It does, however, raise questions as to what role in-vacuum recovery plays in test facilities that characteristically operate in the 10^{-6} and 10^{-7} torr pressure ranges. It might, for example, affect the rate of recovery more profoundly than the extent. Were this the case, the elapsed time from end of exposure to reflectance measurement would take on increased significance, as indeed it already has in even the 10^{-8} and 10^{-9} torr pressure ranges. Measurements made during this program just minutes after the end of an exposure are felt to have "captured" or recorded the full degradation values sustained during exposure. This is based on the measurement of appreciable in-vacuum reflectance recovery only after passage of several hours following end of exposure (Figures 41-43, 45-51, and 58-63). Directional reflectance measurements made in other programs during exposure confirm this (Reference 7).

It must be remembered that the extent of recovery can only be determined from a baseline of spectral reflectance obtained immediately after exposure. The current industry-wide practice is to make one hemispherical reflectance measurement at a convenient time which may be minutes, hours, or the next working day after exposure, and attribute the indicated reflectance change solely to the damaging radiation. It is now seen that for certain types of samples the recorded damage will vary inversely with elapsed time from termination of exposure to reflectance measurement. The proportionality factor is probably a complex function including chamber residual atmosphere pressures (both component and total), sample surface temperature, particle and/or photon energy, irradiation rate and

sample composition. Since no two testing facilities identically produce a given test environment, it would be suspected that the proportionality factor would be different for each facility.

While the above discussion is necessarily speculative, the fact of in-vacuum recovery after 20-, 50-, and 80-keV electron exposure at rates from 10^{10} electrons/cm^2-second to 5×10^{11} electrons/cm^2-second cannot be denied for a considerable number of important types of coatings. Since this phenomenon has not been systematically explored, it is unknown just how many types of coatings are subject to it. Further, it is unknown as to existence and extent for the cases of electromagnetic radiation, proton exposure and combined electromagnetic and particle radiation. It is apparent that another effect has been isolated which bears on the validity of past and present laboratory test data. This effect is analogous to the in-air recovery effect which resulted in complete reappraisal of then-current measurement techniques for most kinds of coatings. In both cases, and in additional cases that may come to light in the future, it is the lack of understanding damage mechanisms that allows unrealistic testing procedures to continue.

Past and current testing philosophy encompasses rectifying test deficiencies as they are identified and anticipation of further deficiencies resulting from known imperfections in environment simulation, but includes only token interest in understanding damage mechanisms. It appears to these investigators that considerable progress toward the goal of formulating damage models could be achieved using existing data. For example, this laboratory has literally thousands of high resolution spectral reflectance charts of representative types of coatings exposed to a large variety of simulated environments. No program to date has encompassed a comprehensive integration of these data into a coherent theoretical framework.

In addition to the mass of reflectance data, other information has accumulated which should provide further insight into identifying damage mechanism modes. Both in-air and in-vacuum recovery are examples. Another example is a "noise" phenomenon discovered during exploration of in-vacuum recovery. It was found that an in situ reflectometer detector exhibited extreme noise when freshly

irradiated samples were positioned in the measurement port of the in situ integrating sphere. Different types of samples produced different noise levels and decay rates. Placement of a portion of the sample holder, rather than a sample, at the measurement port drastically reduced the noise level. The companion reflectometer detector, sensitive to a different spectral region, exhibited no measurable noise under the same conditions. Here again, pursuit of knowledge about a potentially rewarding phenomenon was beyond the work planned for, and time available during, the program.

Further investigation of these observed phenomena could provide additional information to be used in constructing damage models. The formulation of such models is admittedly a complex undertaking but one which should eventually be done.

2.5 ELECTRON ENERGY DEPENDENCE AND EQUIVALENCE

In this Section the dependence of sample reflectance degradation upon incident electron energy is discussed for sample types showing sufficient damage, and equivalences of various electron fluences for causing degradation are listed.

2.5.1 Dependence of Damage Upon Electron Energy

Data from the electron tests at 20, 50, and 80 keV have been combined and plotted together in Figures 64 through 73, to present the electron energy dependence of reflectance degradation over the 20- to 80-keV electron spectrum, and to allow a direct comparison of the performance of ZnO—methyl silicone, TiO_2—methyl silicone, metal oxide—potassium silicate, Kapton H-film, and Alzak coatings at the several test energies. The preirradiation reflectance of each specimen used at the several test energies, and specimen reflectance after exposure to selected electron fluences, are portrayed in Figures 64-73.

Figures 64 through 68 present test data for samples in methyl silicone binders (types B, M, R, L_1, and O). These figures show in common the ability of 80-keV electrons to eradicate infrared-region absorption bands at the higher fluences; on the other hand, the samples are able to retain infrared structure under 20-keV electron exposure. These figures also reveal the different response of these sample types in the visible wavelength region, to 10^{16} electrons/cm^2 of 20- and 80-keV energy. Especially in types B (S-13) and M (S-13G), the wavelength shift of the so-called "UV edge" is seen to cut more deeply under 20-keV electron exposure, than it does under 80-keV exposure.

Figure 64 shows that degradation in S-13 from 20-keV electrons is sufficiently confined as to extent, that 10^{14} electrons/cm^2 of either 50-keV or 80-keV energy cause more damage than 10^{16} 20-keV electrons/cm^2.

Figure 65 reveals that S-13G does not behave quite the same way, 10^{16} 20-keV electrons/cm^2 causing greater degradation at wavelengths shorter than 1.7 microns, than 10^{14} 50-keV or 80-keV electrons/cm^2 cause. However, the figure also shows an interesting effect—that the "soft" electrons (speaking of 10^{16} 20-keV

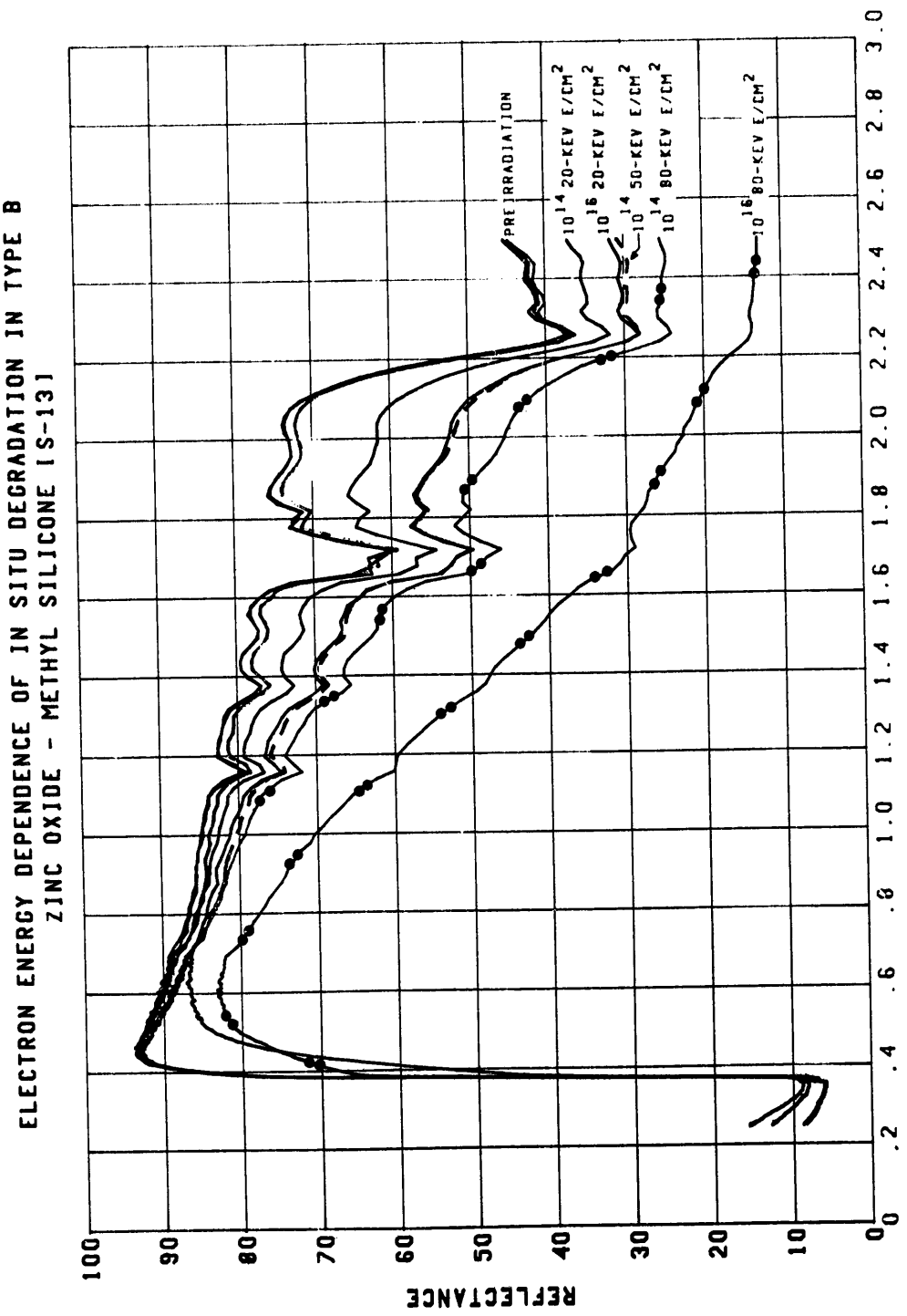

Figure 64. Dependence of Reflectance Degradation in S-13 (Type B) Upon Electron Energy

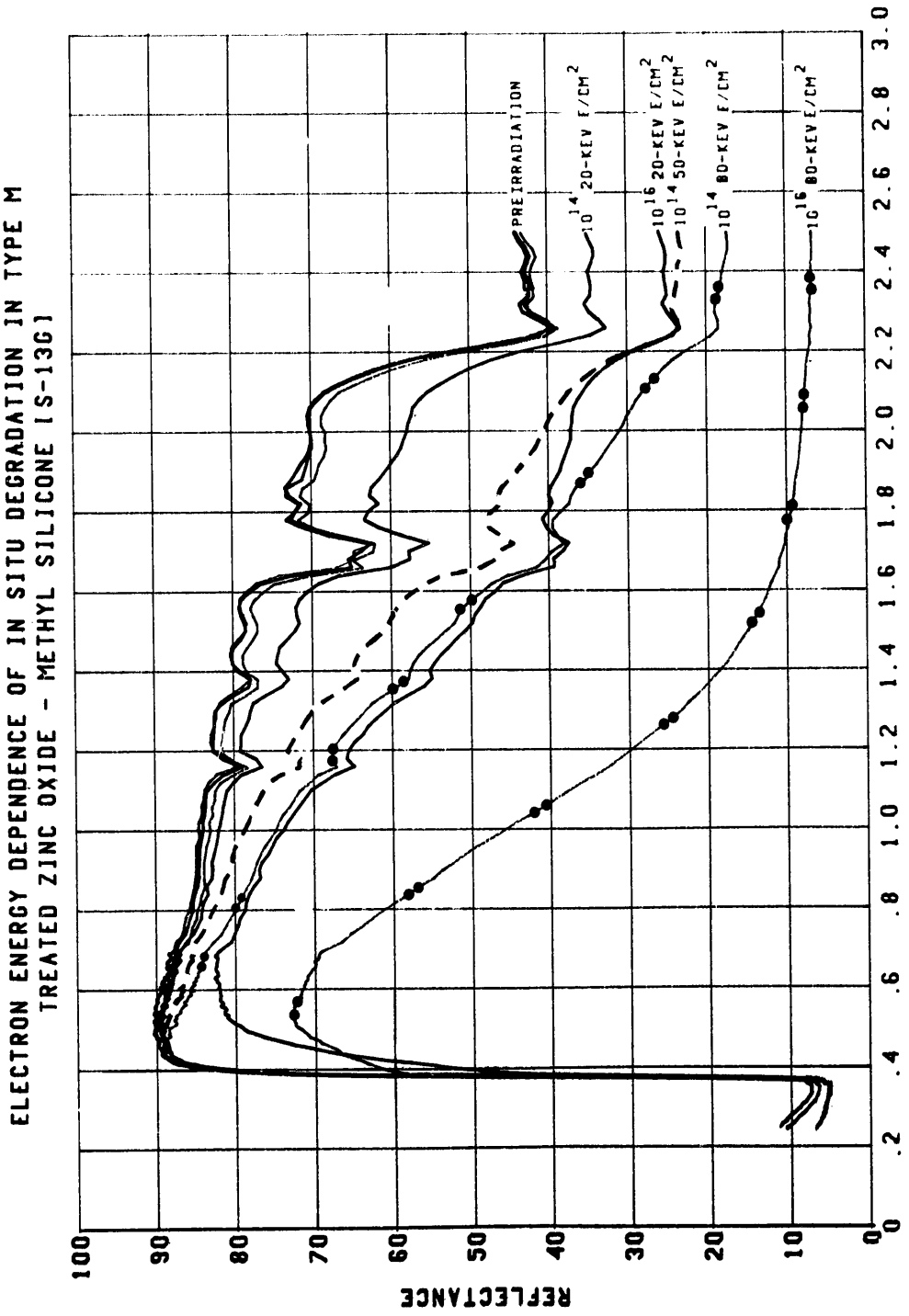

Figure 65. Dependence of Reflectance Degradation in S-13G (Type M) Upon Electron Energy

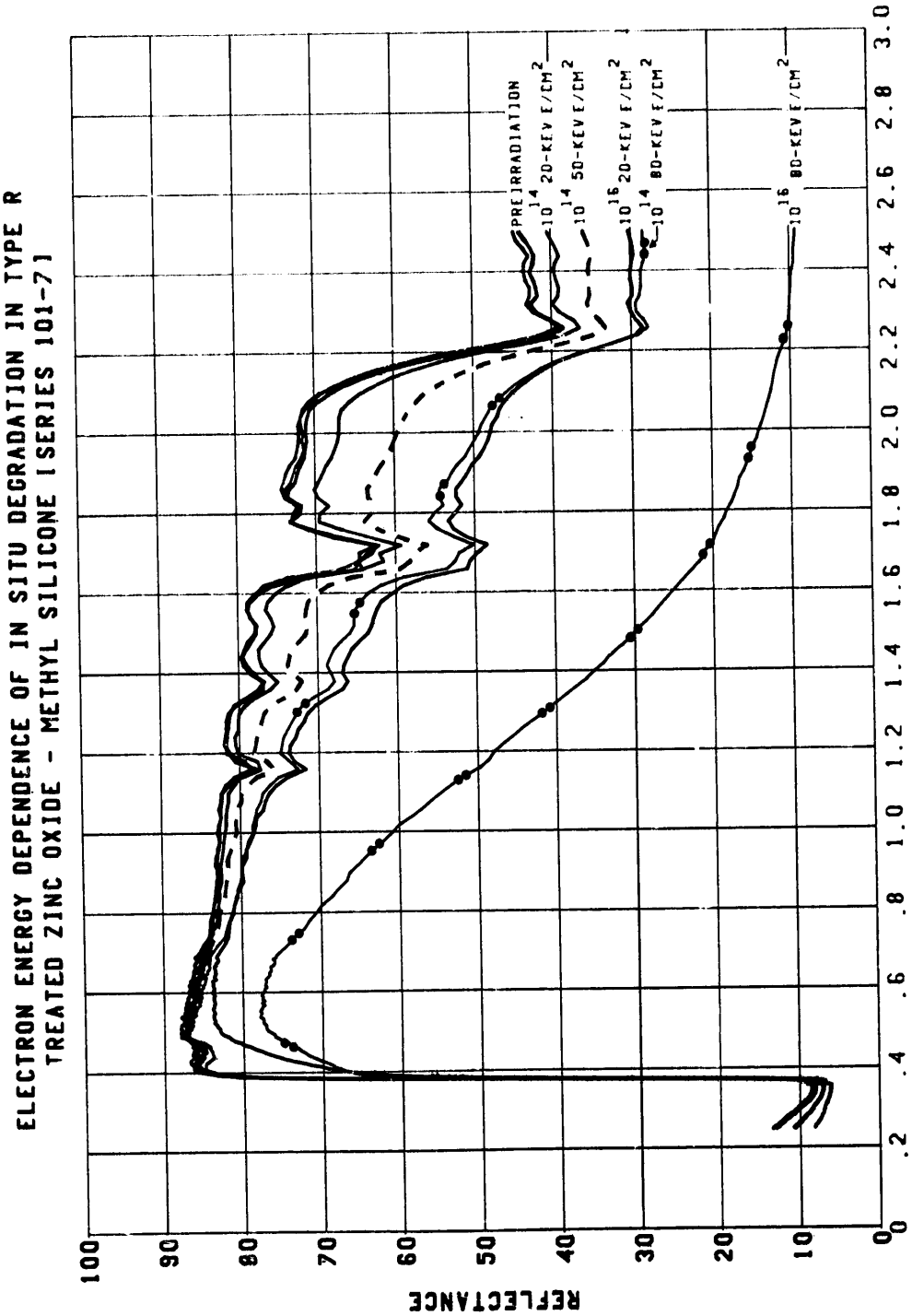

Figure 66. Dependence of Reflectance Degradation in Goddard Series 101-7-1 (Type R) Upon Electron Energy

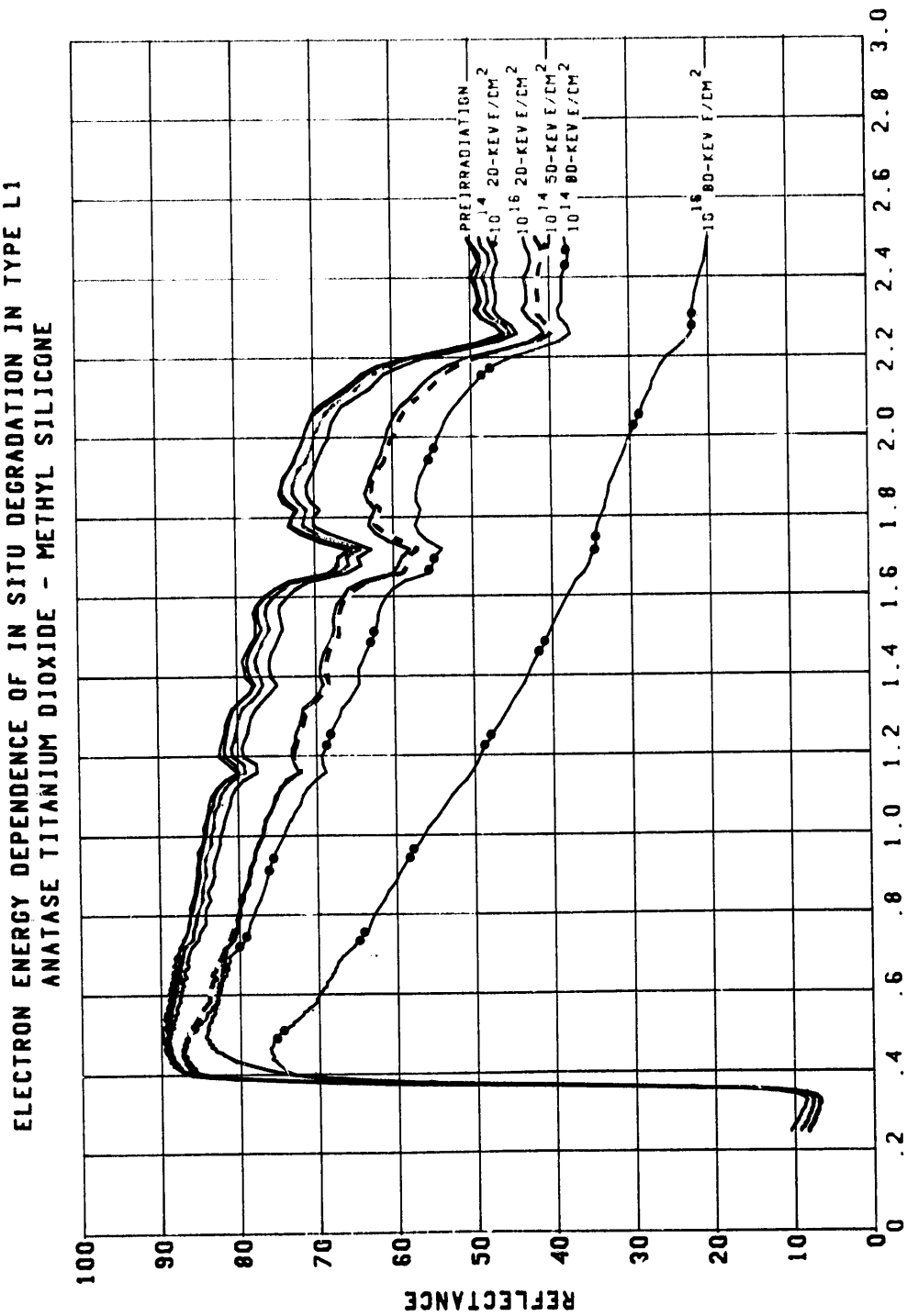

Figure 67. Dependence of Reflectance Degradation in Anatase TiO_2—Methyl Silicone (Type L_1) Upon Electron Energy

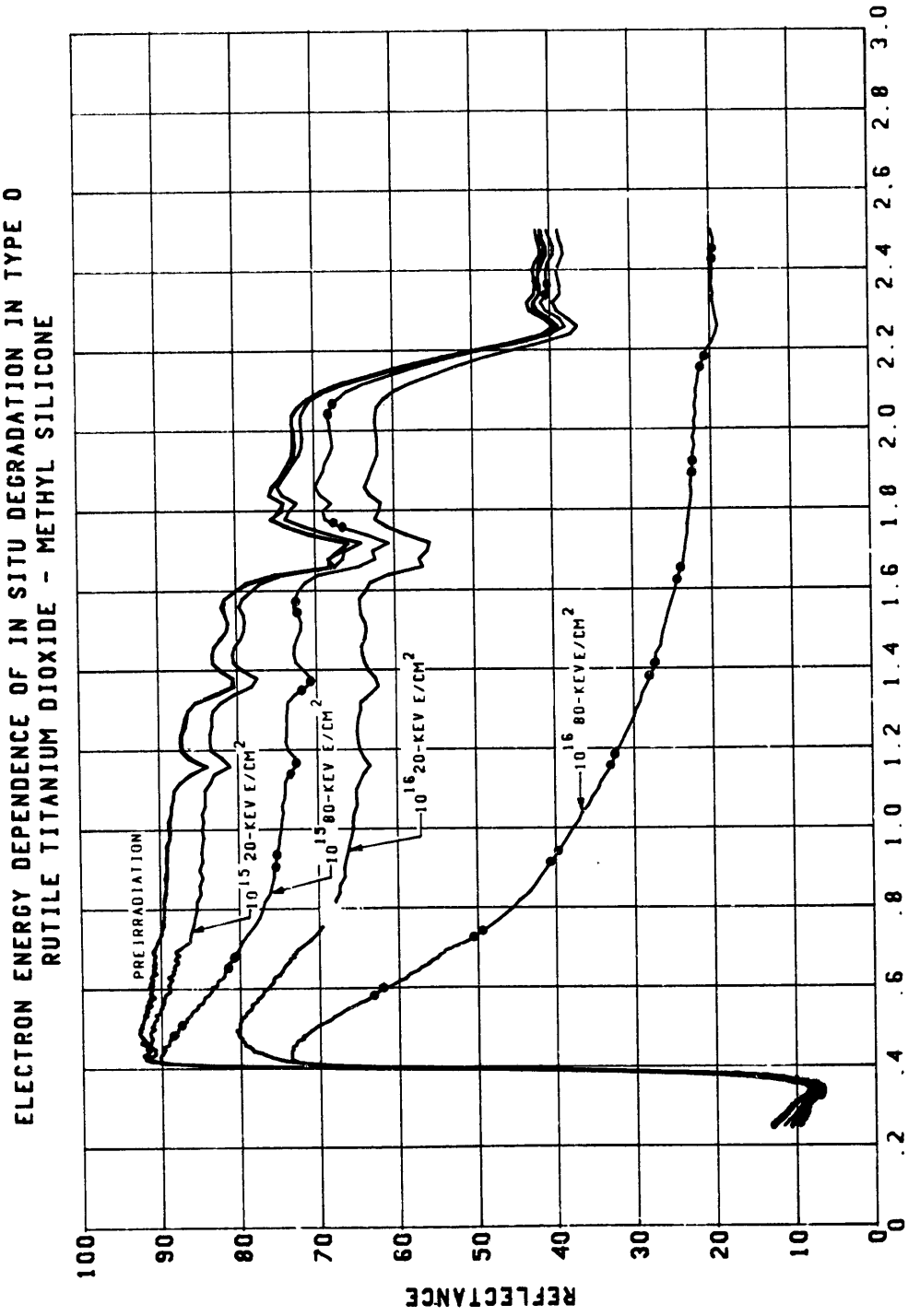

Figure 68. Dependence of Reflectance Degradation in Rutile TiO_2—Methyl Silicone (Type O) Upon Electron Energy

electrons/cm^2) are limited much more as to ability to degrade S-13G reflectance at wavelengths longer than 1.7 microns. The 10^{16} 20-keV curve crosses both the 10^{14} 80-keV curve and the 10^{14} 50-keV curve, the latter at 2.2 microns.

In Figures 66 and 67 (types R and L_1), the only "catastrophic" degradation shown is the 10^{16} 80-keV exposure case.

Figure 68, for type O TiO_2—methyl silicone, like Figures 5 and 22, shows this sample's resistance to damage at lower electron fluences, and its poor response as fluences become greater than 10^{15} electrons/cm^2. Again, catastrophic degradation is indicated following exposure to 10^{16} 80-keV electrons/cm^2.

Figure 69 indicates that 20-keV and 80-keV electrons effect different spectral profiles of degradation in the visible-region "silicate band" of type D_3 (Al_2O_3—potassium silicate) and in the near-ultraviolet region. The visible-region absorption band is deeper and more sharply defined after 80-keV exposure than after 20-keV exposure. In contrast, damage in the near-ultraviolet is greater after 20-keV electron exposure.

Data for types E_3 and F_3 (TiO_2/Al_2O_3—potassium silicate and ZnO/Al_2O_3—potassium silicate, respectively), shown in Figures 70 and 71, indicate the severe damage incurred from exposure to 10^{16} electrons/cm^2 of energy at either extreme studied, 20 keV or 80 keV. The reflectance curves also indicate correctly that degradation from 50-keV electrons in the mid-10^{14} fluence range (3×10^{14} is shown) is virtually indistinguishable from degradation caused by exposure to the same 80-keV electron fluence. The visible-region spectral profiles noted for type D_3 carry over to types E_3 and F_3. That is, 20-keV electron damage in the "silicate bands" of types E_3 and F_3 is confined to values small enough that there is a smooth coupling at 0.7 micron wavelength to the near-infrared region degradation resulting from the presence of TiO_2 and ZnO pigments in types E_3 and F_3 respectively. In the case of 80-keV degradation, however, the silicate band damage in types E_3 and F_3 is deep enough that the spectral profile reveals a distinct trough between 0.5 and 0.7 micron, as with type D_3. This profile of damage stands out most

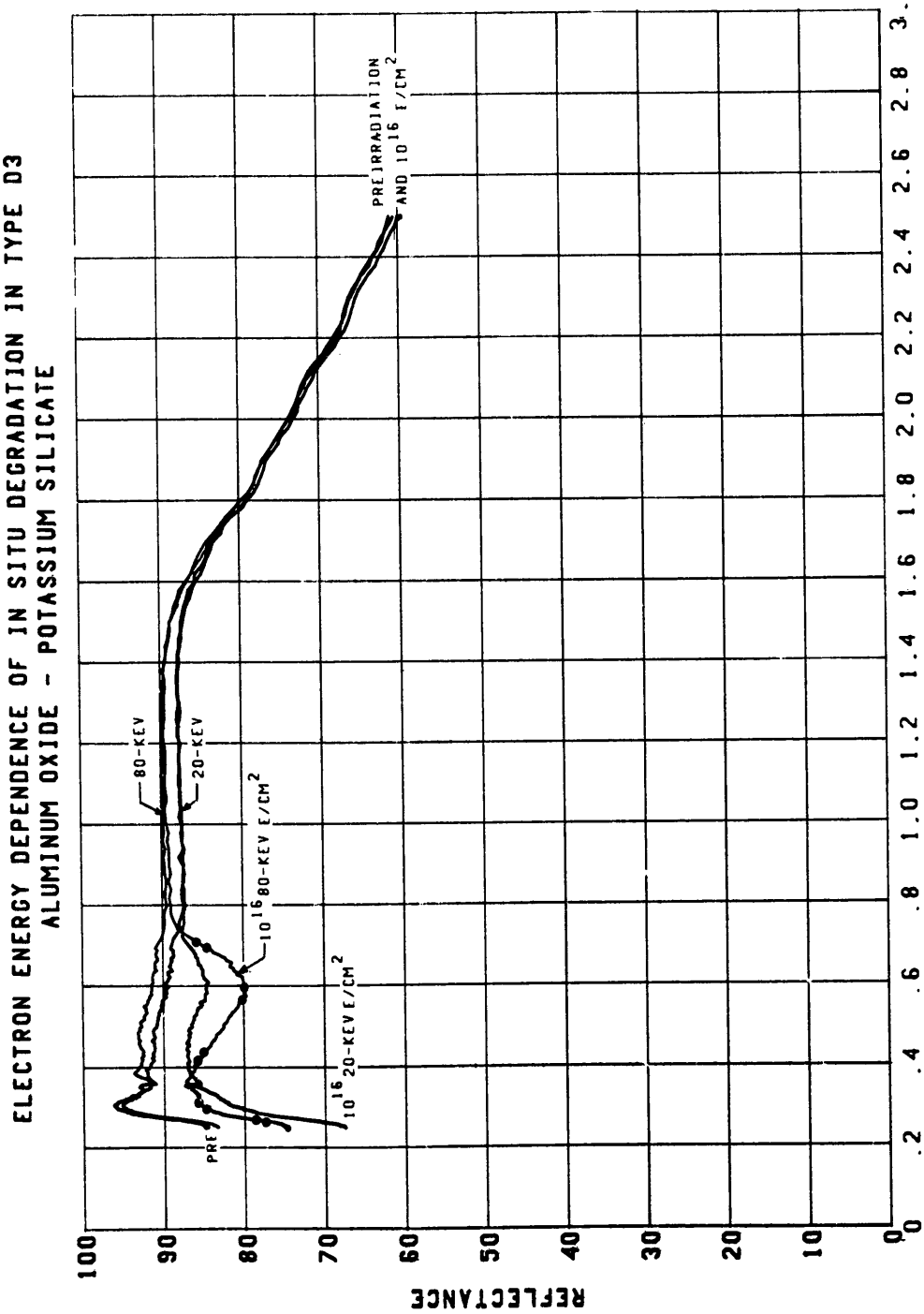

Figure 69. Dependence of Reflectance Degradation in Al_2O_3—K_2SiO_3 (Type D_3) Upon Electron Energy

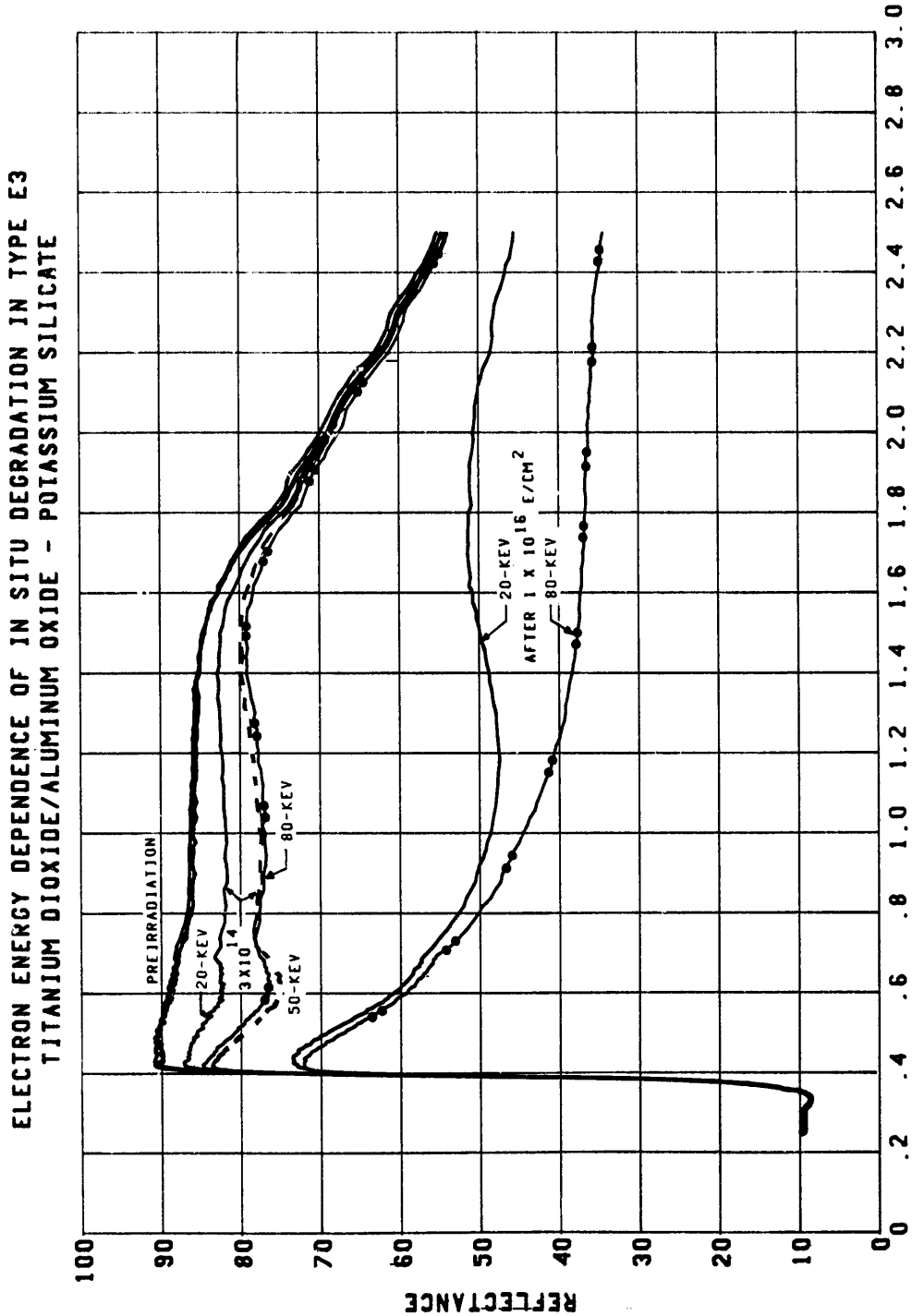

Figure 70. Dependence of Reflectance Degradation in TiO_2/Al_2O_3—K_2SiO_3 (Type E_3) Upon Electron Energy

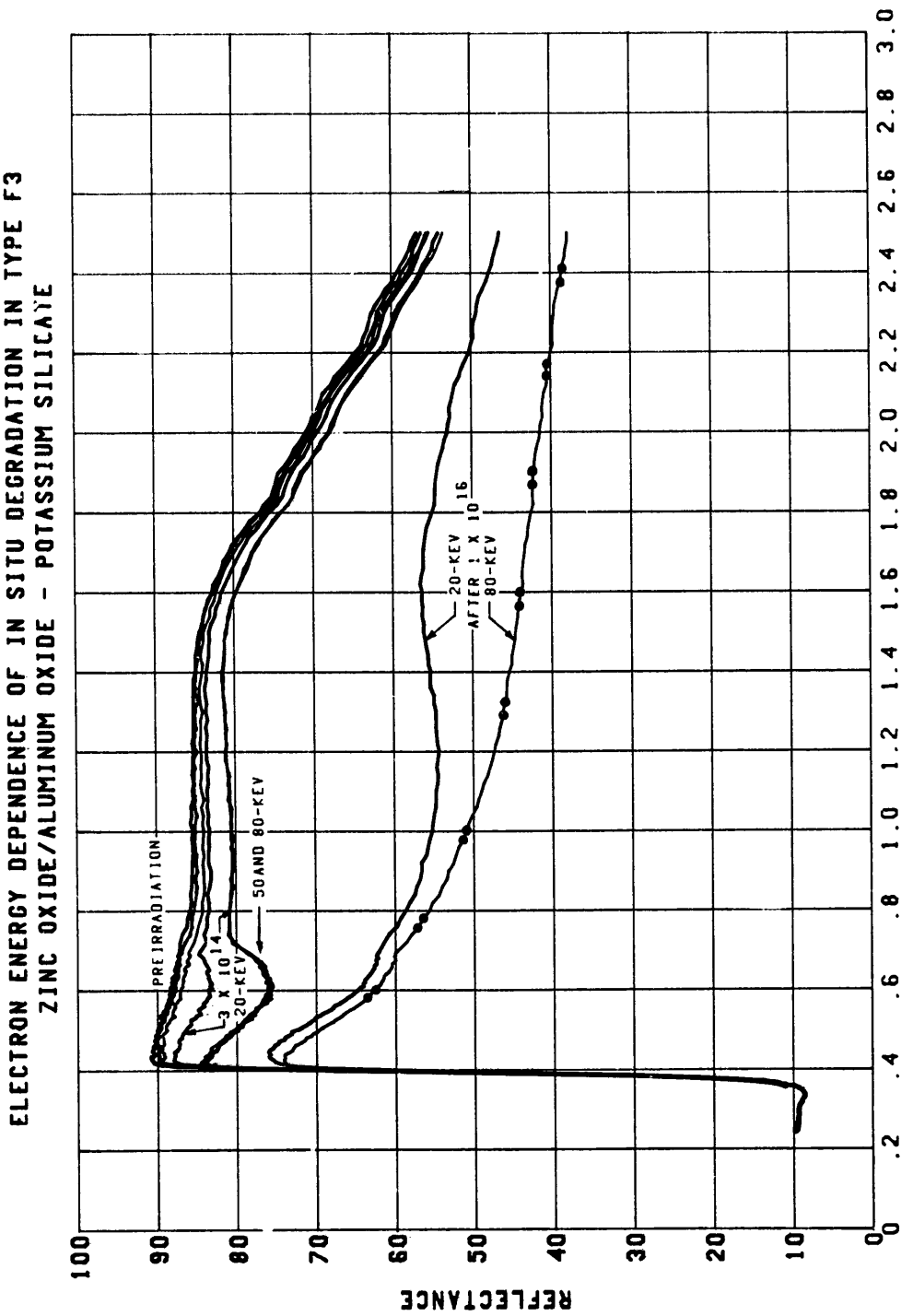

Figure 71. Dependence of Reflectance Degradation in ZnO/Al_2O_3—K_2SiO_3 (Type F_3) Upon Electron Energy

strongly in the 10^{14} electron fluence range; at 10^{16} electrons/cm^2, total degradation in types E_3 and F_3 is so severe that the visible-region absorption is almost entirely masked.

Reflectance-change data in Kapton H film (type N) following 20-, 50-, and 80-keV exposures are compared in Figure 72. The highest 50-keV exposure data obtained is 10^{15} electrons/cm^2. The limited extent of 20-keV degradation, when contrasted with that resulting from 50-keV or 80-keV exposure, is readily apparent. An exception is the greater ultraviolet-region degradation of Kapton H-film which results from exposure to 20-keV electrons.

In all cases heretofore examined — diffuse white coatings and Kapton H-film — it is evident that degradation from 20-keV electrons is confined to much smaller amounts than occurs with 50- or 80-keV electrons. A contrasting case is Alzak, in which 20-keV electron damage is greater. A comparison of Figures 9, 10, and 11 (Alzak after 20-keV exposure) with Figures 26, 27, and 28 (Alzak after 80-keV exposure) shows this to be the case. The largest differences are found in 0.15-mil Alzak (Type Z_3), the thinnest overcoating tested. For type Z_3 the reflectance changes following exposure to the higher 20-keV and 80-keV electron fluences are shown together in Figure 73.

The significant improvement in the ultraviolet-region reflectance of SiO_x over aluminum (type H) after 20-keV and 80-keV electron exposure can be compared in Figures 14 and 31.

2.5.2 Electron Energy/Fluence Equivalences

For several coatings tested, it has been possible to determine electron fluence values of the different energies — 20-, 50- and 80-keV — which give closely matched or equivalent reflectance-change results. These equivalences are listed in Table 4. Most of the fluence equivalences listed are very closely matched (typically within 2 percent) over most or all of the 0.25 - to 2.5 micron wavelength region measured. In three cases specifying a fluence equivalent to 1×10^{16} 20-keV electrons/cm^2, the infrared wavelength region from 0.7 to 2.5 microns has been considered in selecting the equivalent fluence.

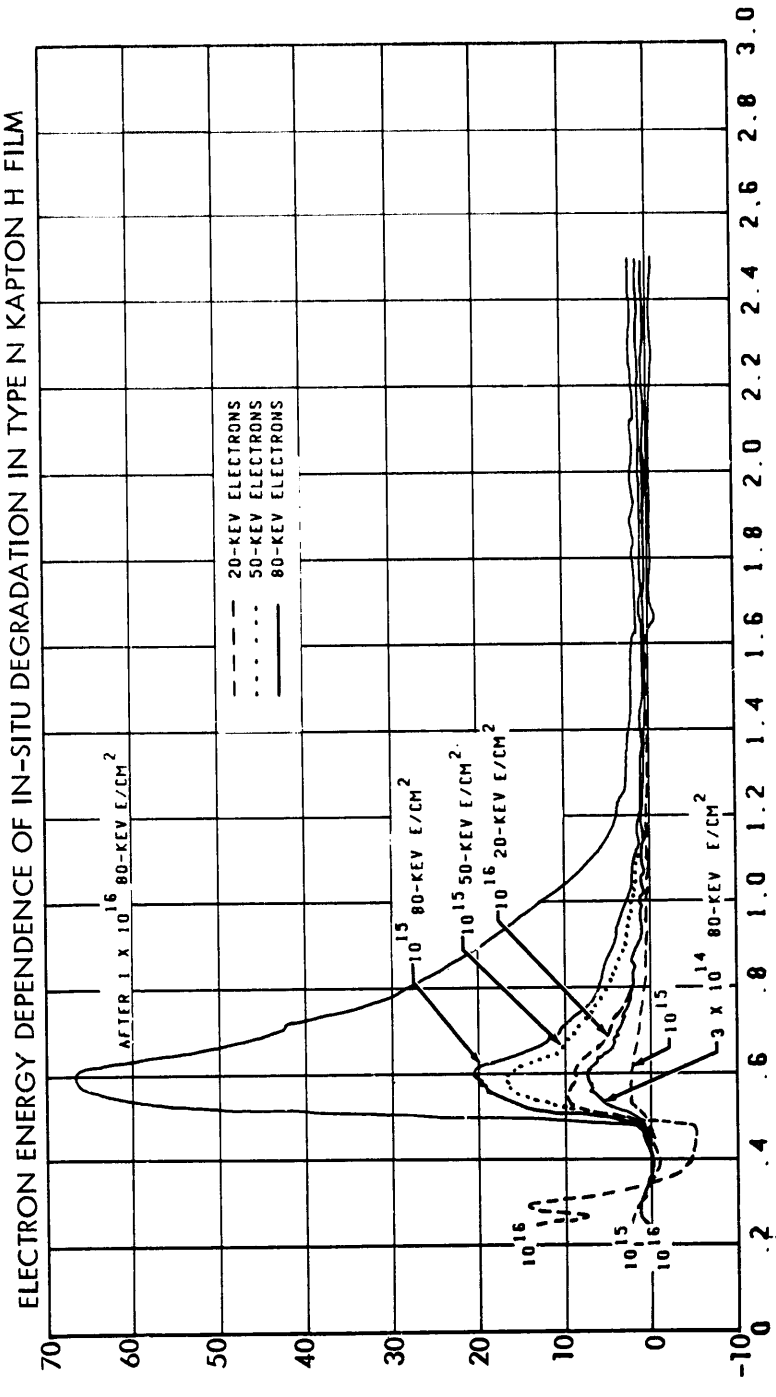

Figure 72. Dependence of Reflectance Degradation in Kapton H Film (Type N) Upon Electron Energy

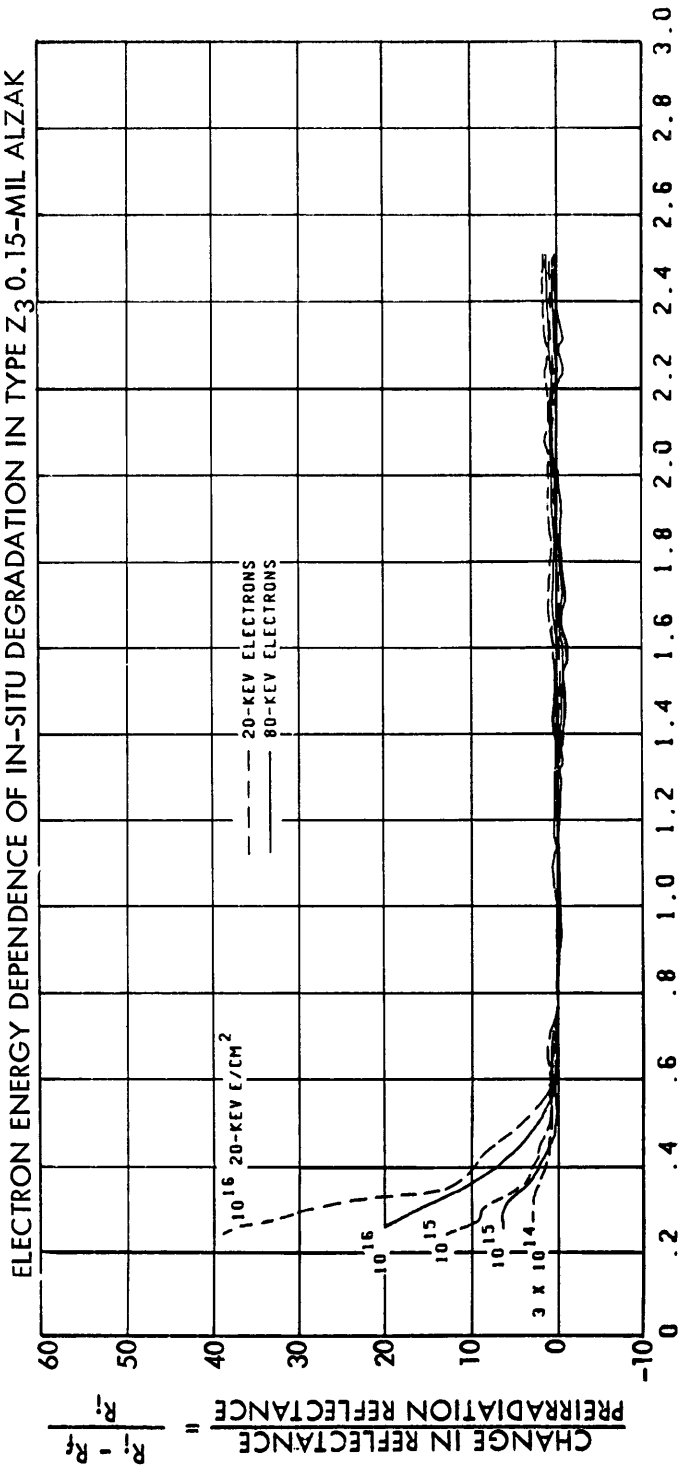

Figure 73. Dependence of Reflectance Degradation in 0.15-mil Alzak (Type Z_3) Upon Electron Energy

Table 4. Equivalence of Various Electron Fluences of Different Energies for Causing Similar Reflectance Degradation

Type of Coating		Electrons/cm^2 Equivalences			Reflectance Curves Match Within *
		20-keV	50-keV	80-keV	
ZnO—methyl silicone	S-13 (B)	5×10^{13}		1×10^{13}	0 - 1 Percent
		3×10^{14}	5×10^{13}		0 - 2 Percent
		1×10^{15}		5×10^{13}	0 - 3 Percent
		1×10^{16}	1×10^{14}		0 - 1 Percent
	S-13G (M)	5×10^{13}		1×10^{13}	0 - 2 Percent
		1×10^{14}	5×10^{13}		0 - 2 Percent
		1×10^{16}		1×10^{14}	0 - 5 Percent
	101-7-1 (R)	1×10^{14}	5×10^{13}		0 - 2 Percent
		3×10^{14}	1×10^{14}	5×10^{13}	0 - 2 Percent
		1×10^{15}		1×10^{14}	0 - 3 Percent
TiO_2—methyl silicone	L_1	**5×10^{14}		5×10^{13}	0 - 1 Percent
		1×10^{15}	5×10^{13}		1 - 2 Percent
		1×10^{16}	1×10^{14}		1 - 2 Percent
			3×10^{14}	1×10^{14}	0 - 2 Percent
	O	3×10^{14}		1×10^{14}	0 - 1 Percent
		1×10^{15}		3×10^{14}	0 - 2 Percent
Silicate-bound (E_3 and F_3)		3×10^{14}		1×10^{14}	0 - 3 Percent
		1×10^{15}	3×10^{14}	3×10^{14}	0 - 4 Percent
Kapton H-Film (N)		1×10^{16}		3×10^{14}	0 - 4 Percent

* Reflectance match over most or all of the 0.25- to 2.5-micron wavelength region measured; where a 1×10^{16} fluence is compared, the match refers to the infrared region only (except type N).

** Not a test point, but provides closest match.

2.6 DATA COLLECTION AND PROCESSING

2.6.1 General Description

Sample spectral reflectance over the wavelength region from 0.25 to 2.5 microns is simultaneously recorded on standard charts and IBM cards. An in situ integrating sphere reflectometer coupled to a far ultraviolet Beckman DK-2A spectrophotometer provides standard charts of percent reflectance versus wavelength. A separate chart for the ultraviolet, visible and near infrared regions is utilized to provide superior wavelength resolution. Datex precision encoders coupled to the spectrophotometer's ordinate and abscissa drive systems operate an IBM 526 card punch through a Datex interfacing module.

2.6.2 Collection Frequency

The standard charts provide continuous spectral reflectance data from 0.25 to 0.36 microns in the ultraviolet, 0.36 to 0.71 microns in the visible and 0.71 to 2.50 microns in the near infrared. Reflectance-wavelength pairs are punched on IBM cards at 2 millimicron intervals in the ultraviolet, 5 millimicron intervals in the visible region, and at 20 millimicrons in the near infrared region. More frequent data collection requires operating the spectrophotometer at reduced scanning speeds which significantly increases test costs. Less frequent card data collection affords no economic advantage since optimum spectrophotometer scanning speeds cannot be increased without sacrificing spectral resolution. Data collection modes other than pre-selected wavelength interval can be selected with the Datex interfacing module and are discussed further in Section 2.6.5.

2.6.3 Test Parameter Card Entries

The Datex system allows ten digits of identification data to be entered manually on each IBM card. Card columns 67 through 76 are used for this purpose and contain the following information:

Card Column(s)	Information
67-68	Sample type (NASA letter designation)
69-70	Sample wheel number location during test and NASA--designated number identification
71	Date(s) applicable to collection of sample spectral reflectance
72	Type of radiation, rate and total fluence
73-74	Identification of corresponding reference deck
75	Test chamber pressure during reflectance measurement period
76	Wavelength region wherein data lies (ultraviolet, visible or near infrared; using blue, white and red IBM cards respectively)

A table containing information specific to a particular test accompanies each set of card decks.

2.6.4 Relative Spectral Reflectance Measurements

In addition to ten digits of parameter data, each IBM card contains from one to six reflectance-wavelength data pairs. Independently considered, these reflectance-wavelength pairs simply describe the sample spectral reflectance relative to the reference spectral reflectance. Such relative measurements provide accurate percentage changes in sample reflectance resulting from exposure to damaging radiation, when processed to effect spectral plots of reflectance (R) or $\Delta R/R_i$ (ratio of change in reflectance to initial reflectance as a function of wavelength). Since the sample spectral reflectance is dependent upon the reference spectral reflectance (a fixed portion of the magnesium oxide coated sphere wall), each sample value is divided by the corresponding reference value to normalize the measurement prior to entry into the $\Delta R/R_i$ calculation.

2.6.5 Interference Effects

The method of recording sample reflectance at fixed wavelength intervals, as described in Section 2.6.2, can be used to produce a computer plot with any

degree of fidelity required, disregarding economic considerations. However, samples which exhibit numerous, closely spaced interference fringes (maxima and minima) present a problem essentially independent of data collection techniques but directly bearing on subsequent data handling methods. In general, interference-type samples (i.e., types G, H, and Alzak) change both in reflectance and wavelength as a result of interaction with damaging radiation. The usual point-by-point spectral subtraction to determine ΔR cannot be used when the interference peaks and valleys have spectrally shifted from their original positions. Alternate procedures must be employed.

Selecting a wavelength collection interval sufficiently small to reproduce accurately, on IBM cards, the oscillating sample reflectance curve generated on the spectrophotometer chart, would require unreasonably long measurement times. An alternate method is to treat this class of samples manually. Types G, H, and Alzak have therefore been analyzed for $\Delta R/R_i$ working directly from the standard spectrophotometer charts. IBM cards were also taken for these samples, at the same wavelength intervals used for the balance of samples, but are misleading in those wavelength regions where interference minima and maxima occur. Delivery of these cards to NASA is therefore not recommended.

For types G, H, and Alzak, ΔR was determined by arithmetically fairing an average spectral reflectance curve through interference peaks and valleys (maxima and minima) present on pre- and post-exposure standard spectrophotometer charts, followed by normalization and point-by-point subtraction. A Peak and Valley Detector accessory is currently on order for installation into the Datex interfacing module to automate this procedure on future programs and produce meaningful data cards for this class of sample.

2.6.6 Highly Reflective Specular Surfaces

As discussed in Section 2.6.4, reflectance-wavelength pairs punched on any given IBM card simply indicate a sample's reflectance compared to the reference's reflectance at the same wavelength. Since the reference is a fixed location on the MgO coated sphere wall, its spectral reflectance is essentially that of MgO

as degraded by time elapsed since its application. Throughout the visible region the reflectance of freshly prepared MgO remains uniformly high, drops off gradually in the near infrared and decays rapidly in the ultraviolet. These characteristics are further degraded by continued exposure to air. The net result of these factors is that some specular sample surfaces exhibit a higher ultraviolet, and sometimes visible, spectral reflectance than does the reference. For the purpose of calculating $\Delta R/R$ this consequence is of limited importance. If, however, sample card decks are used directly to generate sample spectral reflectance, the resultant departure from absolute requires correction. An alternate procedure is to apply the spectral $\Delta R/R$ values to typical absolute spectral reflectance data obtained with an absolute bench-type instrument. The validity of this technique rests on the assumption that sample-to-sample variations in spectral reflectance, within a given sample batch, are insignificant. This basic premise underlies all environmental simulation testing since materials selected for actual hardware may be from a particular test batch but obviously cannot be the selfsame test specimen.

3.0 NEW TECHNOLOGY

The research performed under Contra t NAS5-11164 has been reviewed for the purpose of uncovering potential reportable New Technology items. The review activities have considered both the results of each test in turn, and the correlation of those results to derermine the overall performance of each thermal control coating. To the best of our knowledge, there is no New Technology to report.

4.0 CONCLUSIONS AND RECOMMENDATIONS

The effort expended during this program causes us to reach the following conclusions and to make the following recommendations:

4.1 CONCLUSIONS

From the 20-keV electron test, it is concluded that:

1. Degradation in white paints builds up more slowly than was found in earlier tests at 50 keV for Contract NAS5-9650. Absorptance bands in the infrared wavelength region are apparent in reflectance vs. wavelength curves, even after exposure to high electron fluences.

2. Goddard Series 101-7-1 (type R) has successfully been made more resistant to low-energy electron damage. Nevertheless, substantial degradation builds up in type R at 10^{15} and 10^{16} 20-keV electron fluences.

3. The visible-region "silicate-band" damage in types D_3, E_3, and F_3 occurs in substantial amounts, even for this low energy. Additional damage due to the presence of TiO_2 and ZnO occurs in the types possessing them as pigments. Thus, type D_3 with Al_2O_3 pigment only, is the most stable of the three types under electron exposure.

4. Other coatings exposed to 20-keV electrons (Kapton, Alzak, overcoated aluminum) sustain only limited amounts of reflectance degradation, if any.

From the 80-keV electron test, it is concluded that:

5. Degradation in white paints is more severe at each exposure fluence, compared to damage resulting from lower energy electrons. Absorptance structure in the infrared wavelength region is removed at lower fluences than happens with lower energy electrons. Damage is chiefly in the infrared except for the case of aluminum oxide—potassium silicate (type D_3), in which degradation is confined to the visible and ultraviolet wavelength regions.

6. The visible-region silicate absorption band is induced to even greater amounts by 80-keV electrons. In addition, the presence of TiO_2 and ZnO pigments

in coating types E_3 and F_3 causes them to incur "catastrophic" amounts of reflectance degradation at 10^{16} 80-keV electrons/cm^2.

7. Similar "catastrophic" reflectance damage is measured in the following coatings after exposure to 10^{16} 80-keV electrons/cm^2:

a. types M and R ZnO—methyl silicone
b. type O rutile TiO_2—methyl silicone
c. type N Kapton H-film

8. In all six types of metallized Teflon, the exposure to 10^{16} 80-keV electrons/cm^2 is sufficient to convert the specular appearance of the coatings to a crazed, mottled gray appearance.

Upon comparison of test results at different energies, it is concluded that:

9. Degradation in white paints is substantial for each energy studied, and quite severe in some cases. In every case, exposure to 20-keV electrons causes less damage than exposure to electrons of higher energy. Degradation caused by 50-keV electrons (for those surfaces tested) is rather like degradation caused by 80-keV electrons. In a few cases, in fact, results at 50 keV are virtually indistinguishable from those at 80 keV. Degradation in the white paints from 20-keV electrons is less able to mask or eliminate infrared absorption bands than is degradation from 50-keV and 80-keV electrons.

10. Type O rutile TiO_2—methyl silicone offers the greatest stability of the white diffuse coatings tested in an electron environment, provided fluences above 10^{15} electrons/cm^2 are not expected to be encountered in the application or mission. Because of type O's poor performance above 10^{15}, however, type L with anatase TiO_2 is a better TiO_2—silicone selection for such an application.

11. The following coatings and surface are extremely resistant to reflectance change when exposed to electrons in the 20-keV to 80-keV range: leafing aluminum—silicone (type I), vapor-deposited aluminum over lacquer (type J), aluminum oxide over aluminum (type G), silicon dioxide over aluminum (type H),

and buffed aluminum (type K). The principal change in type H is an improvement in reflectance in the ultraviolet wavelength region.

12. Alzak (types Z_3, Z_4, and Z_5) sustains more degradation from 20-keV electrons than from 80-keV electrons. Reflectance losses are chiefly in the ultraviolet wavelength region.

13. The concept of potassium silicate (K_2SiO_3) actually being best represented by ($K_2O \cdot SiO_2$) fits well with results obtained in this program. Damage in coatings bearing potassium silicate (D_3, E_3, and F_3) correlates well as to wavelength region in which it peaks (0.6 micron) with that historically observed and reported for optical materials, including silica, Corning 7940, and borosilicate glass (Reference 8).

From the additional tests conducted during the program it is concluded that:

14. The newly-obtained 50-keV test data fit well, though not perfectly, with earlier 50-keV data from Contract NAS5-9650.

15. In-vacuum reflectance recovery or improvement with time after the end of an electron exposure is a real, validly observed phenomenon in some types of coatings. The amount or rate of recovery may be easily observed, or difficult to detect, depending upon the type of material or coating involved. Possession of instrumentation with high signal-to-noise ratio and spectral resolution aids in its detection and measurement.

16. In-vacuum reflectance recovery proceeds more quickly to remove greater fractions of the original degradation caused by exposure to 20-keV electrons, compared to that removed with time after 50-keV or 80-keV electron exposure. Previous observations of reflectance improvement when exposure to ultraviolet radiation follows electron exposure (Reference 1) may also be interpreted as in-vacuum reflectance recovery successfully competing with ultraviolet-induced degradation.

17. Segmented and unsegmented electron exposures yield substantially the same results (reflectance changes) in the types of coatings tested, when compared at a fluence of 3×10^{14} 20-keV electrons/cm^2.

18. Both the rate and the extent of in-vacuum reflectance recovery in the various coatings and surfaces studied are functions of electron energy, electron fluence, and time after end of exposure. There is some indication that rate and extent of recovery are dependent upon specimen temperature. Additional study would be needed to determine any dependence upon the type of radiation received before recovery is observed (e.g., protons, solar photons, etc.), and any dependence upon exposure flux or intensity.

4.2 RECOMMENDATIONS

This program should be followed by:

1. Continuation of coating exposures to additional simulated space environmental conditions, and further test technique development to increase accuracy of simulation. This will allow better prediction of coating performance and survival (see Figure 74).

   (a) An electron exposure test should be performed at an energy of 35 keV. This test would complete the definition of energy-dependent damage between 20 and 80 keV. In addition, it would provide supplemental information on the performance of Teflon-based coatings that were fundamentally altered after the 80-keV electron exposure.

   (b) Additional testing should be performed to establish the dependence for damage on proton energy and evaluate the most recent NASA-Goddard coatings.

   (c) Simultaneous electron and proton tests should be performed. This is deemed to be important since low energy electrons and protons affect coatings in a significantly different manner over the spectral range from 0.25 to 2.5 microns, and since the ultraviolet plus either electron or proton damage is significantly nonadditive. Consequently, computer analysis of the integrated effects (both electrons and protons) of a near Earth

Figure 74. Simulation Test Techniques for Evaluating Coatings for a Near Earth Environment

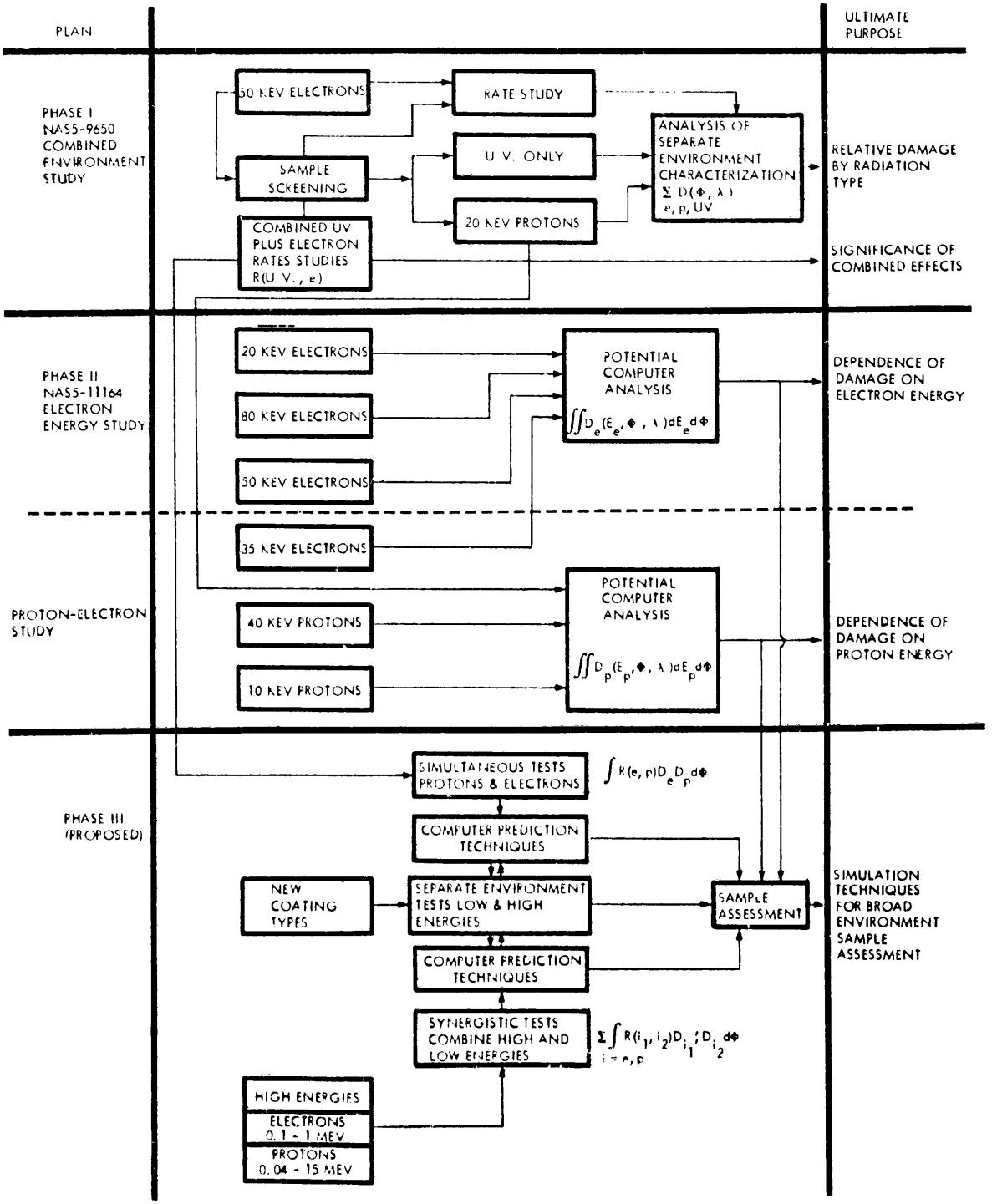

environment cannot assume simple additiveness.

(d) To complete the ability to simulate and predict space radiation effects, high-energy electron and proton tests should be conducted in situ and coupled with low-energy tests to determine anticipated synergistic effects.

2. Studies to determine damage mechanisms, in order to effect hardened coating development (see Figure 75).

(a) Spectral reflectance results already accumulated and indicating "photon bleaching" of particle-induced damage, in-air recovery and in-vacuum recovery, should be analyzed in terms of optical structure and shifts in interference peaks.

(b) Spectral reflectance charts now accumulated and showing the dependence of damage on particle type and energy should be analyzed in terms of penetration depth, ionization deposition, and displacement cross section for the exposure radiation.

(c) Results of 2(a) and 2(b) should be blended with knowledge of the interaction of solar energy (as a function of wavelength) with the coating material, to develop a model for damage.

(d) The model should be verified experimentally by following up on clues revealed during the performance of this contracted study. Coating specimens involved should have controlled and documented properties. This test program could include:

(i) Measurement of spectral properties in the infrared wavelength region, not only to evaluate in-vacuum emittance changes, but for determination of structural changes in optical signature. This would extend beyond 2.5 microns data on large reflectance changes now observed following electron exposure as well as allow investigation of significant sample "noise" now sensed in the infrared region

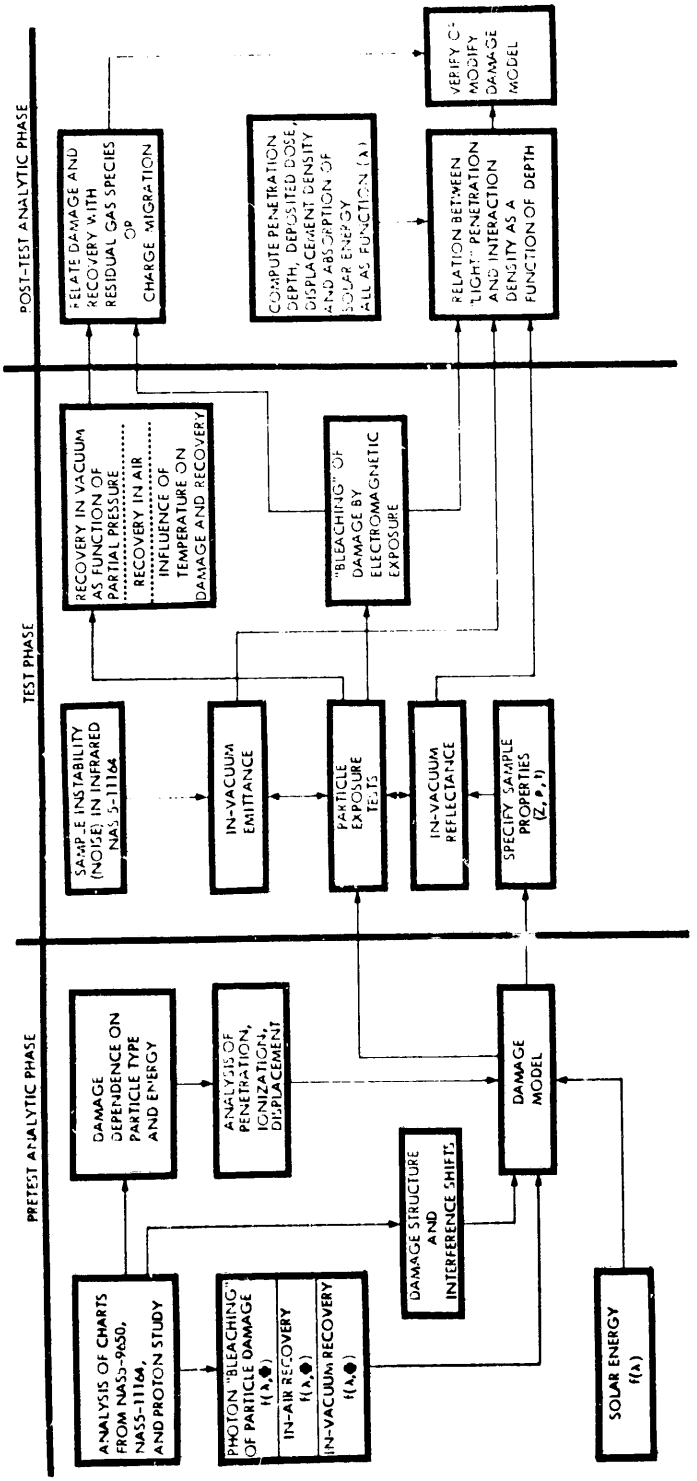

Figure 75. Proposed Future Studies of Damage Mechanisms

immediately following exposure.

(ii) Investigation of in-vacuum recovery as to its extent following proton, electron or ultraviolet radiation damage, either separately or simultaneously. This work would provide information on damage mechanisms and is also important in order to evaluate current testing practices.

(iii) Further controlled tests to evaluate in-air reflectance recovery, in-vacuum recovery, the influence of temperature on recovery, and the "bleaching" of damage by electromagnetic exposure.

(e) Analysis of new test data, directed toward revealing:

(i) The relative roles of residual chamber environment species and charge migration (charge storage measurements) on the damage and recovery of coatings, and

(ii) The correlation between absorption of solar energy as a function of wavelength and radiation penetration depth, dose, and displacement density.

REFERENCES

1. L.B. Fogdall, S.S. Cannaday, and R.R. Brown, "In Situ Electron, Proton, and Ultraviolet Radiation Effects on Thermal Control Coatings." Final Report to NASA-Goddard Space Flight Center for the Program, "Space Environment Effects on Thermal Control Coatings," Contract NAS5-9650, January, 1969, Boeing Document D2-84118-9.

2. S.S. Cannaday, L.B. Fogdall, and R.R. Brown, "In Situ Ultraviolet Radiation Effects on Thermal Control Coatings." Eighth Quarterly Progress Report to NASA-Goddard Space Flight Center for the Program, "Space Environment Effects on Thermal Control Coatings," Contract NAS5-9650, November 1967 , Boeing Document D2-84118-8.

3. J.E. Drennan and D.J. Hamman, "Space Radiation Damage to Electronic Components and Materials." Report No. 39, Radiation Effects Information Center, Battelle Memorial Institute, January, 1966.

4. R.B. Gillette, B.A. Kenyon, and S.S. Cannaday, "Investigation of the Effects of Low-Energy Protons on Specular Reflectance of Surfaces for Space Mirrors." Quarterly Progress Report No. 5 to NASA-Langley Research Center for Contract NAS1-7627, November, 1968.

5. A. Goldsmith "Thermophysical Properties of Solid Materials." WADC Report TR 58-476, Volume 4.

6. G.A. Zerlaut, personal communication.

7. S.J. Babjak, personal communication.

8. "Radiation Effects State of the Art (1965-1966)". Report No. 42, Radiation Effects Information Center, Battelle Memorial Institute, June, 1966.